CHARACTERIZATION AND MODELING OF CROSSTALK NOISE

IN DIGITAL SYSTEMS AND MICROWAVE APPLICATIONS

by

Prasit Teekaput

Dissertation submitted to the Faculty of

The Bradley Department of Electrical Engineering

Virginia Polytechnic Institute and State University

in partial fulfillment of the requirements for the degree of

Doctor of Philosophy

in

Electrical Engineering

APPROVED:

Aicha Elshabini-Riad

Prof. Aicha A. Elshabini-Riad, Chairperson

Prof. Shinzo Onishi, Co-Chairperson

Prof. Sedki M. Riad

Prof. Ira Jacobs

Prof. Margaret A. Murray

December 1990

Blacksburg, Virginia

CHARACTERIZATION AND MODELING OF CROSSTALK NOISE IN DIGITAL SYSTEMS AND MICROWAVE APPLICATIONS

by

Prasit Teekaput

Prof. Aicha A. Elshabini-Riad, Chairperson

Prof. Shinzo Onishi, Co-Chairperson

Electrical Engineering

(ABSTRACT)

This dissertation presents the characterization and modeling of crosstalk noise based on the theory of coupled microstrip lines. An equivalent circuit model used in this work comprises of the addition of mutual inductances and mutual capacitances to the fundamental transmission line model. Characterization of crosstalk noise along adjacent lines, current-voltage characteristics, characteristic impedance, effective dielectric impedance, and maximum crosstalk are performed analytically. Computer simulations and computations of these parameters are also performed. The circuits are realized experimentally, and an investigation of crosstalk noise using time domain and frequency domain measurement techniques is conducted. The results illustrate that the computation matched closely the experimental data and explained the physical phenomena bettter.

ACKNOWLEDGEMENTS

I would like to express my sincere gratitude to my advisors, Dr. A. A. Elshabini-Riad and Dr. S. Onishi, for giving their time, counselling, materials, and encouragement through out my research work. Special thanks is due to Dr. S. M. Riad, a member of my committee, for his help and for providing the opportunity of using some specialized equipment necessary for measurement experiments.

I am appreciative of the time and efforts of the other members of my committee,Dr. I. Jacobs, and Dr. M. A. Murray.

I would like to thank Dr. D. B. Hodge, former electrical engineering department head, for his help, support, and guidance.

I am deeply indebted to Dr. R. L. Carter, director of the center for advanced electron devices and systems and my advisor at The University of Texas at Arlington, who provided me a great deal of help in academic and nonacademic areas.

This work was performed using facilities in both the Time Domain Laboratory, the Hybrid Microelectronics Laboratory, and the Electronic Materials Laboratory at Virginia Tech. So, I would like to take this opportunity to thank my colleagues in both laboratories for their assistance.

I would like to extend my deep gratitude and appreciation to my parents, brothers, and sisters for their love and support.

I am especially thankful to my fiancee, Dr. Nonthima Chandramphorn, who has cheered me up and given the assistance on this final work. Also, thanks is due to her father, General Suthep Chandramphorn of the Thai Army, for his agreement on her assistance.

I also give the utmost praise and thanks to my lord, who is my constant companion and guide .

Finally, I hope to dedicate my success to encourage all the youngsters who wish to have a better life. I do believe that everyone has a chance to be successful if he or she has faith and never gives up.

TABLE OF CONTENTS

CHAPTER 1

INTRODUCTION

Crosstalk noise is an undesirable signal produced by either voltage drop due to current flow, electromagnetic fields, or both. The transmission of energy takes place in the region outside the conductor and the circuit model of a transmission line contains inductances, capacitances, and resistances associated with an incremental line length so that the occurrence of crosstalk noise is related to these inductances, capacitances, and resistances. Since microstrip lines are used in digital systems and microwave applications, high density circuitry always emphasizes the problem of crosstalk noise.

This dissertation describes work carried out to examine the characterization and modeling of crosstalk noise based on theory of coupled microstrip lines. An equivalent circuit model used in this work comprises of the addition of inductances and capacitances to the fundamental transmission line model. Characterization of crosstalk noise along adjacent lines, current - voltage characteristics, characteristic impedance, effective dielectric impedance, and maximum crosstalk are performed analytically. Computer simulations of these electrical parameters are also performed. The circuits are realized experimentally and an investigation of the crosstalk noise in the time domain and the frequency domain using various measurement techniques is also conducted.

This dissertation is organized into six chapters. The first chapter, Chapter 1, consists of this introduction. The next chapter, Chapter 2, presents the fundamentals of crosstalk noise theory. The theoretical background needed to understand the crosstalk noise equivalent circuit model, such as transmission line theory, microstrip line theory, and coupled microstrip lines theory, is also discussed.

Chapter 3 presents an equivalent circuit model of crosstalk noise between adjacent lines. The characterization of equivalent circuit model, current - voltage characteristics, characteristic impedance, effective dielectric impedance, and maximum crosstalk are developed analytically. The computer simulation and computation of these parameters are conducted. Maxwell Software is used to simulate data of physically based equivalent circuit model. The data are used to determine the characterization of crosstalk noise. TOUCHSTONE Software is used to simulate the data on crosstalk noise on adjacent lines using frequency domain measurement techniques. On the other hand, Spice Software is used to simulate the data using time domain measurement techniques.

An experimental realization of these microstrip structures is demonstrated in Chapter 4. The fabrication processes of these structures consist of etching copper-cladded teflon-ceramic composites, as well as screen printing various metallizations. An investigation of crosstalk noise in both time domain measurements and frequency domain of these structures is also demonstrated.

In Chapter 5, crosstalk noise considerations to verify the model, such as different line lengths, different loss lines, efficiency test on stripline are discussed. These structures are realized experimentally.

Finally, Chapter 6 summarizes the major findings of this dissertation.

CHAPTER 2

FUNDAMENTAL OF CROSSTALK NOISE THEORY AND OVERVIEW

2.1 Transmission line

Transmission line is used to transmit energy and information from one location to another. There are numerous types of transmission lines, such as microstrip lines, strip lines, and coplanar lines. Each of these structures possesses electrical characteristics upon the propagation of the current along the line length.

A transmission line is different from a waveguide in the sense that it has electrical characteristics distributed in each conductor per unit length. The field distribution along the uniform transmission line is known as transverse electromagnetic wave (TEM) because both electric and magnetic waves propagate in a perpendicular direction to the propagation direction. The electrical characteristics comprise of the resistance (R), the conductance (G), the capacitance (C), and the inductance (L) throughout the line. The transmission line may be analyzed using an equivalent circuit of a small section of the line as shown in Figure (2.1). In the case of lossless transmission line, the series resistance (R) and the shunt conductance (G) can be neglected.

The voltage between conductor may be expressed as,

$$V = V_0 \cos (wt-\beta z+\phi) \qquad (2.1)$$

where V is a function of time and distance in z direction.

Applying Euler's identity, gives the equation,

$$V = \text{Re} [V_0 \exp j (wt - \beta z + \phi)]$$
$$= \text{Re}\ V_0 \exp (j\phi) \exp (-j\beta z) \exp(jwt)$$

In phasor form, the voltage can be written as,

$$V_s = V_0 \exp (j\phi) \exp (-j\beta z)$$

Applying an increment length of a uniform transmission line where R, G, L, and C are functions of the transmission line configuration and material as shown in Figure (2.1), gives the voltage of the form,

$$V_s = (\tfrac{1}{2} R\, \delta z + j \tfrac{1}{2} w L\, \delta z) I_s + (\tfrac{1}{2} R\, \delta z + j \tfrac{1}{2} w L\, \delta z)(I_s + \delta I) + V_s + \delta V_s \qquad (2.2)$$

Dividing eq.(2.2) by δz, reduces the equation to the form,

$$\frac{\delta V_s}{\delta z} = - (R + j w L) I_s - (\tfrac{1}{2} R + j \tfrac{1}{2} w L) \delta I_s \qquad (2.3)$$

when δz is very small and approaches zero, δI_s approaches zero. Then, equation (2.3) can be written as,

$$\frac{\delta V_s}{\delta z} = - (R + j w L) I_s \qquad (2.4)$$

The voltage across the central branch is approximated to be equal to V_s, and the second equation is of the form,

$$\frac{\delta I_s}{\delta z} = -(G + jwC)V_s \quad (2.5)$$

In a sinusoidal time variation, Maxwell's curl equations for the uniform plane wave are of the form,

$$\nabla \times E_s = -jw\mu H_s \quad (2.6)$$

and

$$\nabla \times H_s = (\sigma + jw\epsilon)E_s \quad (2.7)$$

where both E_s and H_s are functions of z only as,

$$E_s = E_{xs}\, a_x$$

and

$$H_s = H_{ys}\, a_y$$

Then, eqs. (2.6, 2.7) take the forms,

$$\frac{d\,Exs}{dz} = -jw\mu H_{ys} \quad (2.8)$$

and

$$\frac{d\,Hys}{dz} = -(\sigma + jw\epsilon)E_{xs} \quad (2.9)$$

The boundary conditions in field equations of E_{xs} and V_s are the same as those for I_s and H_{ys}, the solution of the field equations can be written as,

$$E_{xs} = E_{x0} \exp(-\tau z)$$

and

$$V_s = V_0 \exp(-\tau z)$$

Applying the boundary conditions, $V_s = V_0$ at $z = 0$ and $V = V_0$ at $z = 0$, $t = 0$, gives the propagation constant (τ) for the uniform plane wave in the form,

$$\gamma = [\, j\, w\, \mu\, (\sigma + j\, w\, \epsilon)]^{\frac{1}{2}}$$
$$= \alpha + j\, \beta$$
$$= [\, (R + j\, w\, L)\, (G + j\, w\, C)\,]^{\frac{1}{2}} \qquad (2.10)$$

where the real and imaginary parts, α and β, are the attenuation constant (Np/m) and the phase constant (rad/m) of the line, respectively.

The coupled time-harmonic transmission line equations, eqs. (2.4-2.5), can be combined to solve for V(z) and I(z) as,

$$\frac{\delta^2 V(z)}{\delta z^2} = \gamma^2 V(z)$$

and

$$\frac{\delta^2 I(z)}{\delta z^2} = \gamma^2 I(z)$$

which provides the solution of the form,

$$V(z) = V^+(z) + V^-(z)$$
$$= V^+ \exp(-\gamma z) + V^- \exp(\gamma z) \qquad (2.11)$$

and

$$I(z) = I^+(z) + I^-(z)$$
$$= I^+ \exp(-\gamma z) + I^- \exp(\gamma z) \qquad (2.12)$$

where the plus and minus superscripts denote wave traveling in the + Z and - Z directions, respectively. The relationship among wave amplitudes V^+, V^-, I^+, and I^- takes the form,

$$\frac{V^+}{I^+} = -\frac{V^-}{I^-} = \frac{R + j\,w\,L}{\gamma} \qquad (2.13)$$

The ratio of voltage and current at any Z in equation (2.13) for an infinitely long line is called characteristic impedance (Z_0), written as,

$$Z_0 = \frac{R + j\,w\,L}{\gamma} = \frac{\gamma}{G + j\,w\,C}$$

$$= \left[\frac{R + j\,w\,L}{G + j\,w\,C}\right]^{\frac{1}{2}} \;\Omega \qquad (2.14)$$

In the case of lossless transmission line, R = 0, G =0. The propagation constant γ equals j β, α = 0.

$$\gamma = [\,(j\,w\,L)\,(j\,w\,C)\,]^{\frac{1}{2}}$$

$$= j\,w\,(L\,C)^{\frac{1}{2}} \qquad (2.15)$$

The phase velocity v equals w / β.

$$v = (L\,C)^{\frac{1}{2}} \qquad (2.16)$$

and

$$Z_0 = R_0 + j\,X_0$$

$$= (L / C)^{\frac{1}{2}} = \text{constant value} \qquad (2.17)$$

where $R_0 = (L / C)^{\frac{1}{2}}$, and $X_0 = 0$

In the case of low-loss transmission line, $R \ll w L$ and $G \ll w C$, the propagation constant τ equals $\alpha + j \beta$.

$$\tau = j w (L C)^{\frac{1}{2}} \left[1 + \frac{R}{j wL} \right]^{\frac{1}{2}} \left[1 + \frac{G}{j wC} \right]^{\frac{1}{2}}$$

$$\approx j w (L C)^{\frac{1}{2}} \left[1 + \frac{R}{2 j wL} \right] \left[1 + \frac{G}{2 j wC} \right]$$

$$\approx j w (L C)^{\frac{1}{2}} \left[1 + \frac{1}{2 j w} \left[\frac{R}{L} + \frac{G}{C} \right] \right] \quad (2.18)$$

where

$$\alpha \approx \frac{1}{2} \left[R \left[\frac{C}{L} \right]^{\frac{1}{2}} + G \left[\frac{L}{C} \right]^{\frac{1}{2}} \right]$$

$$\beta \approx j w (L C)^{\frac{1}{2}}$$

The phase velocity v equals to w / β

$$v \approx (L C)^{\frac{1}{2}} \quad (2.19)$$

and

$$Z_0 = R_0 + j X_0$$

$$= \left[\frac{L}{C} \right]^{\frac{1}{2}} \left[1 + \frac{R}{j wL} \right]^{\frac{1}{2}} \left[1 + \frac{G}{j wC} \right]^{-\frac{1}{2}}$$

$$Z_0 \approx \left[\frac{L}{C}\right]^{\frac{1}{2}} \left[1 + \frac{1}{2\,j\,w}\left[\frac{R}{L} - \frac{G}{C}\right]\right] \qquad (2.20)$$

where

$$R_0 = (L / C)^{\frac{1}{2}}$$

and

$$X_0 \approx - \left[\frac{L}{C}\right]^{\frac{1}{2}} \left[1 + \frac{1}{2\,j\,w}\left[\frac{R}{L} - \frac{G}{C}\right]\right]$$

$$\approx 0$$

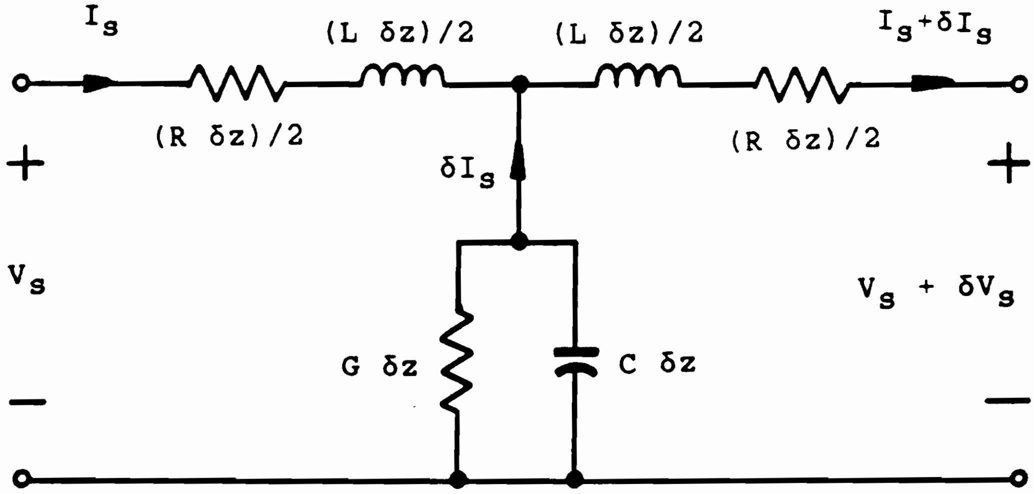

Figure 2.1 Elementary Section of A Transmission Line

2.2 Microstrip Line

A microstrip line has a metal strip and a ground plane separated by dielectric material, Figure (2.2). The distributions of electric and magnetic fields are presented in Figure (2.3). Due to the concentration of electric field in the dielectric region below the strip, most of the wave energy is concentrated there. The distribution of the electric field lines approaches the air dielectric interface. Using maxwell's equation, pure TEM mode cannot propagate in a microstrip. This leads to the conclusion that a pure TEM mode cannot support a microstrip line. Since most of the electric field lines are concentrated below the strip, and the electric flux crossing the air dielectric boundary is small, the deviation from TEM mode is small and may be ignored for most of the circuit design application. The mode propagating along the microstrip line is quasi-TEM mode. The effective dielectric constant is lower than the dielectric constant of the substrate due to the external fields. Many approaches to characterize the microstrip line require extensive calculations. The closed form expressions for computer aided design of microstrip is provided and some expressions are programmed in FORTRAN for calculation to support the theory in Appendix I. Some examples of these simulation results are demonstrated in Figures (2.4) - (2.5).

a) Characteristic Impedance and Effective Dielectric Constant

The closed form expressions for Z_0 and ϵ_{eff} have been reported by Wheeler (1965, 1977) , Schneider (1969), and Hammerstad (1975). Owens (1976) investigated the applications of expressions given by Wheeler, comparing numerical computations requiring elaborate algorithm that was known to be very accurate. Expression for ϵ_{eff} (Z_0) furnished by Owens (1976) is of the form,

$$\epsilon_{eff} = \frac{(\epsilon_r+1)}{2}\left[1+\frac{29.98}{Z_0}\left[\frac{2}{\epsilon_r+1}\right]^{\frac{1}{2}}\left[\frac{\epsilon_r-1}{\epsilon_r+1}\right]\left[\ln\frac{\pi}{2}+\frac{1}{\epsilon_r}\ln\frac{4}{\pi}\right]\right]^2 \tag{2.21}$$

The effect of thickness (t), which influences the field distribution, is very small and negligible in most single microstrip lines. For microstrip lines designed to carry at least moderate power, the thickness may be significant. Several researchers have investigated the effects of finite strip thickness. The simple and accurate formula for Z_0 and ϵ_{eff} have been reported by Bahl (1977). The following expressions are summarized.

For $W/h \le 1$,

$$Z_0 = \frac{60}{(\epsilon_{eff})^{\frac{1}{2}}}\ln\left[8\frac{h}{W_e}+0.25\frac{W_e}{h}\right] \tag{2.22}$$

For $W/h \geq 1$,

$$Z_0 = \frac{120\pi}{(\epsilon_{eff})^{\frac{1}{2}}} \left[\frac{W_e}{h} + 1.393 + 0.667 \left[\frac{W_e}{h} + 1.444 \right] \right]^{-1} \tag{2.23}$$

where

$W/h \leq \pi/2$

$$\frac{W_e}{h} = \frac{W}{h} + \frac{1.25t}{\pi h} \left[1 + \ln \frac{4\pi W}{t} \right] \tag{2.24}$$

and

$W/h \geq \pi/2$

$$\frac{W_e}{h} = \frac{W}{h} + \frac{1.25t}{\pi h} \left[1 + \ln \frac{2h}{t} \right] \tag{2.25}$$

The effective microstrip permittivity ϵ_{eff} due to the effects of thickness can be written in the simple form,

$$\epsilon_{eff}(t) = \epsilon_{eff} - \delta\epsilon_{eff}(t) \tag{2.26}$$

where

$$\delta\epsilon_{eff}(t) = \frac{(\epsilon_r - 1)\ t/h}{4.6\ (W/h)^{\frac{1}{2}}} \tag{2.27}$$

The effect of frequency on ϵ_{eff} is described accurately through the dispersion model given by Getsinger (1973). The expression of ϵ_{eff} based on the same foundation is of the form,

$$\epsilon_{eff}(f) = \epsilon_r - \frac{\epsilon_r - \epsilon_{eff}}{1 + G(f/f_p)^2} \qquad (2.28)$$

where $\mu_0 = 4\pi * 10^{-7}$ H/m, $f_p = Z_0 / 2\mu_0 h$, and $G = 0.6 + 0.009 Z_0$

This model requires at least optimization of the G - factor for any given microstrip lines on a particular substrate. Edwards and Owens (1976) carried out extensive measurements on microstrip lines and established the expression for G - factor by curve fitting in the form,

$$G = \left[\frac{Z_0 - 5}{60}\right] + 0.004 Z_0 \qquad (2.29)$$

This work applies well in the range $10 \le Z_0 \le 100\ \Omega$, and $2 \le f \le 18$ GHz.

Based on extensive measurements, Edwards and Owens suggest the following expression for dispersion having accuracy better than 0.8 per cent.

$$\epsilon_{eff}(f) = \epsilon_r - \frac{\epsilon_r - \epsilon_{eff}}{1+(h/Z)^{1.33} + (0.43 f^2 - 0.009 f^3)} \qquad (2.30)$$

where f is in gigahertz and h is in millimeters.

The effect of frequency on Z_0 has been described by several investigators. The results of Bianco et.al. (1974), providing accurate results, may be written as,

$$Z_0(f) = Z_{OT} - \frac{Z_{OT} - Z_0}{1 + G\ (\ f/f_p\ )^2} \qquad (2.31)$$

where Z_{OT} is twice the characteristic impedance calculated for a triplate transmission line having the same width W as the microstrip line but twice the substrate height (2h). Referring to Edwards (1981), this expression for 50 ohm line on an alumina substrate yields an increase of only 5 percent over the 0 - 16 GHz frequency range.

The wavelength λ can be given by,

$$\lambda = \frac{c}{f\ (\epsilon_{eff}\ )^{1/2}} \qquad (2.32)$$

and the physical length of microstrip element is approximated to be a quarter wavelength.

b) Losses

The total loss comprises of the conductor loss and the dielectric loss, α_c and α_d, respectively.

The closed form expressions for losses have been reported by Pucel et al.(1968). The expression for conductor loss (α_c) is of the form,

$$\alpha_c = 1.38 \; A \; \frac{R_S}{h \; Z_O} \; \frac{32 - (W_e/h)^2}{32 + (W_e/h)^2}$$

$$= 6.1 * 10^{-5} \; A \; \frac{R_S \; Z_O \; \epsilon_{eff}}{h} \left[W_e/h + \frac{0.667 \; W_e/h}{W_e/h + 1.444} \right] \quad (2.33)$$

where

$A = 1 + h/W_e \; (1 + \ln (2B/t) / \pi,$

$B = h$, for $W/h \geq 1 / 2\pi$

$= 2 \pi W$, for $W/h \leq 1 / 2\pi$

$R_S = (\pi f \mu_O \rho)^{\frac{1}{2}}$

ρ is the resistivity of the strip conductor

The dielectric loss α_d (in dB / unit length) has been reported by Gupta et al. (1979) as,

$$\alpha_d = 27.3 \; \frac{\epsilon_r}{\epsilon_r - 1} \; \frac{\epsilon_{eff} - 1}{\epsilon_{eff}^{\frac{1}{2}}} \; \frac{\tan \delta}{\text{wave length}} \quad (2.34)$$

where tan δ is the loss tangent of the dielectric.

Also, this dielectric loss (in dB/microstrip wavelength) has been reported by Hammerstad and Bekkadal (1975) as,

$$\alpha_d = 27.3 \; \frac{\epsilon_r \; (\epsilon_{eff} - 1)}{(\epsilon_r - 1) \; \epsilon_{eff}} \tan \delta \quad (2.35)$$

c) Pulse Propagation Along Microstrip Lines

There are many applications in which microstrip lines are used to conduct pulses rather than microwave energy such as high speed computer logic, high bit-rate digital communication, high speed samplers for time domain reflectometers, etc. The important property of the microstrip lines in these applications is propagation delay, which can be written as,

$$\begin{aligned} \text{delay} &= 1 \,/\, \text{velocity} \\ &= 1 \,/\, v_p \qquad \text{s/m} \\ &= \epsilon_{eff}^{\frac{1}{2}} \,/\, c \qquad \text{s/m} \end{aligned} \qquad (2.36)$$

To increase the effective propagation delay, the capacitive placing along the microstrip line can be introduced. The delay and velocity are changed by these capacitances as shown in the following equations.

$$\begin{aligned} \text{delay} &= 1 \,/\, \text{velocity} \\ &= 1 \,/\, v_p \qquad \text{s/m} \\ &= (\, L \; C \,)^{\frac{1}{2}} \end{aligned} \qquad (2.37)$$

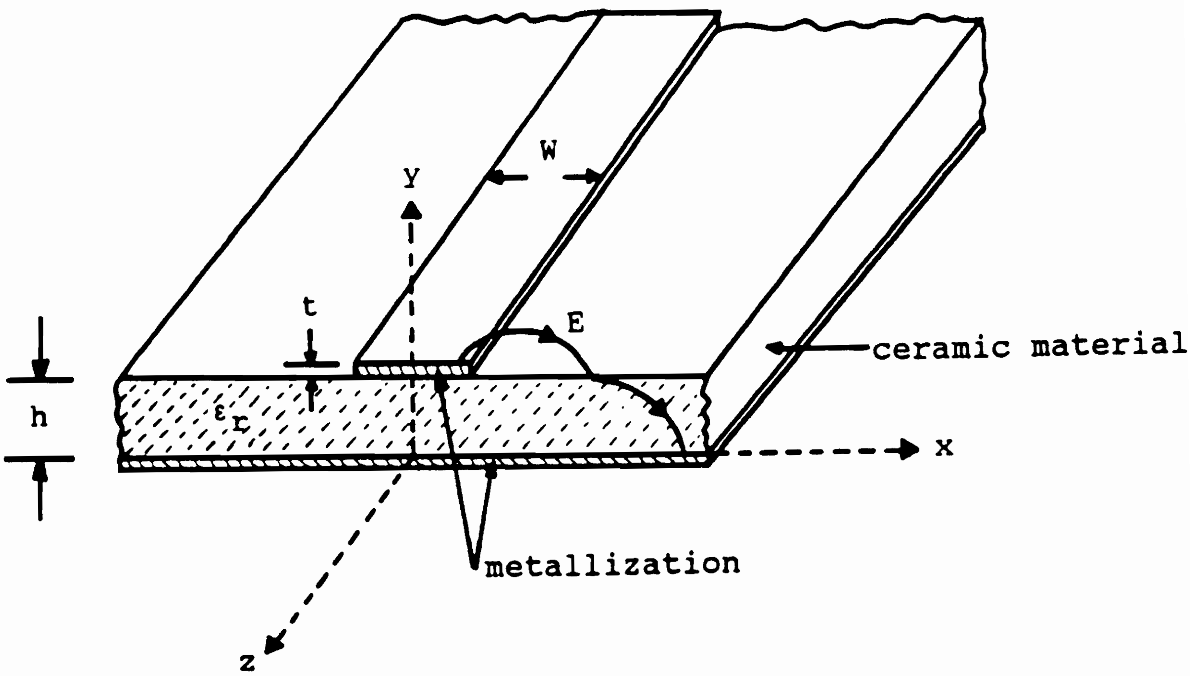

Figure 2.2 Microstrip Line Configuration

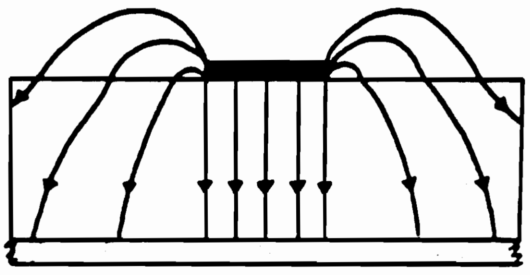

Electric Field

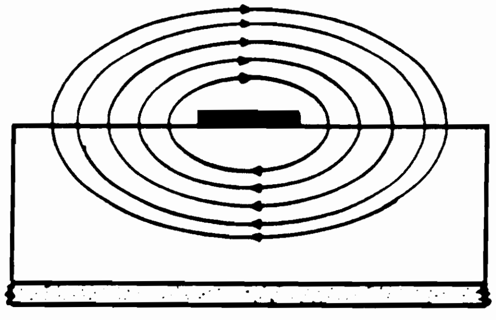

Magnetic Field

Figure 2.3 Distribution of Electric and Magnetic Fields in A Microstrip Line

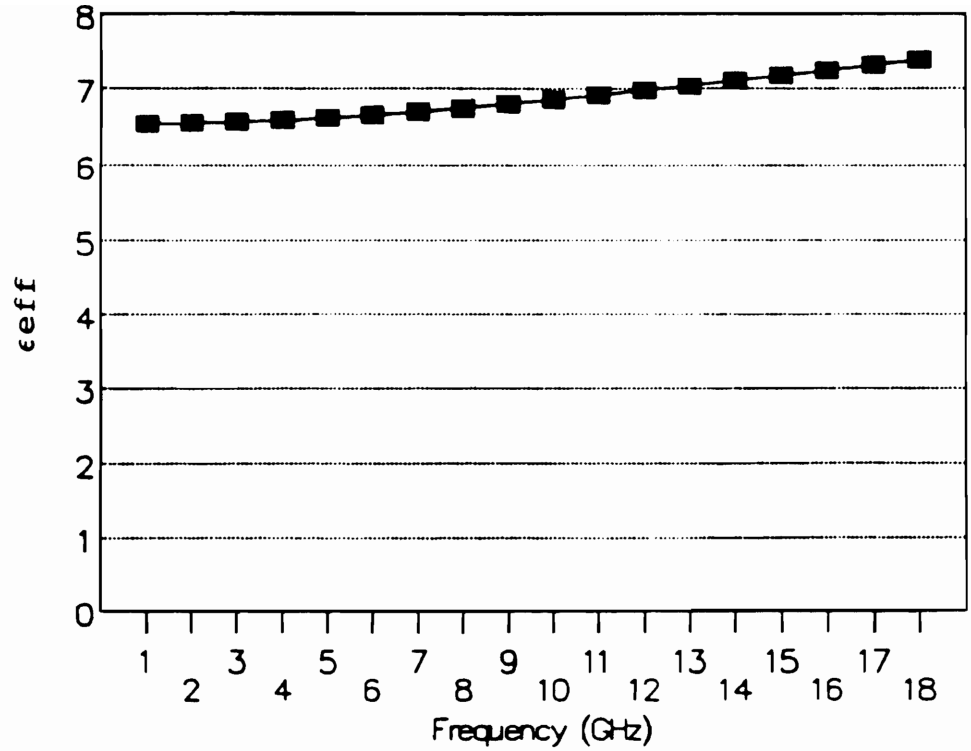

Figure 2.4 Simulated Effective Dielectric Constant versus Frequency, (Microstrip Line Configuration) (ϵ_r=9.8, w=24 mils, t=0.01 mil, h=25 mils)

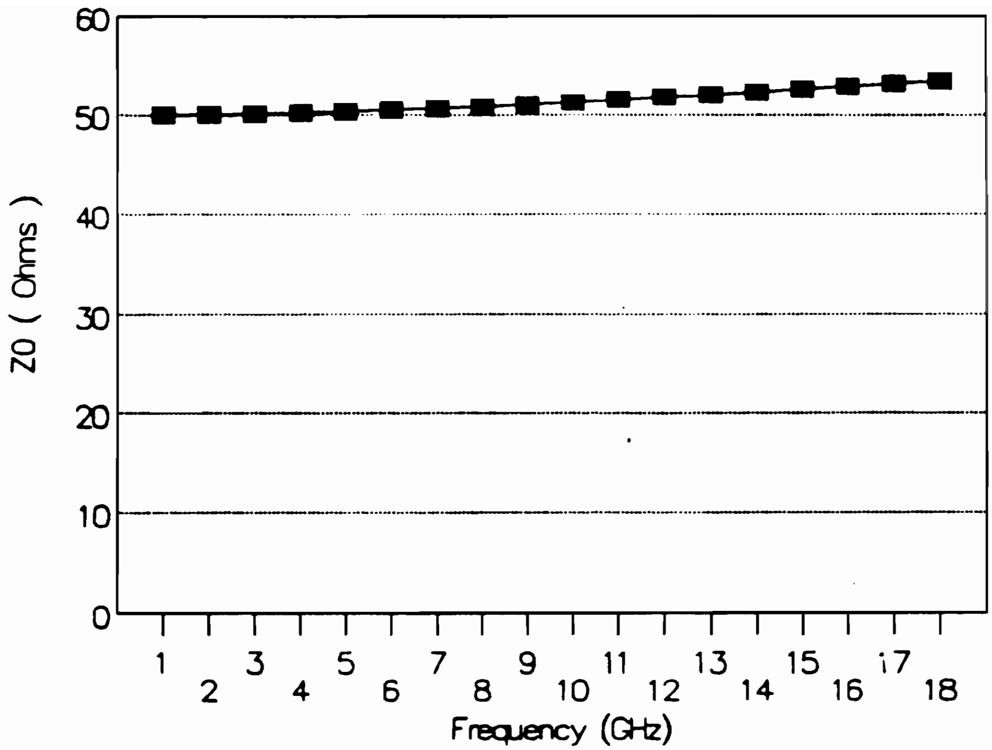

Figure 2.5 Simulated Characteristic Impedance versus Frequency, (Microstrip Line Configuration) (ϵ_r=9.8, w=24 mils, t=0.01 mil, h=25 mils)

2.3 Coupled Microstrip Lines

Microstrip lines can be used in moderate to high speed digital systems. The problem of crosstalk noise can be considerable when high density circuitry and short rise time pulses are involved. On the same substrate, the design purpose is to have microstrip lines isolated from each other. In practice, crosstalk noise can exist even when the lines are separated by several strip widths. In this work, methods to characterize crosstalk noise are introduced.

Crosstalk noise is a critical obstacle in the pulse system. Methods for understanding the characterization of crosstalk noise require a good understanding of the coupled microstrip lines area. Figure (2.6) presents the coupled microstrip lines configuration. Figures (2.7) - (2.8) show the even and odd mode fields in coupled microstrip lines, respectively. Figure (2.9) shows the capacitance model of coupled microstrip lines for the analysis purpose. The computation of this model is written in FORTRAN program shown in appendix B. Some examples of these simulation results are demonstrated in Figures (2.10) - (2.11).

a) Characteristic Impedance and Effective Dielectric Constant

The analysis formula for characteristic impedance have been reported by Garg and Bahl (1979). The approach is to represent the total capacitance of a line in terms of a parallel plate capacitance and two fringing capacitances. Using these capacitances, the total even and odd mode capacitances, Figure (2.9), can be given by,

$$C_e = C_p + C_f + C'_f \tag{2.38}$$

$$C_o = C_p + C_f + C_{ga} + C_{gd} \tag{2.39}$$

where

$$C_p = \epsilon_o \epsilon_r \frac{W}{h} \tag{2.40}$$

C_f is the fringing capacitance of a microstrip line with width W/h , impedance Z_0, and effective dielectric constant ϵ_{re}, and is of the form,

$$2 C_f = (\epsilon_{re})^{1/2} / (c Z_o) - C_p \tag{2.41}$$

and $c = 3 * 10^8$ m/s

C_f' is obtained empirically in the term,

$$C'_f = \frac{C_f}{1 + A (h / s) \tanh (10 s/h)} \tag{2.42}$$

and

$$A = 1 + \exp[-0.1 \exp(2.33 - 2.53 W/h)] \tag{2.43}$$

C_{ga} is the capacitance term in odd mode for the fringing field across the gap in air region and is obtained as,

$$2 C_{ga} = \epsilon_o \frac{K(k')}{K(k)} \tag{2.44}$$

and

$$K = \frac{s/h}{s/h + 2W/h} \tag{2.45}$$

$$K' = (1 - K^2)^{\frac{1}{2}} \tag{2.46}$$

Cgd is the capacitance in odd mode for the fringing field across the gap in dielectric region and is given as,

$$C_{gd} = \frac{\epsilon_o \epsilon_r}{\pi} \ln\left[\coth\left[\frac{\pi S}{4h}\right]\right] + 0.65 C_f \left[\frac{0.02}{s/h} (\epsilon_r)^{\frac{1}{2}} + 1 - \epsilon_r^{-2}\right] \tag{2.47}$$

The characteristic impedances and effective dielectric constants for even and odd modes can be obtained from the capacitance expression,

$$Z_{oi} = [c (C(i) \; C^a(i))^{\frac{1}{2}}]^{-1} \tag{2.48}$$

$$\epsilon^i(e) = \frac{C_i}{C^a(i)} \tag{2.49}$$

where $\quad i \;=\;$ even or odd, e or o, respectively.

and C_a denotes the capacitance with air as the dielectric medium.

Jansen (1978) gave the expression for effective width W_t which was valid for $S \geq 2t$,

$$\frac{W_t^e}{h} = \frac{W}{h} + \frac{\delta W}{h} \left(1 - 0.5 \exp \frac{-0.69 \; \delta W}{\delta t} \right) \tag{2.50}$$

$$\frac{W_t^o}{h} = \frac{W_t^e}{h} + \frac{\delta t}{h} \tag{2.51}$$

where,

$$\frac{\delta t}{h} = \frac{1}{\epsilon r} \frac{t/h}{s/h} \tag{2.52}$$

b) Losses

Coupled microstrip lines have two kinds of losses, ohmic loss (α_c) and dielectric loss (α_d). These losses can be represented in the forms,

$$\alpha_c{}^i = \frac{8.68\ Rs}{240\ \pi\ Z_{0i}} \frac{2}{h} \frac{1}{c(C_{at}{}^i)^2} \left[\frac{d\ C_{at}{}^i}{d(W/h)} \left(1 + 2 \frac{W}{2h} \right) - \frac{d\ C_{at}{}^i}{d(S/h)} \left(1 - 2 \frac{S}{2h} \right) + \frac{d\ C_{at}{}^i}{d(t/h)} \left(1 + 2 \frac{t}{2h} \right) \right] \tag{2.53}$$

and

$$\alpha_d{}^i = 27.3 \frac{\epsilon r\ (\epsilon_{re}{}^i - 1)}{(\epsilon_{re}{}^i)^{\frac{1}{2}}\ (\epsilon r - 1)} \tan \delta \tag{2.54}$$

where i = even (e) or odd (o)

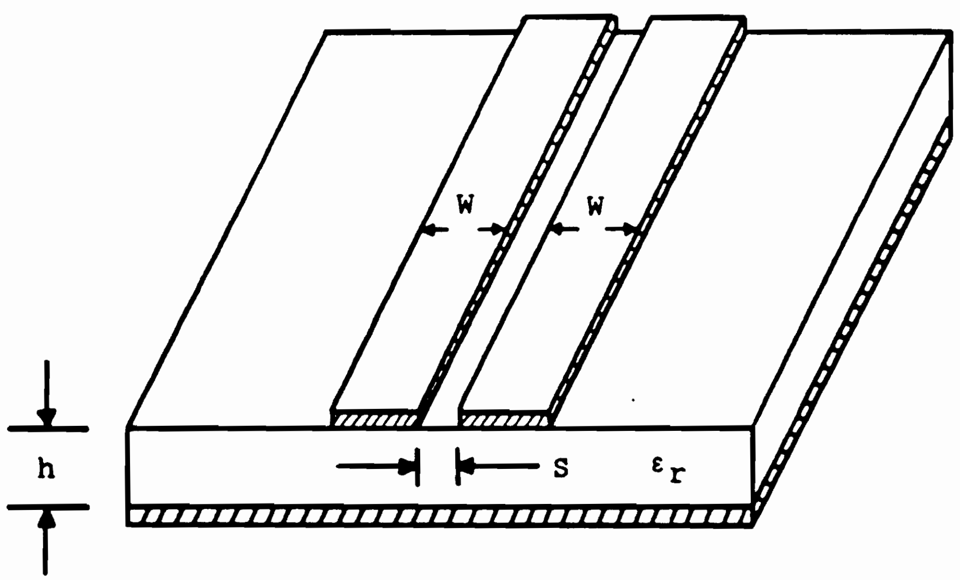

Figure 2.6 Coupled Microstrip Lines Configuration

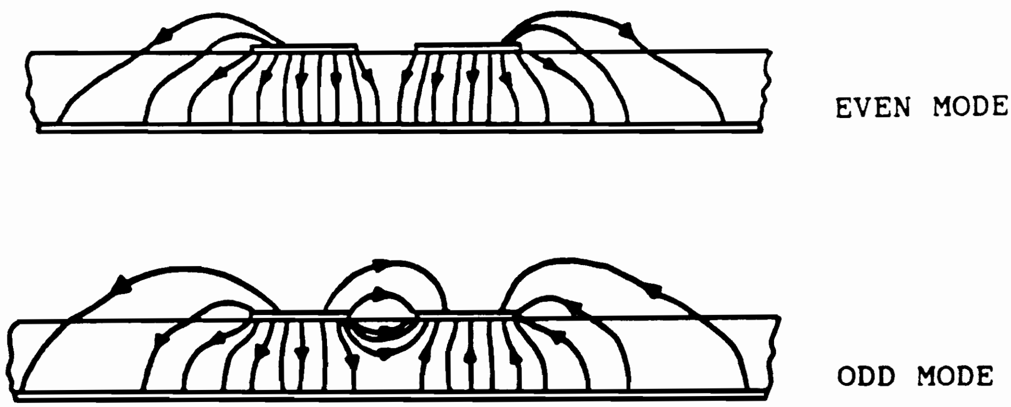

Figure 2.7 Even and Odd Mode Electric Fields in Coupled Microstrip Lines

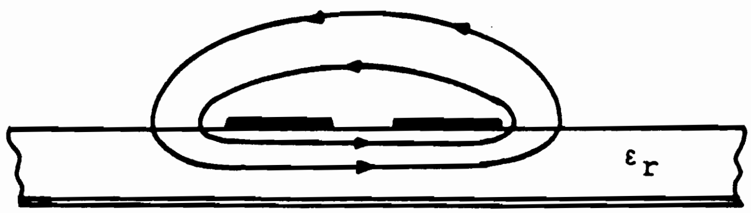

EVEN MODE

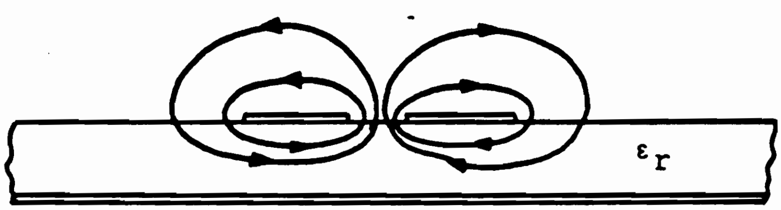

ODD MODE

Figure 2.8 Even and Odd Mode Magnetic Fields in Coupled Microstrip Lines

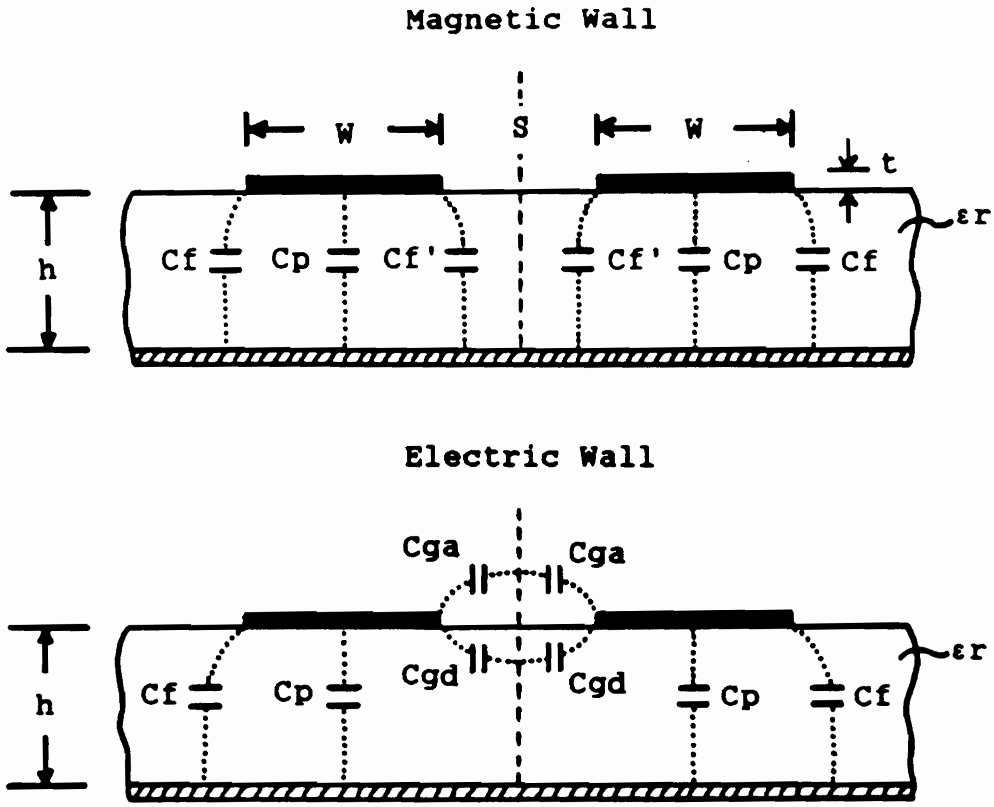

Figure 2.9 Capacitance Model of Coupled Microstrip Lines

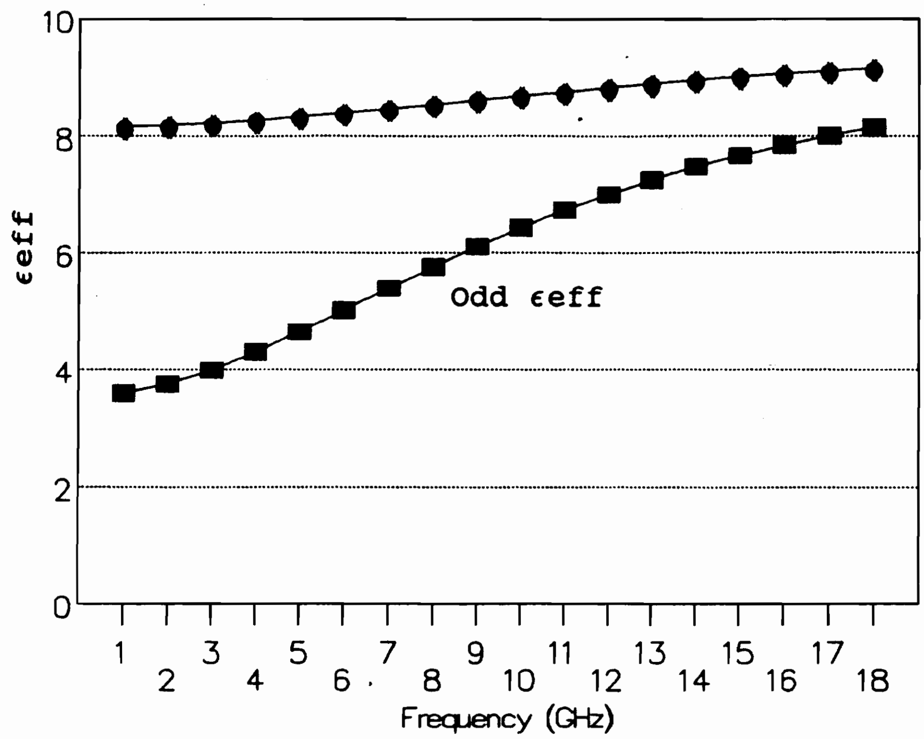

Figure 2.10 Simulated Effective Dielectric Constant versus Frequency, (Coupled Microstrip Lines Configuration) (ϵ_r=9.8, w=20 mils, t=0.01 mil, h=25 mils and S=10 mils)

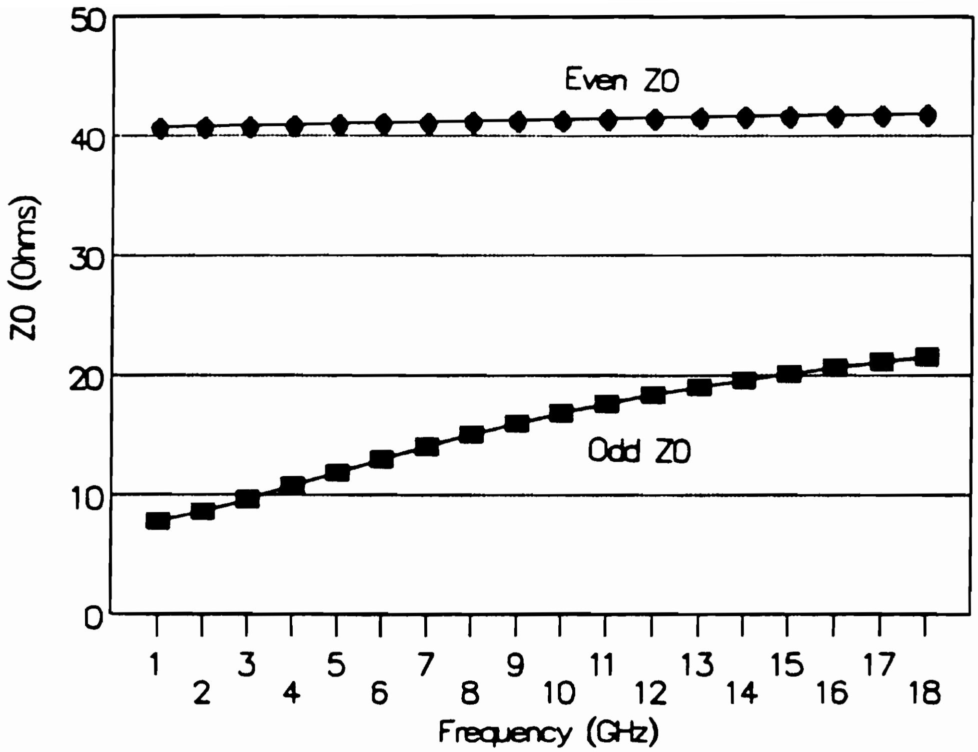

Figure 2.11 **Simulated Characteristic Impedance versus Frequency, (Coupled Microstrip Lines Configuration) (ϵ_r=9.8, w=24 mils, t=0.01 mil, h=25 mils, and S=10 mils)**

2.4 Overview of Crosstalk Noise Theory

Cohn (1955) demonstrated that two fundamental TEM modes could exist on a pair of parallel conductor strips between parallel ground planes. He had a formula for Z_{0e} and Z_{0o} for buried lines. Jarvis (1963) discussed the effects of interconnections on high speed logic circuits. This included the source, calculation, and minimization of interconnection crosstalk noise. Wheeler (1965) analyzed the characteristic impedance and propagation velocity of a single line using a modified conformal mapping, and Yamashita (1968) computed these quantities using variational mapping. Connolly (1966) did an analysis of cross-coupling from line to line in multilayers when excitation function was a fast rise time voltage pulse. Catt (1967) defined crosstalk noise and coupling noise in digital systems. Silvester (1968) proposed the method using Green's function and integral equation for the TEM wave properties of microstrip lines. His work had no restriction on the thickness of stripline conductor and got along with the experimental work presenting by Kaupp (1967). Bryant and Weiss (1968) analyzed the characteristics of coupled lines. Their work had a restriction on line thickness. Okugawa and Hagiwara (1970) calculated the crosstalk waveform in lossless coupled microstrip lines using Silvester's method and a numerical method. Garg and Bahl (1979) proposed a method to calculate the characteristics of coupled microstrip lines. Their approach represented the total capacitance of a line to ground in terms of a parallel plate capacitance and two fringing capacitances. The capacitance expressions were used to determine characteristic impedances and effective dielectric constants. Hamilton (1982) presented the construction and performance of a compact chip mount for making multiple, high speed, low crosstalk contacts to a Josephson integrated circuit. Seki and Hasegawa (1984) analyzed crosstalk in very high speed LSI/VLSI using a coupled multiconductor metal-insulator-semiconductor (MIS) microstrip line model. They proposed a shielded multilevel interconnect scheme for reduction of crosstalk without reducing wiring capacity. Bakoglu (1985) proposed a model that included the effects of scaling transistor, interconnection, and chip dimensions for interconnection lines in optimal interconnection circuits for VLSI. Kwon (1987) noted that the chip-to-chip interconnections can limit overall performance of VLSI circuits. He proposed a two-level structure to offer an attractive combination of high speed, low crosstalk noise, low loss, and high density. This included a new model of circuit configuration of coupled microstrip lines for crosstalk noise study. Hatta (1988) introduced a three-phase three-conductor transmission line in an inductive radio system for detecting the position of a linear synchronous motor car. His work showed the relation between the crosstalk between positive and negative-phase-sequence components in a helically wound transmission line, and deviations of the line conductors from their normal positions.

2.5 Research Topic Identification

The line length in the work is assumed to be long in order to observe the characteristics of crosstalk noise, in order to provide an approximate shape of pulse waveform in time domain measurement techniques. This assumption is quite acceptable in high speed computers and VLSI applications, but not in high frequency applications. Considering the fact that the wavelength of transmission line operated at high frequency is very short, the length of this line should be correspondent to its wavelength in order to perform satisfactory. Therefore, the assumption of a long transmission line may not be an appropriate one to adopt in some applications.

This work demonstrates the method to characterize crosstalk noise when the circuit is operated at high frequency. An equivalent circuit model used in this work comprises of the addition of inductances and capacitances to the fundamental transmission line model. Characterization of crosstalk noise along adjacent lines, current-voltage characteristics, characteristic impedance, effective dielectric impedance, and maximum crosstalk, are performed analytically in Chapter 3. Computer simulation and computation of these parameters are also conducted. MAXWELL Software is used to simulate data of physically based equivalent circuit model. The data are used to determine the characterization of crosstalk noise. TOUCHSTONE Software is used to simulate the data on crosstalk noise on adjacent lines in frequency domain, where SPICE Software is used to simulate the data in time domain. The circuits are realized experimentally using both conventional thick film printing technique on alumina substrates, as well as selective etching of copper cladded teflon-ceramic duriod composite substrates. An investigation of the crosstalk noise using both time domain measurements and frequency domain measurements of these structures is demonstrated in Chapter 4. Crosstalk noise considerations to verify the model, such as different line lengths, different loss lines, and efficiency test on stripline are discussed in Chapter 5.

2.6 Summary

This chapter presents an overview of crosstalk noise. A summary of transmission line theory related to this work is demonstrated. The characterization of microstrip lines and coupled microstrip lines based on literature review is reviewed. Section 2.5 presents the problems encountered in crosstalk noise theory when the circuit is operated at high frequency, thus identifying the research topic.

In the next chapter, an equivalent circuit model used in this work is presented. Characterization of crosstalk noise along adjacent lines, current-voltage characteristics, characteristic impedance, effective dielectric constant, and maximum crosstalk are performed analytically. Computer simulations and computations of these parameters are performed in order to support the theory.

CHAPTER 3

MODELING, ANALYSIS AND SIMULATION OF CROSSTALK NOISE

3.1 Introduction

TEM waves are not possible in an inhomogeneous medium. Since a digital signal is not significantly distorted when it travels down the surface conductor, the propagation mode can be approximated to TEM. The concept of crosstalk modeling comes from a simple model of a transmission line as shown in Figure (3.1) Then, two parallel transmission lines are presented in Figure (3.2) In this work, the circuit configuration is presented in Figure (3.3). The crosstalk model between the microstrip lines can be demonstrated in Figures (3.4) - (3.5). Figure (3.4) represents primary crosstalk model while Figure (3.5) represents transient model.

In this model, the mutual inductance M1 and the mutual capacitance Cm1 represent primary crosstalk. The model is treated as forward signal system, Figure (3.4). The effect of mutual inductance and mutual capacitance associated with a forward signal can be classified as primary crosstalk. Applying the relationship of transmission line, provides the relationship of these physical elements. The equations are given by,

$$- \frac{d V_A}{dx} = L \frac{d I_A}{dt} + M_1 \frac{d I_B}{dt} \qquad (3.1)$$

$$- \frac{d V_B}{dx} = M_1 \frac{d I_A}{dt} + L \frac{d I_B}{dt} \qquad (3.2)$$

$$- \frac{d I_A}{dx} = C \frac{d V_A}{dt} - Cm_1 \frac{d V_B}{dt} \qquad (3.3)$$

$$- \frac{d I_B}{dx} = - Cm_1 \frac{d V_A}{dt} + C \frac{d V_B}{dt} \qquad (3.4)$$

where V_A and I_A are the voltage and current on the excitation line, respectively. V_B and I_B are the voltage and current on the pick-up line, respectively. L, C, M1, and Cm1 are the self inductance, the self capacitance, the mutual inductance, and the mutual capacitance per unit length, respectively.

Using approximation, gives the result,

$M_1 << L$, $Cm_1 << C$, $V_B << V_A$, and $I_B << I_A$

Applying Laplace Transform to equations (3.1)-(3.4), gives a relationship of the form,

$$- \frac{d V_A}{dx} = L\ S\ I_A \qquad (3.5)$$

$$- \frac{d V_B}{dx} = M_1\ S\ I_A + L\ S\ I_B \qquad (3.6)$$

$$- \frac{d\, I_A}{dx} = C\, S\, V_A \tag{3.7}$$

$$- \frac{d\, I_B}{dx} = -\, C_{m1}\, S\, V_A + C\, S\, V_B \tag{3.8}$$

Differentiating equations (3.5) - (3.6), provides the following results,

$$- \frac{d^2\, V_A}{dx^2} = L\, S\, \frac{d\, I_A}{dx} \tag{3.9}$$

$$- \frac{d^2\, V_B}{dx^2} = M_1\, S\, \frac{d\, I_A}{dx} + L\, S\, \frac{d\, I_B}{dx} \tag{3.10}$$

Substituting equations (3.9) - (3.10) with equations (3.7) - (3.8), provides the final relationship of these physical elements.

$$- \frac{d^2\, V_A}{dx^2} = -\, L\, C\, S^2\, V_A \tag{3.11}$$

or

$$\frac{d^2\, V_A}{dx^2} + L\, C\, S^2\, V_A = 0 \tag{3.12}$$

and

$$- \frac{d^2\, V_B}{dx^2} = -\, (\, M_1\, C\, S^2\, V_A\,) + L\, S\, (\, Cm1\, S\, V_A - C\, S\, V_B\,) \tag{3.13}$$

or

$$\frac{d^2 V_B}{dx^2} - L\ C\ S^2\ V_B = (\ M_1\ C - L\ Cm1\ )\ S^2\ V_A \qquad (3.14)$$

let the speed light in vacuum v equals to 1 / LC

Then, Equations (3.12) - (3.14) can be written as,

$$\frac{d^2 V_A}{dx^2} - \frac{S^2}{v^2} V_A = 0 \qquad (3.15)$$

$$\frac{d^2 V_B}{dx^2} - \frac{S^2}{v^2} V_B = [\ (\ M_1\ /\ L) - (Cm1\ /C)\ ]\ \frac{S^2}{v^2} V_A$$

(3.16)

Applying the boundary condition, at t = 0, x = 0, V_A = V Volt, reduces the solution to the form,

$$V_A = V \exp(\ - S\ x\ /\ v\ ) \qquad (3.17)$$

and

$$V_B = V \exp(\ - S\ x\ /\ v)\ [\ A1 + B1\ ]$$

$$+ V \exp(\ S\ x\ /\ v)\ [\ A2 + B2\ ] \qquad (3.18)$$

where A1 and A2 are constants, B1 and B2 are in form of exponential functions [reference # 13], V_A is a step function and V_B can be interpreted as a square pulse function, Figure (3.6), where V is the applied voltage.

The net crosstalk noise waveform is the result of the addition of primary crosstalk and transient crosstalk, Figure (3.7). Since the microstrip line is not a lossless line, losses occur when the signal is transmitted along the line. This situation can be applied with the crosstalk signal. The crosstalk signal distribution from the beginning to the end of the adjacent lines is presented in Figure (3.8). Due to the losses, the signal near the end of line, Figure (3.9), is small, but it still has the same properties as that at the beginning of the line. When signal is transmitted to the end of the line, the shape of the signal is predicted to have the same magnitude with opposite phase, Figure 3.10 (a). In general, the reflected signal may be compressed to be a differential signal, Figure 3.10 (b). Compared to a normal signal, the differential signal possesses larger magnitude but smaller bandwidth.

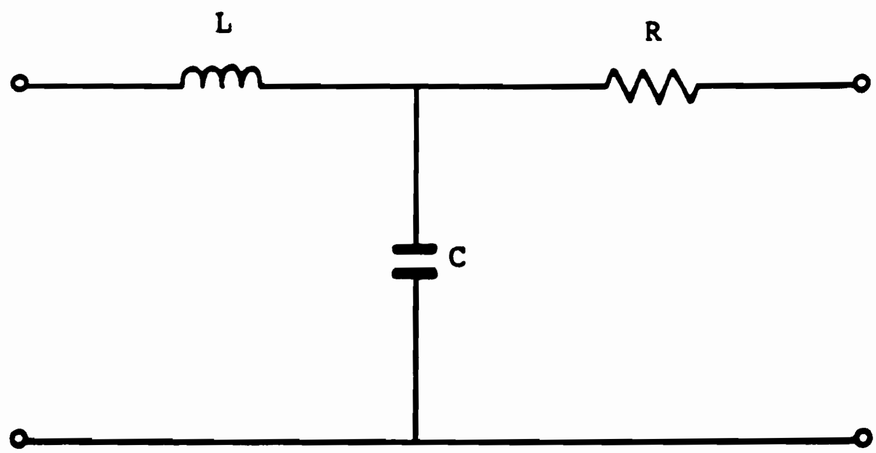

Figure 3.1 Simple Model of A Transmission Line

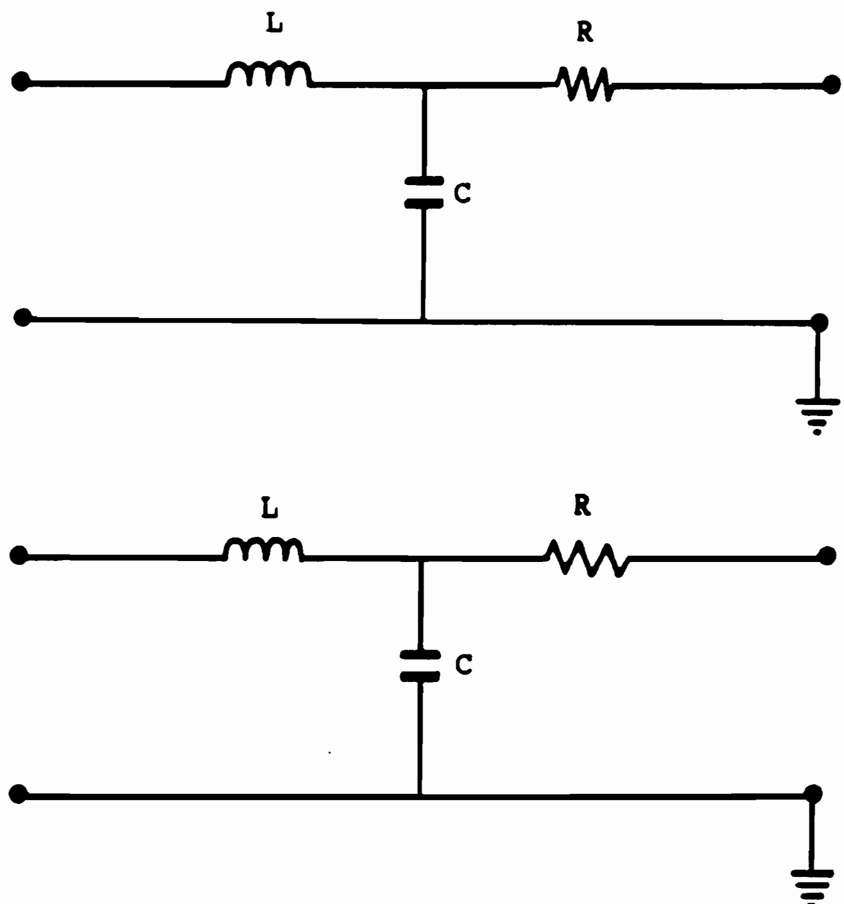

Figure 3.2 Simple Model of Two Parallel Transmission Lines

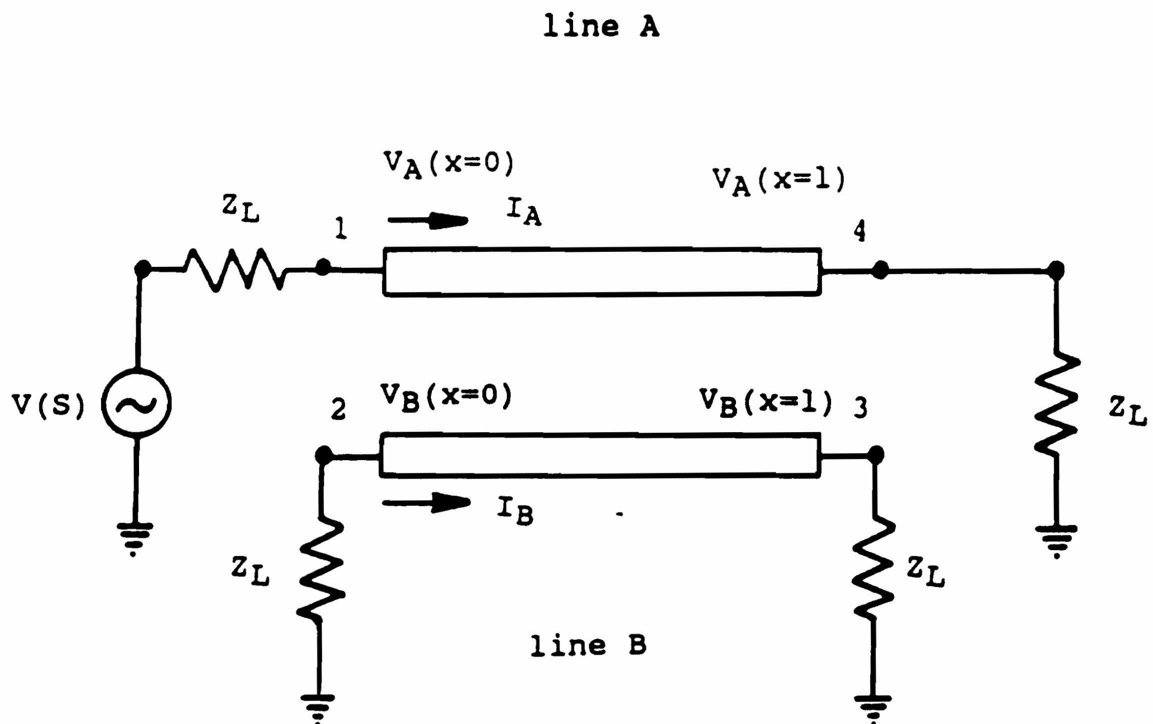

Figure 3.3 Circuit Configuration for Crosstalk Study

(Z_L = 50 ohms)

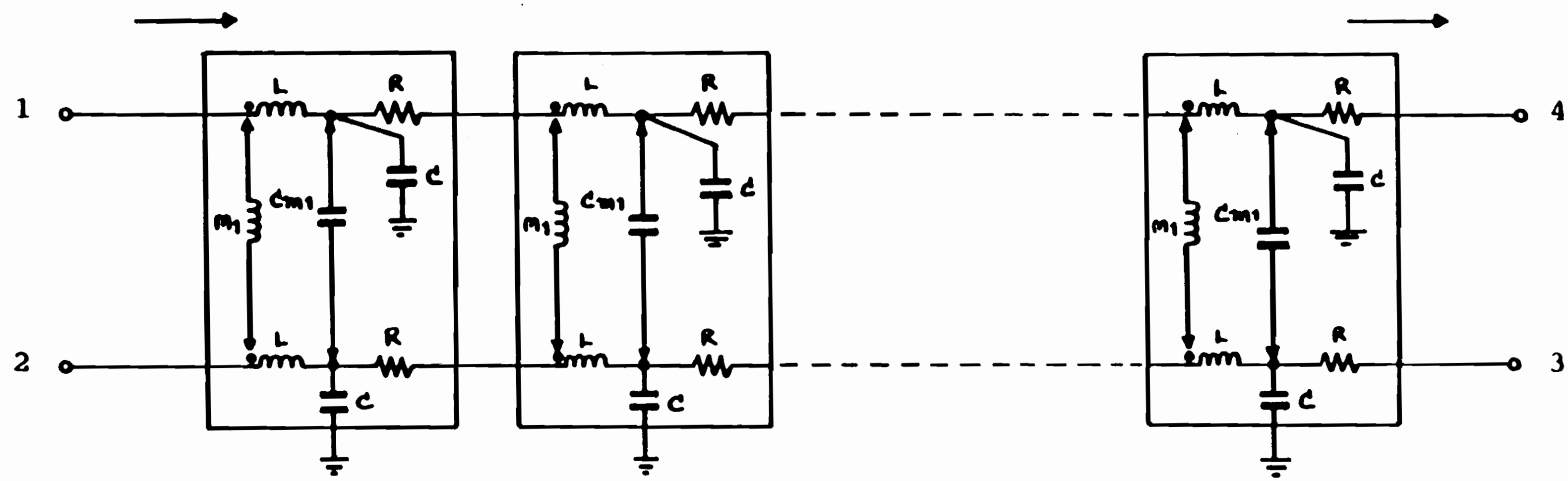

Figure 3.4 Primary Crosstalk Model

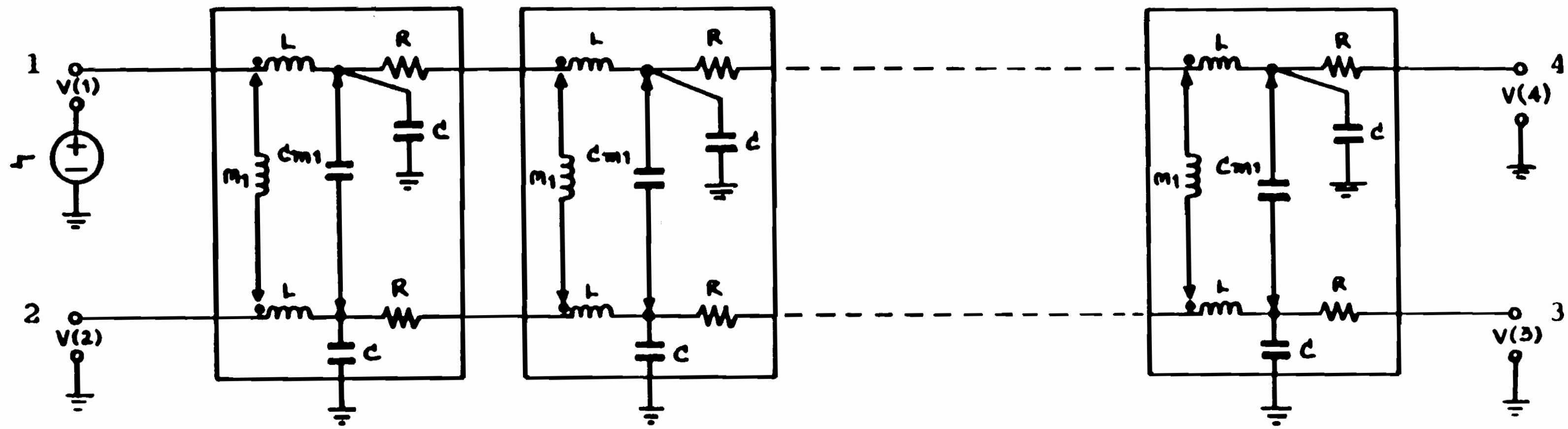

Figure 3.5 Transient Model

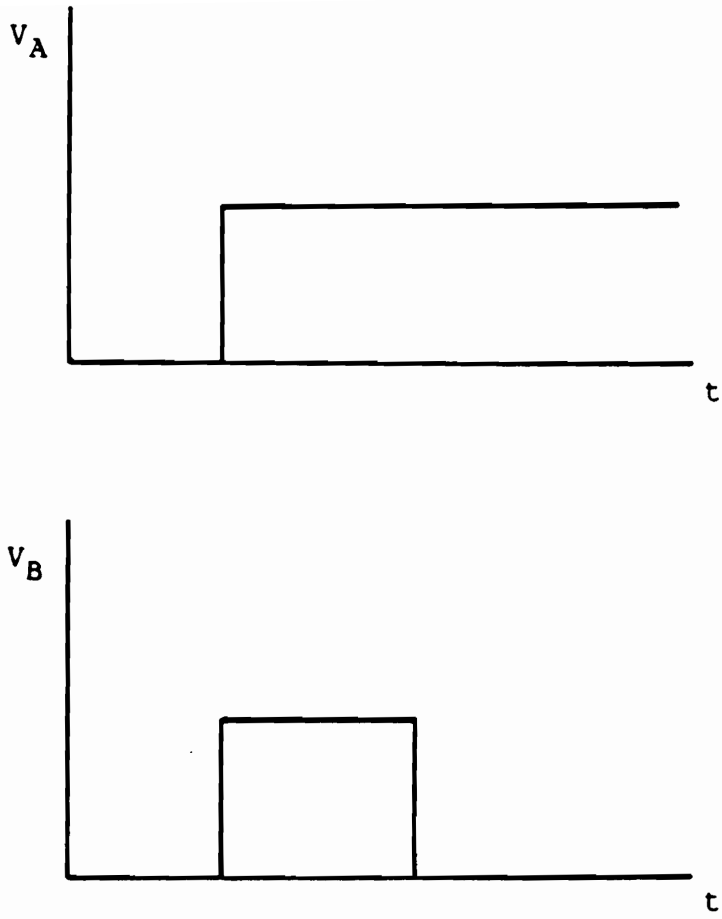

Figure 3.6 Waveform at The Main Line (V_A) and Waveform at The Pick Up Line (V_B) in Section A Analysis

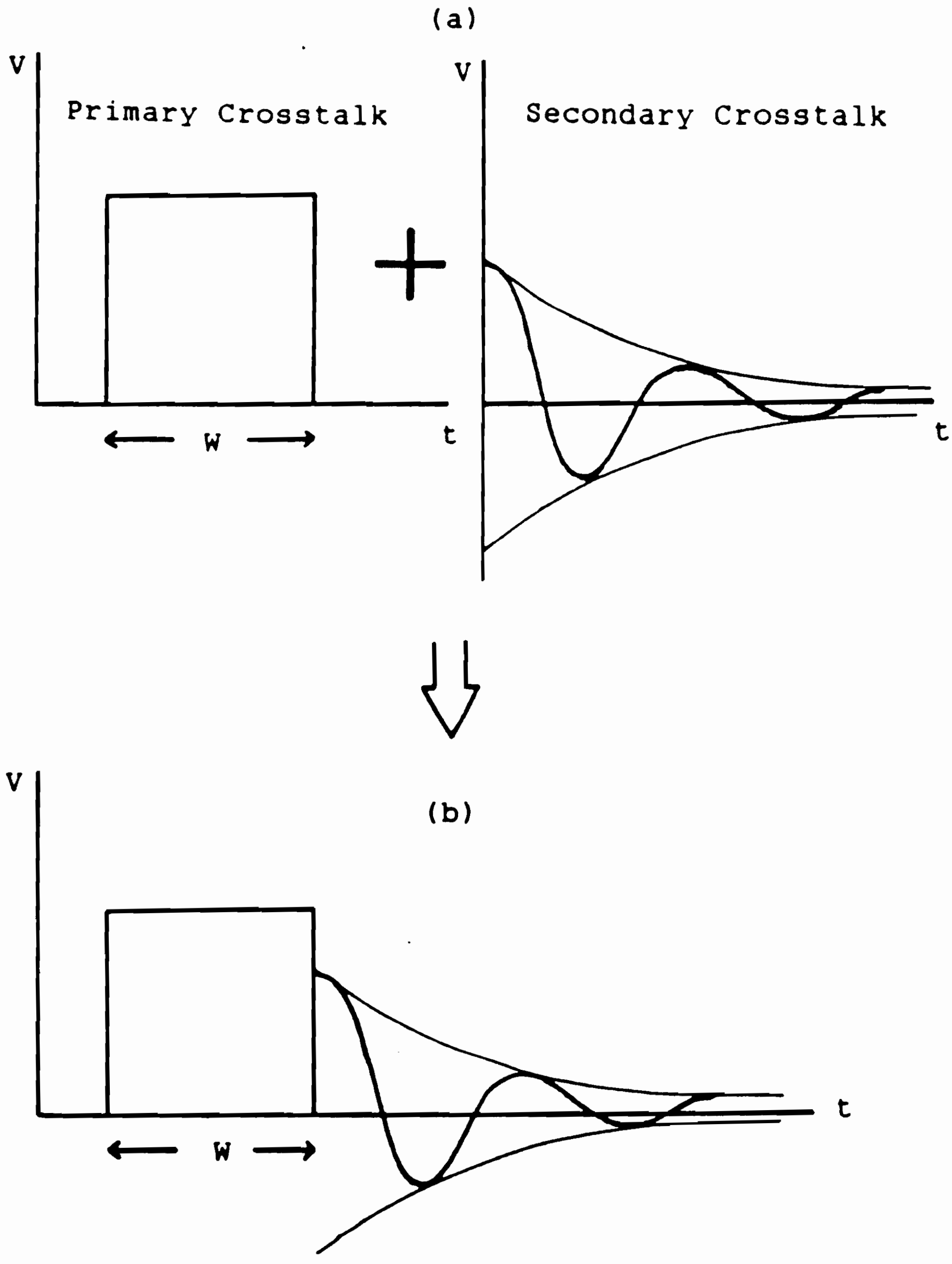

Figure 3.7 Crosstalk Noise Waveform at The Beginning of Pick Up Line

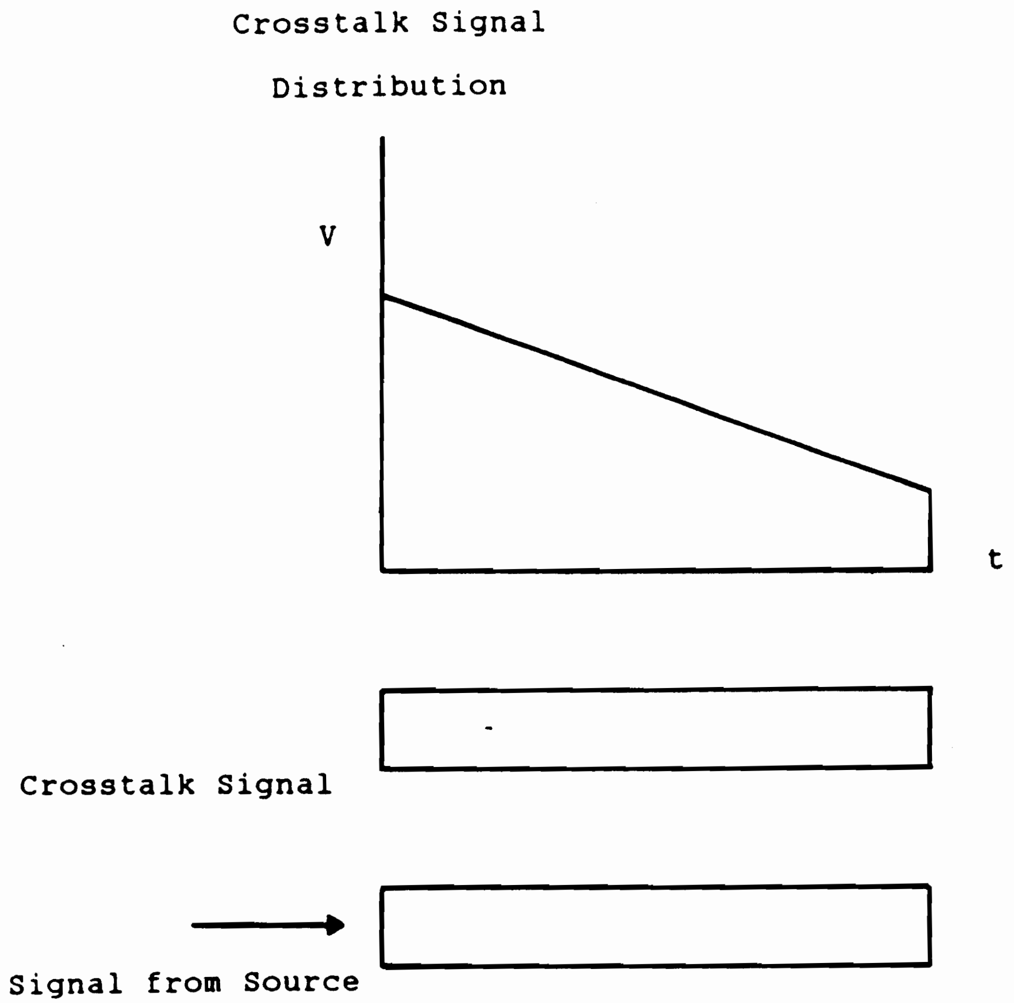

Figure 3.8 Crosstalk Noise Distribution from The beginning to The End of Pick Up Line

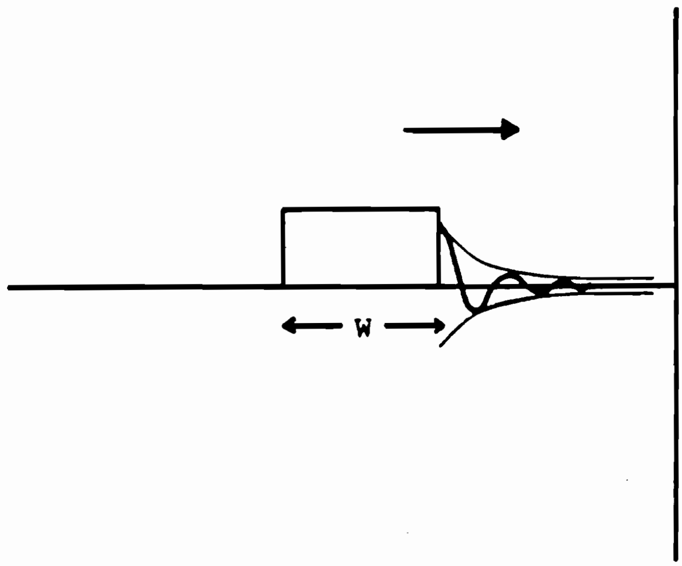

Figure 3.9 Crosstalk Noise Waveform near The End of Pick Up Line

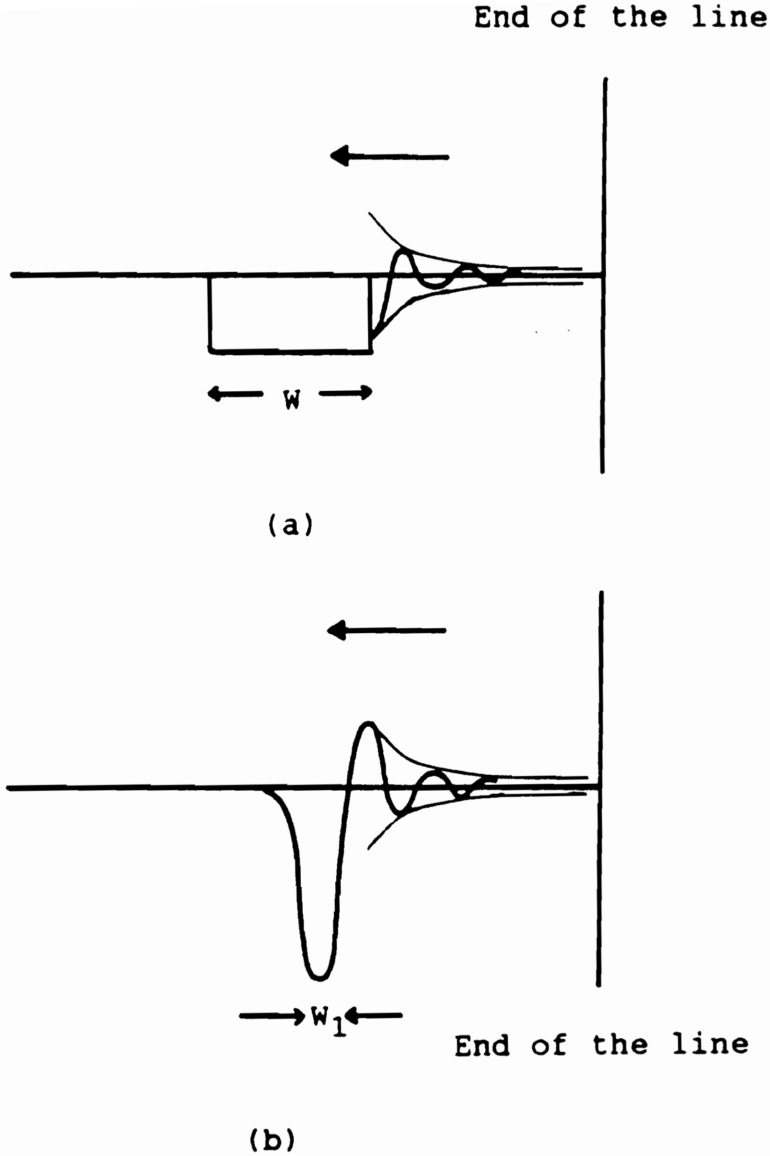

Figure 3.10 Crosstalk Noise Waveforms at The End of Pick Up Line; a) Same Shape But Opposite Phase and b) Different Shape from (a)

3.2 CURRENT AND VOLTAGE CHARACTERISTICS

In this model, Figure (3.4), M1 and Cm1 give the primary crosstalk. The total signals on adjacent lines are presented in Figure (3.7).

Applying Laplace Transform to equations (3.1) - (3.4), gives the relationship in the form,

$$-\frac{d\,V_A}{dx} = L\,S\,I_A + M_1\,S\,I_B \tag{3.19}$$

$$-\frac{d\,V_B}{dx} = M_1\,S\,I_A + L\,S\,I_B \tag{3.20}$$

$$-\frac{d\,I_A}{dx} = C\,S\,V_A - C_{m1}\,S\,V_B \tag{3.21}$$

$$-\frac{d\,I_B}{dx} = -C_{m1}\,S\,V_A + C\,S\,V_B \tag{3.22}$$

Differentiating equations (3.19) and (3.20), gives the following results,

$$-\frac{d^2\,V_A}{dx^2} = L\,S\,\frac{d\,I_A}{dx} + M_1\,S\,\frac{d\,I_B}{dx} \tag{3.23}$$

$$-\frac{d^2\,V_B}{dx^2} = M_1\,S\,\frac{d\,I_A}{dx} + L\,S\,\frac{d\,I_B}{dx} \tag{3.24}$$

Substituting equations (3.23) and (3.24) in equations (3.21) and (3.22), gives the final relationship of these physical elements,

$$-\frac{d^2 V_A}{dx^2} = L\, S\, [-\, C\, S\, V_A + C_{m1}\, S\, V_B\,] + M_1\, s\, [\, C_{m1}\, S\, V_A - C\, S\, V_B\,]$$

$$= -\, L\, C\, S^2\, V_A + L\, C_{m1}\, S^2\, V_B + M_1\, C_{m1}\, S^2\, V_A - M_1\, C\, S^2\, V_B$$

$$= [\, -\, L\, C + M_1\, C_{m1}\,]\, S^2\, V_A + [\, -\, M_1\, C + L\, C_{m1}\,]\, s^2\, V_B$$

or

$$\frac{d^2 V_A}{dx^2} = [\, L\, C - M_1\, C_{m1}\,]\, S^2\, V_A + [\, M_1\, C - L\, C_{m1}\,]\, S^2\, V_B \qquad (3.25)$$

and

$$-\frac{d^2 V_B}{dx^2} = M_1\, S\, [\, -\, C\, S\, V_A + C_{m1}\, S\, V_B\,] + L\, S\, [\, C_{m1}\, S\, V_A - C\, S\, V_B\,]$$

$$= -\, M_1\, C\, s^2\, V_A + M_1\, C_{m1}\, S^2\, V_B + L\, C_{m1}\, S^2\, V_A - L\, C\, S^2\, V_B$$

$$= [\, M_1\, C + L\, C_{m1}\,]\, s^2\, v_A$$

$$+ [\, - L\, C + M_1\, C_{m1}\,]\, s^2\, v_B$$

or

$$\frac{d^2\, v_B}{dx^2} = [\, M_1\, C - L\, C_{m1}\,]\, s^2\, v_A$$

$$+ [\, L\, C - M_1\, C_{m1}\,]\, s^2\, v_B \qquad (3.26)$$

Applying the even and odd mode theory, gives the relationship as,

$$V_{even} = V_A + V_B$$

$$I_{even} = I_A + I_B$$

$$V_{odd} = V_A - V_B$$

$$I_{odd} = I_A - I_B$$

Adding equation (3.25) to equation (3.26), gives a new equation as,

$$\frac{d^2\, v_A}{dx^2} + \frac{d^2\, v_B}{dx^2} = [\, L\, C - M_1\, C_{m1} + L\, C_{m1}\,]\, s^2\, v_A$$

$$+ [\, M_1\, C - L\, C_{m1} + L\, C - M_1\, C_{m1}\,]\, s^2\, v_B$$

$$= [\, (\, L + M_1\,)\, (\, C - C_{m1}\,)\,]\, s^2\, v_A$$

$$+ [\, (\, L + M_1\,)\, (\, C - C_{m1}\,)\,]\, s^2\, v_B$$

$$= [\, L + M_1\,]\, [\, C - C_{m1}\,]\, [\, v_A + v_B\,]\, s^2 \qquad (3.27)$$

or

$$\frac{d^2 V_{even}}{dx^2} = [L + M_1] [C - C_{m1}] s^2 V_{even} \qquad (3.28)$$

Subtracting equation (3.26) from equation (3.25), gives a new equation as,

$$\frac{d^2 V_A}{dx^2} - \frac{d^2 V_B}{dx^2} = [L C - M_1 C_{m1} - M_1 C + L C_{m1}] S^2 V_A$$

$$+ [M_1 C - L C_{m1} - L C + M_1 C_{m1}] S^2 V_B$$

$$= [(L + M_1) (C + C_{m1})] S^2 V_A$$

$$- [(L - M_1) (C + C_{m1})] S^2 V_B$$

$$= [L - M_1] [C + C_{m1}] [V_A - V_B] S^2 \qquad (3.29)$$

or

$$\frac{d^2 V_{odd}}{dx^2} = [L - M_1] [C + C_{m1}] S^2 V_{odd} \qquad (3.30)$$

Rewriting new coefficients for convenience, gives the equations in the form,

$$[(L + M_1) (C - C_{m1})]^{\frac{1}{2}} = K_{even}$$

$$[(L - M_1) (C + C_{m1})]^{\frac{1}{2}} = K_{odd}$$

Equation (3.28) and equation (3.30) can be given by,

$$\frac{d^2 V_{even}}{dx^2} = K^2_{even} S^2 V_{even} \tag{3.31}$$

$$\frac{d^2 V_{odd}}{dx^2} = K^2_{odd} S^2 V_{odd} \tag{3.32}$$

The voltage solution is of the form,

$$V_{even} = E_1 exp(S K_{even} x) + E_2 exp(-S K_{even} x) \tag{3.33}$$

$$V_{odd} = E_3 exp(S K_{odd} x) + E_4 exp(-S K_{odd} x) \tag{3.34}$$

where E_1, E_2, E_3, and E_4 are the complementary solutions of second order differential equations.

Differentiating equations (3.33) - (3.34), gives the equations of the form,

$$\frac{d V_{even}}{dx} = E_1 exp(S K_{even} x) S K_{even}$$

$$- E2 exp(- S K_{even} x) S K_{even} \tag{3.35}$$

$$\frac{d V_{odd}}{dx} = E1 exp(S K_{odd} x) S K_{odd}$$

$$- E2 exp(- S K_{odd} x) S K_{odd} \tag{3.36}$$

Adding equation (3.19) to equation (3.20), gives a relationship of voltage in even mode,

$$- \frac{d V_A}{dx} - \frac{d V_B}{dx} = (L + M_1) S (I_A + I_B)$$

or

$$- \frac{d\, V_{even}}{dx} = (L + M_1)\ S\ I_{even} \qquad (3.37)$$

Subtracting equation (3.19) and equation (3.20), gives a relationship of voltage in odd mode,

$$- \frac{d\, V_A}{dx} + \frac{d\, V_B}{dx} = (L - M)\ S\ (I_A - I_B)$$

$$- \frac{d\, V_{odd}}{dx} = (L - M)\ S\ I_{odd} \qquad (3.38)$$

Substituting $\frac{dV_{even}}{dx}$, $\frac{dV_{odd}}{dx}$ of equations (3.35) - (3.36) in equations (3.37) - (3.38), gives the relationship,

$$-[\ E_1 exp(S\ Keven\ x)\ S\ Keven - E_2 exp(-S\ Keven\ x)\ S\ Keven\ ] = (L + M_1)\ S\ I_{even}$$

$$-[\ E_1 exp(S\ Kodd\ x)\ S\ Kodd - E_2 exp(-S\ Kodd\ x)\ S\ Kodd\ ] = (L - M_1)\ S\ I_{odd}$$

or

$$I_{even} = \frac{K_{even}}{L + M_1} [(-E_1 exp(S\ K_{even}\ x) + E2exp(-S\ K_{even}\ x)] \qquad (3.39)$$

$$I_{odd} = \frac{K_{odd}}{L - M_1} [-E_3 exp(S\ K_{odd}\ x) + E_4 exp(-S\ K_{odd}\ x)] \qquad (3.40)$$

$$V_A = (V_{even} + V_{odd}) / 2 \tag{3.41}$$

$$V_B = (V_{even} - V_{odd}) / 2 \tag{3.42}$$

$$I_A = (I_{even} + I_{odd}) / 2 \tag{3.43}$$

$$I_B = (I_{even} - I_{odd}) / 2 \tag{3.44}$$

where V_A and I_A are the voltage and the current on the excitation line, respectively. V_B and I_B are the voltage and the current on the pick-up line, respectively.

Hence, V_A, V_B, I_A, and I_B can be calculated at any points of line.

3.3 Characteristic Impedance

The characteristic impedance; Z_0 is of the form,

(a) even mode, $Z_{0e} = [(L + M) / C_e]^{\frac{1}{2}}$

$$= [(L + M_1) / C]^{\frac{1}{2}} \tag{3.45}$$

(b) odd mode, $Z_{0o} = [(L - M) / C_o]^{\frac{1}{2}}$

$$= [(L - M_1) / C_o]^{\frac{1}{2}}$$

$$= [(L - M_1) / (C + 2\,Cm_1)]^{\frac{1}{2}} \tag{3.46}$$

3.4 Effective Dielectric Constant

The wave velocity; V_0 takes the form,

(a) even mode, $V_{0e} = [1 / C_e (L + M)]^{\frac{1}{2}}$

$$= [1 / C_e (L + M_1)]^{\frac{1}{2}}$$

$$= [1 / C (L + M_1)]^{\frac{1}{2}}$$

(b) odd mode, $V_{0o} = [1 / C_o (L - M)]^{\frac{1}{2}}$

$$= [1 / C_o (L - M_1)]^{\frac{1}{2}}$$

$$= [1/ ((C + 2Cm_1) (L + M_1)]^{\frac{1}{2}}$$

The effective dielectric constant; ϵeff directly effects the impedance of the circuit which is used in circuit design to calculate parameters and is of the form,

(a) even mode,

$$\epsilon eff = (\text{light speed in air} / V_{0e})^2$$
$$= (\text{light speed in air})^2 \times (C (L + M_1)) \qquad (3.47)$$

(b) odd mode,

$$\epsilon eff = (\text{light speed in air} / V_{0o})^2$$
$$= (\text{light speed in air})^2 ((C+2Cm_1) \times (L+M_1)) \qquad (3.48)$$

3.5 Maximum Crosstalk

Based on the measurements performed by Catt (1967), his maximum fast crosstalk can be evaluated as a percentage and have the same formula as coupling in general applications. The percentage of maximum crosstalk is of the form,

$$\text{\% of Maximum Crosstalk} = \frac{Z_{0e} - Z_{0o}}{Z_{0e} + Z_{0o}} \times \text{signal} \times 100\ \% \qquad (3.49)$$

where

$$\text{Coupling Factor (C)} = \frac{Z_{0e} - Z_{0o}}{Z_{0e} + Z_{0o}}$$
$$= 20 \log_{10} \frac{Z_{0e} - Z_{0o}}{Z_{0e} + Z_{0o}}\ \text{dB} \qquad (3.50)$$

3.6 Computer Simulation

The use of computer analysis and optimization programs become very important in design and characterization of circuits of this nature. The capability of some softwares is very broad and the specific aim of the circuit designer can be met by solutions already developed. In this work, the operating frequency is chosen to be .8 GHz, the structure has the line length about a quarter wavelength, 1400 mils. The line spacings are taken equal to 10 mils, 50 mils, 200 mils, and 1500 mils. The computer simulation and computations of the characteristics of the modified model are presented in Tables (3.1) - (3.4). Maxwell Software is used to evaluate the inductances and capacitances versus spacing of the structures as shown in Table (3.1) and Table (3.2), respectively. Table (3.3) and Table (3.4) summarize the computed results of characteristic impedance, wave velocity, effective dielectric constant, and % of maximum crosstalk with various line spacings. Crosstalk noise can also change the circuit parameters, such as characteristic impedance, wave velocity, and effective dielectric constant. The percentage of maximum crosstalk can be used to determine the level of crosstalk noise. As the crosstalk noise increases, the spacing decreases, as demonstrated in Tables (3.3)- (3.4). Also, the crosstalk noise causes an increase of the characteristic impedance and the effective dielectric constant in the case of even mode, but causes a decrease of these quantities in the case of odd mode. When the separation of the line is large enough, the percentage of maximum crosstalk approaches zero. This indicates that the crosstalk noise does not effect the circuit and the circuit parameters in even mode and odd mode are the same. Spice Software is used to simulate the crosstalk noise waveform on the adjacent lines of the circuits in time domain measurements. TOUCHSTONE Software is used to achieve this task in frequency domain measurements. The simulated results are illustrated in Figures (3.11) - (3.14) for frequency domain measurements and in Figures (3.15) - (3.17) for time domain measurements, respectively. Figures (3.11) - (3.14) give the maximum crosstalk at .8 GHz which meets the purpose of the design with a line length equals 1400 mils (equivalent to a quarter wavelength). S21 and S31 represent the near-end and far-end crosstalk components in frequency domain forms , respectively. Figures (3.15) - (3.17) provide a good agreement of the analysis results in Section (3.1). Figure (3.18) summarizes the simulated S21 and S31 at .8 GHz with various spacings.

3.7 Summary

A physically based model of crosstalk noise in the case of parallel transmission lines has been introduced. The analysis of the structures characteristics is carried out by assuming the propagation to be TEM mode. Characterization of crosstalk noise along adjacent lines, current - voltage characteristics, characteristic impedance, effective dielectric impedance, and maximum crosstalk are performed analytically. The computer simulation of these parameters and computations of various electrical parameters in frequency domain and time domain are also performed. In the next chapter, an experimental realization of the circuits is performed. The frequency domain measurements and time domain measurements are used to acquire the results of these experimental circuits in order to support the theory and simulated results.

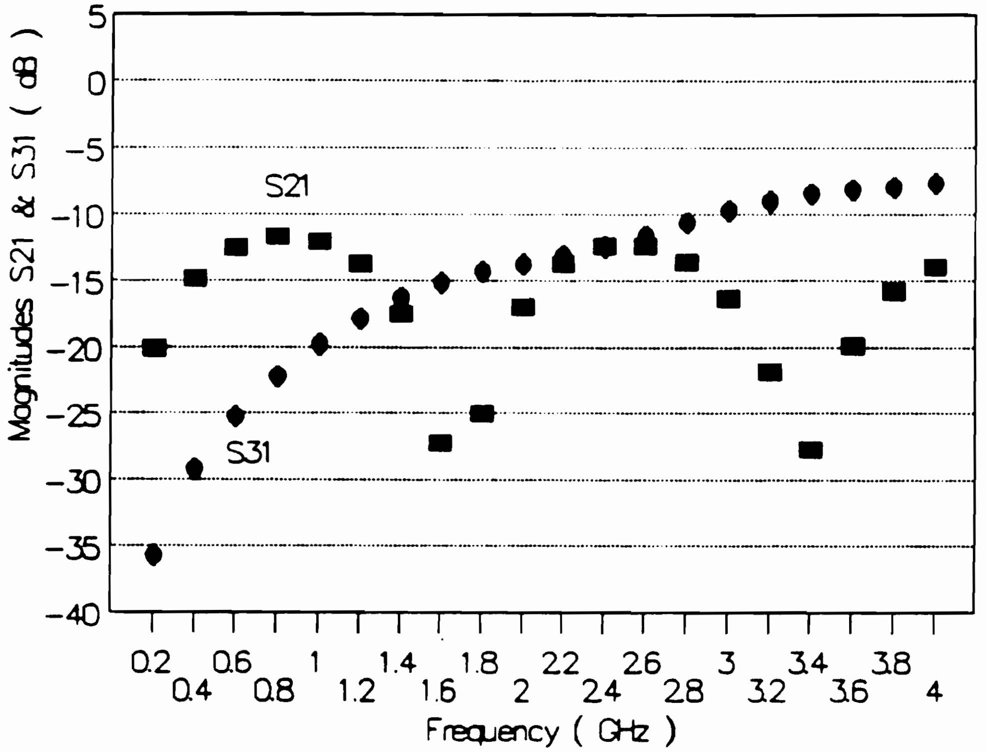

Figure 3.11 Simulated S21 and S31 of The Structure, (Spacing = 10 mils)

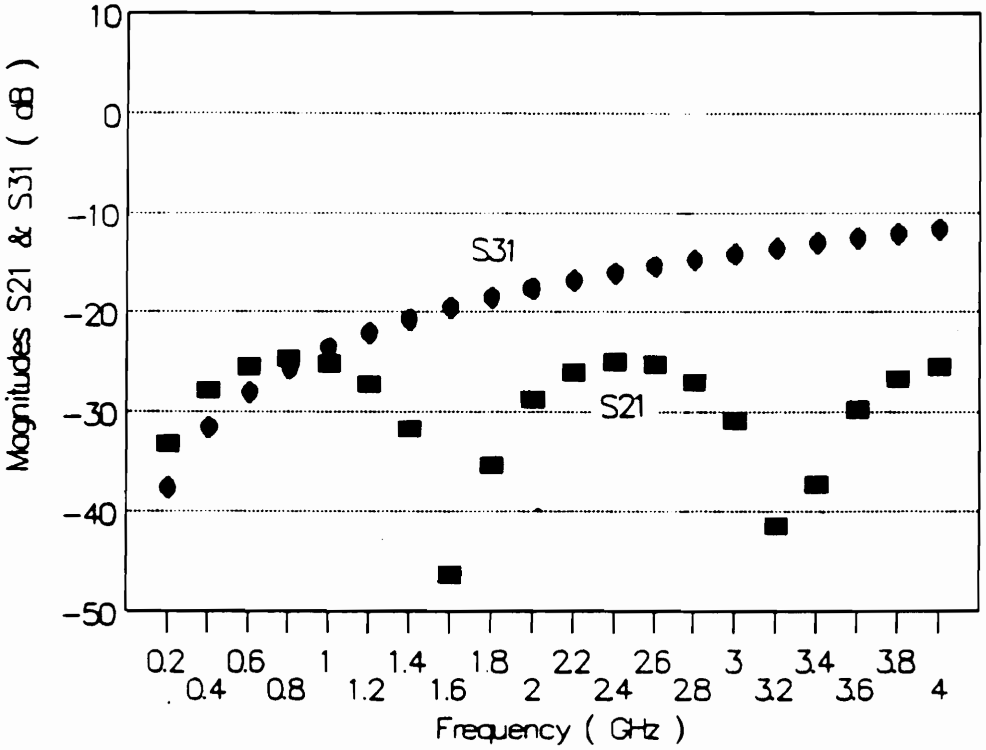

Figure 3.12 Simulated S21 and S31 of The Structure, (Spacing = 50 mils)

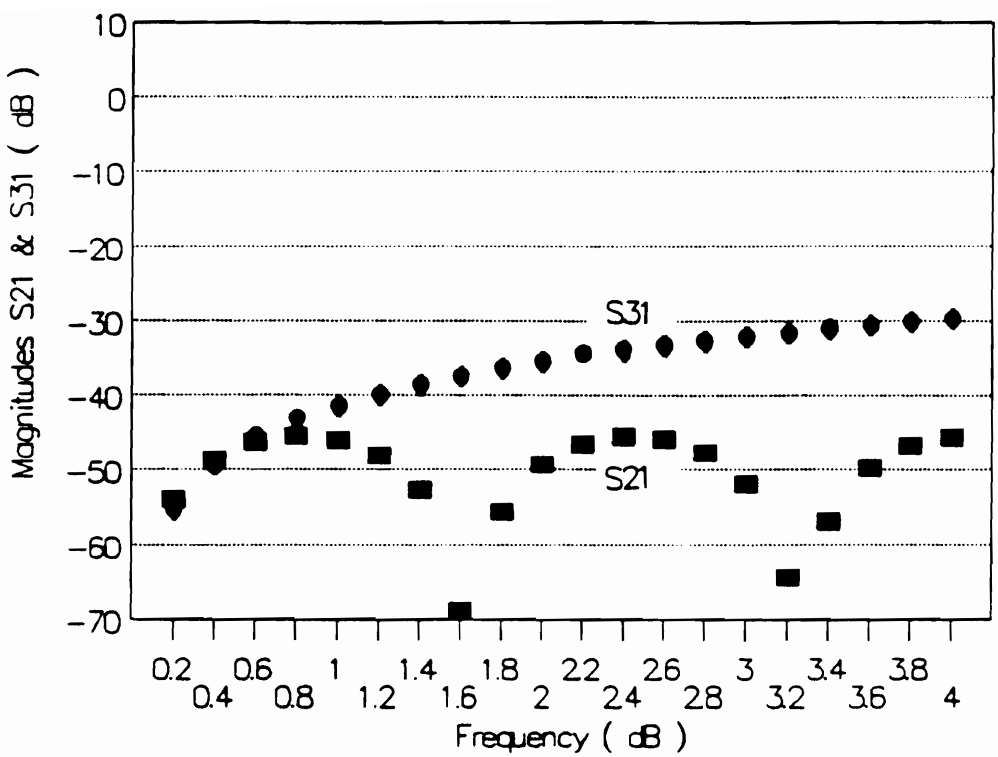

Figure 3.13 Simulated S21 and S31 of The Structure, (Spacing = 200 mils)

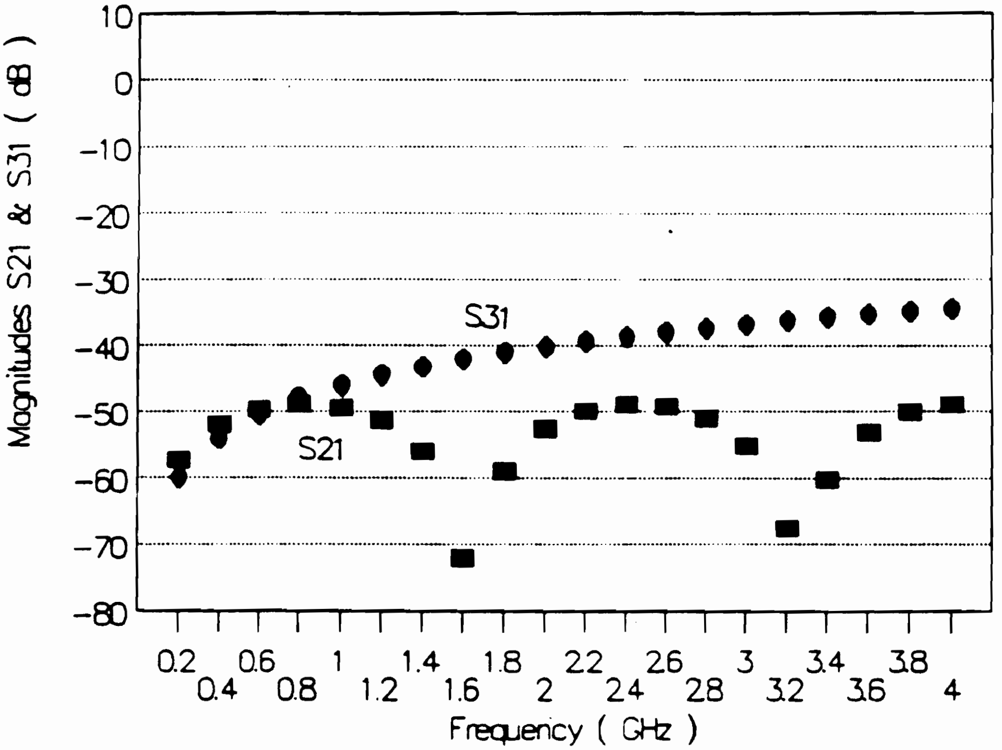

Figure 3.14 Simulated S21 and S31 of The Structure, (Spacing = 1500 mils)

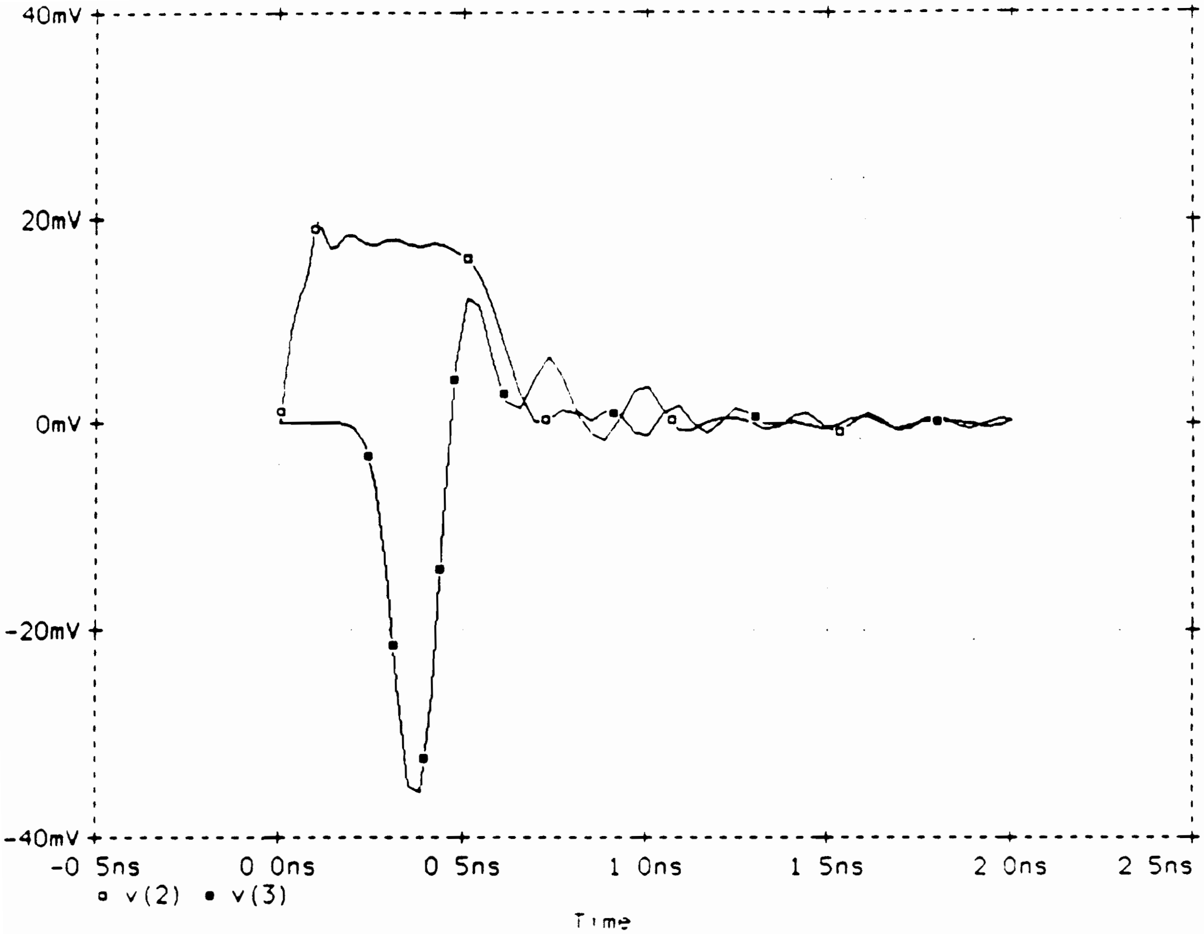

Figure 3.15 Simulated Crosstalk Signals at Port 2 (V2) and Port 3 (V3) versus Time of The Structure, (Spacing = 10 mils)

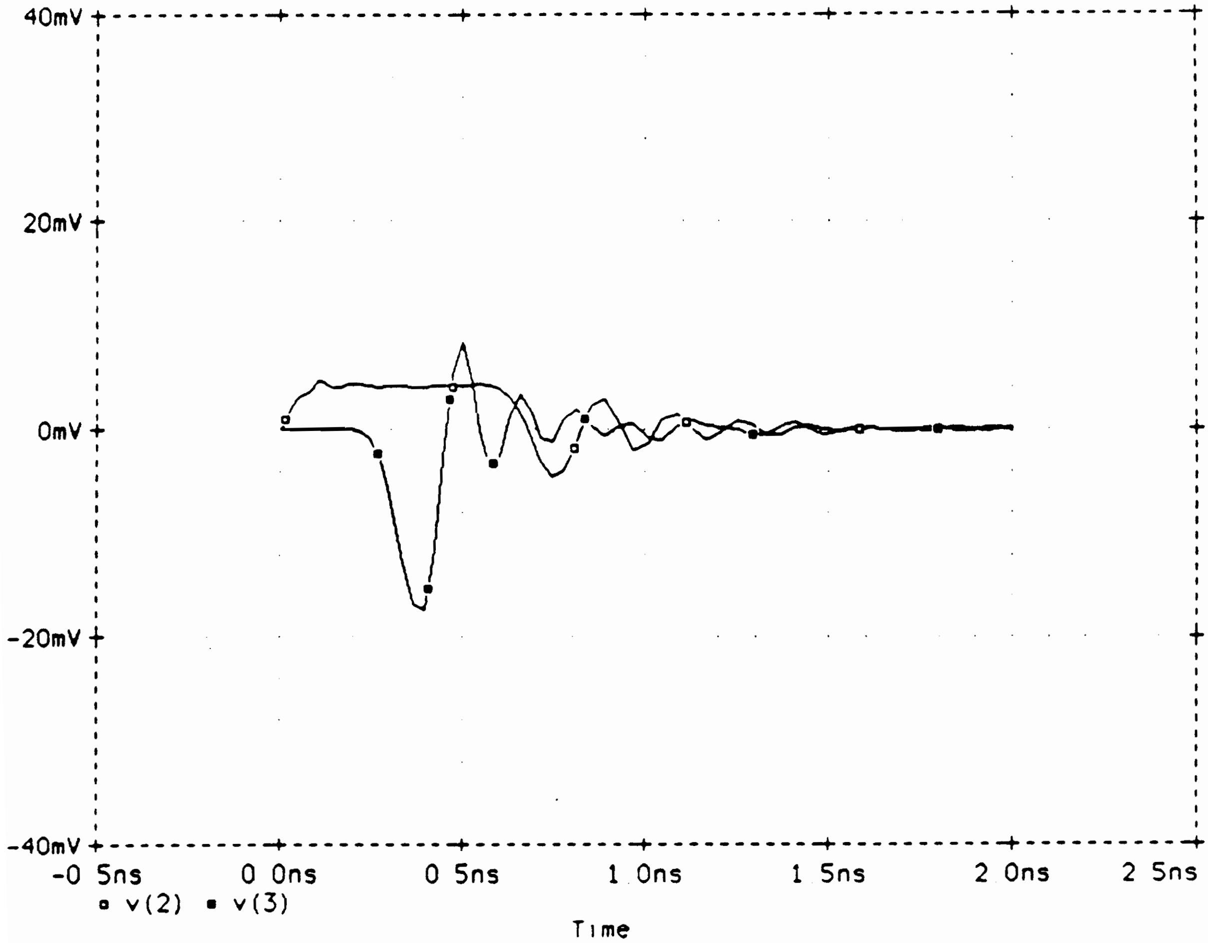

Figure 3.16 Simulated Crosstalk Signals at Port 2 (V2) and Port 3 (V3) versus Time of The Structure, (Spacing = 50 mils)

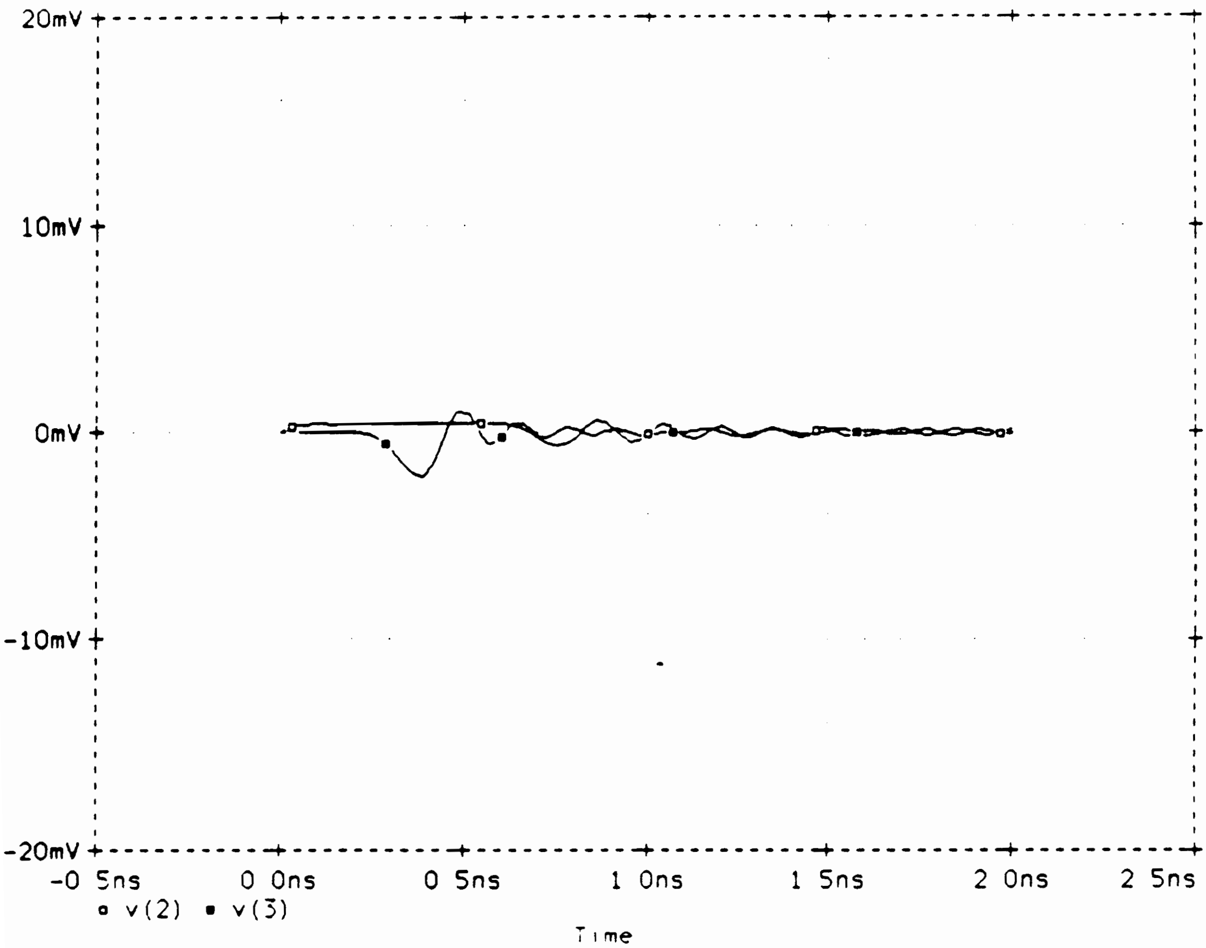

Figure 3.17 Simulated Crosstalk Signals at Port 2 (V2) and Port 3 (V3) versus Time of The Structure, (Spacing = 200 mils)

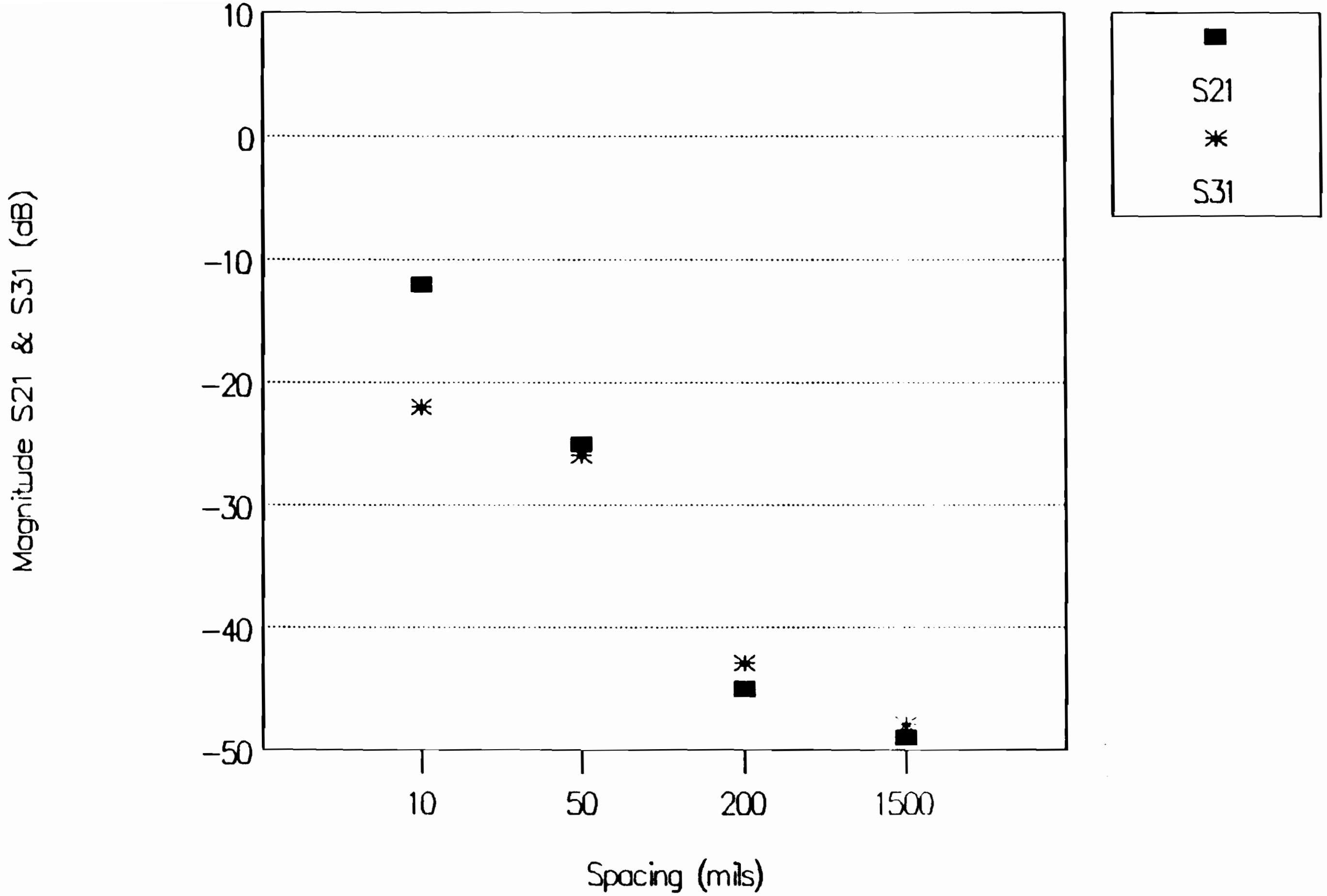

Figure 3.18 Summary of Simulated S21 and S31 at .8 GHz

Table 3.1 Simulated Results of Inductance and Mutual Inductance versus Spacing of the Structure (Using Maxwell Software)

Spacing S (Mils)	Inductance L (Henry)	Mutual Inductance M1 (Henry)
10	3.72×10^{-7}	1.50×10^{-7}
50	3.73×10^{-7}	3.77×10^{-8}
200	3.78×10^{-7}	5.81×10^{-9}
1500	3.80×10^{-7}	2.62×10^{-10}

Table 3.2 Simulated Results of Capacitance and Mutual Capacitance versus Spacing of the Structure (Using Maxwell Software)

Spacing S (Mils)	Capacitance C (Farad)	Mutual Capacitance Cm1 (Farad)
10	1.78×10^{-10}	5.37×10^{-11}
50	1.82×10^{-10}	6.71×10^{-12}
200	1.84×10^{-10}	2.25×10^{-14}
1500	1.85×10^{-10}	3.23×10^{-15}

Table 3.3 Computed Results of Characteristic Impedance, Wave Velocity, Effective Dielectric Constant, % of Maximum Crosstalk, and Coupling Factor versus Spacing of The Structure in Even Mode

	Case of Even Mode			
Spacing S (mils)	10	50	200	1500
Characteristic Impedance Z_0 (Ω)	54.15	47.50	45.67	45.34
Wave Velocity v (x 10^8 m/s)	1.04	1.16	1.19	1.19
Effective Dielectric Constant ϵ_{eff}	8.36	6.73	6.35	6.33
% of Maximum Crosstalk	32.01	6.83	0.78	0.03
Coupling Factor C (dB)	9.89	23.30	42.21	69.03

Table 3.4 Computed Results of Characteristic Impedance, Wave Velocity, Effective Dielectric Constant, % of Maximum Crosstalk, and Coupling Factor versus Spacing of The Structure in Odd Mode

Case of Odd Mode				
Spacing S (mils)	10	50	200	1500
Characteristic Impedance Z_0 (Ω)	27.89	41.42	44.97	45.30
Wave Velocity v (x 10^8 m/s)	1.26	1.24	1.21	1.19
Effective Dielectric Constant ϵ_{eff}	5.70	5.90	6.16	6.32
% of Maximum Crosstalk	32.01	6.83	0.78	0.03
Coupling Factor C (dB)	9.89	23.30	42.21	69.03

CHAPTER 4

EXPERIMENTAL REALIZATION AND RESULTS

4.1 Introduction

The actual realization of the structures is performed using conventional thick film printing technique on alumina substrates, as well as selective etching of copper-cladded teflon-ceramic duriod composite substrates from Rogers Corporation. Measurements are conducted using frequency domain measurement techniques and time domain measurement techniques.

4.2 Fabrication Procedure

In this section, the crosstalk noise is observed at a specific frequency and the wavelength of the line λ is related to frequency as shown below,

$$\text{wavelength } \lambda = 300 \text{ mm} / (f \, \epsilon_{eff})$$

where f is the frequency and ϵ_{eff} is the effective dielectric constant.

To have a good graphical presentation, the line must be long enough to satisfy the condition of operating frequency. From computer simulation results, the maximum crosstalk occurs at a quarter wavelength of microstrip line at the operating frequency. In this work, the operating frequency is selected to be .8 GHz, since the structure has the line length about a quarter wavelength, (1400 mils). The circuits are realized experimentally using conventional thick film printing technique on alumina substrates in this chapter. On the other hand, those structures realized using selective etching of copper cladded teflon-ceramic duriod composite substrates are used to verify the model, Chapter 5. In this chapter, the thick film process is discussed and a typical thick film hybrid process flow chart is presented in Figure (4.1). It includes layout and artwork, preparation of screen, screen printing, drying and firing, and packaging.

a) Layout and Artwork

Basically, there are three steps to produce good microwave artwork: initial drawing, layout, and photo process. The initial drawing is made on special graph paper. The circuit elements are placed on the center of the paper. With the drawing completed, the reference in the lower left corner (0,0) is established. Everything to the right will be the X dimension and everything at the top will be the Y dimension. This will give every point on the drawing an X and a Y coordinate. In this work, the circuit drawing is made by hand. The MicroCad Software (CAD) is used to generate the artwork. The HP plotter is interfaced with the PC to produce the master layout of the circuit drawing using Rubylith. The rubylith, a photographic masking film, consists of a mylar sheet of ruby color that can be easily peeled once scribed, with a plastic backing. A magnification scale 10:1 is used in this case. This results in very high accuracy and resolution. Then the photo process is introduced, and the artwork is photoreduced by placing it on the camera copy board and photographing it to reduce it to its final size. To make a positive, Kodak Kodalith Ortho Films (type 3) are placed in the camera with the emulsion side toward the lens and exposed with the board lights. The film is then developed. After developing, the film is placed in the stop bath for 30 seconds and in the fixer bath for a few minutes. The film is rinsed and then dried. A Pattern of the experimental circuits is shown in Figure (4.2)

b) Screen Preparation

The screen is the most important part of the screen printing process. It is responsible for the design of the printed pattern and is also the major part for controlling the thickness of the film on the substrates. The screen used in this work is of stainless steel mesh type with a 325 mesh count, which is tightly stretched woven mesh fixed to a rigid aluminium metal frame. First, the mesh is cleaned in order to remove dirt, grease, or residue which may result in poor adhesion of the stencil. Then, the screen stencil is formed by exposing a light-sensitive emulsion with the film to ultraviolet light using the hybrid emulsion type.

c) Screen Printing

The screen printer is used to hold the screen and the substrate to be printed in proper relationship while the paste is forced through the screen onto the substrate using a squeegee pressure action during the travel. Figure (4.3) shows a screen printing process schematic, and Figure (4.4) presents a cross section of the screen during and after printing. The paste used in this section is Silver (Ag) metallization, Dupont 6160 conductor paste. The paste is applied to the upper surface of the screen and a flexible squeegee is transversed across the pattern area. The portion of the squeegee presses the screen into contact with the substrate surface and forces paste through the open meshes of the screen.

d) Drying and Firing

After the paste has been deposited onto the substrate, the film is allowed to settle to eleminate the mesh impression. The drying process removes the organic materials in the paste. This process is carried out in an oven for 15 minutes at 150 °C. The subsequent firing process is used to remove the remaining organic binders, to develop the electrical properties of the paste compositions, and to adhere the circuit elements to the substrates. The dried substrates have been fired in a multi-zone moving belt furnace in which the belt speed and zone temperatures can be controlled to obtain the proper firing profile for these films.

e) Packaging

In digital systems and microwave applications, the package is an integral part of the overall circuit design and can mean the difference between a circuit that works and one that does not work satisfactorily. For example, the microstrip has a ground plane supporting the dielectric with air on the top of the circuit while the stripline has a ground plane both above and below the circuit. Since this work has been demonstrated in experiments to support the theory, the substrates after the firing process are ready to be used. The connectors are connected at the end of each microstrip line.

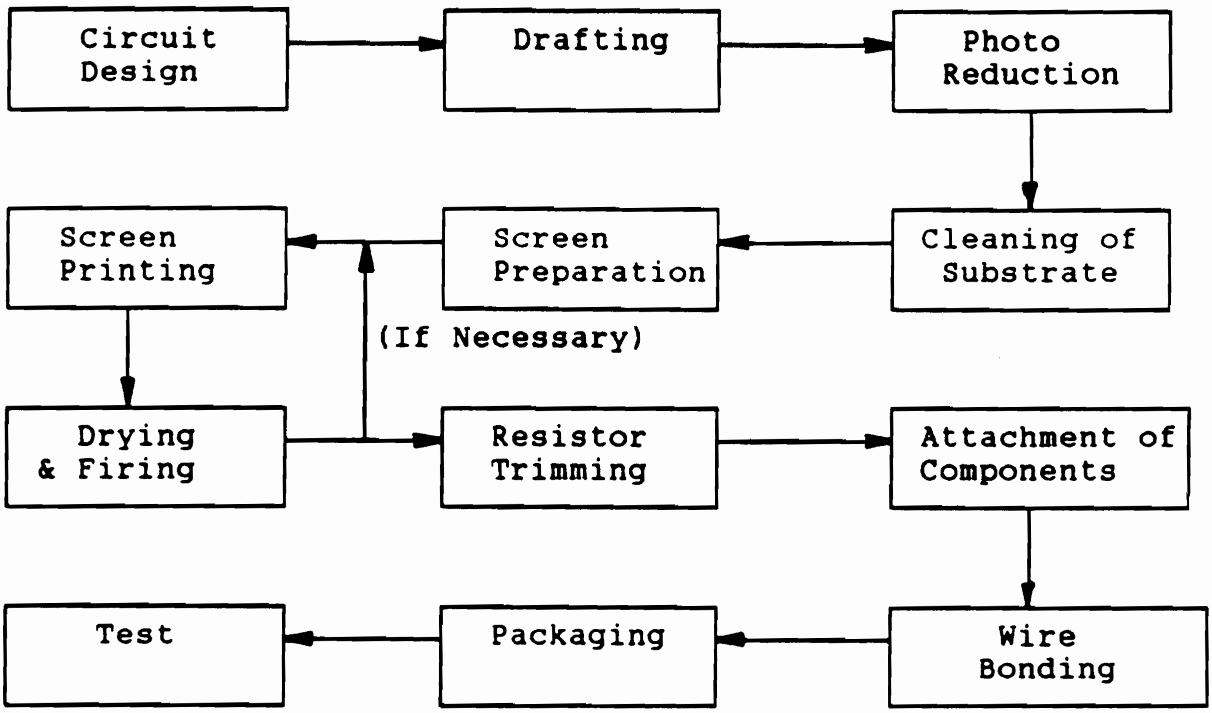

Figure 4.1 Typical Thick Film Hybrid Process Flow Chart

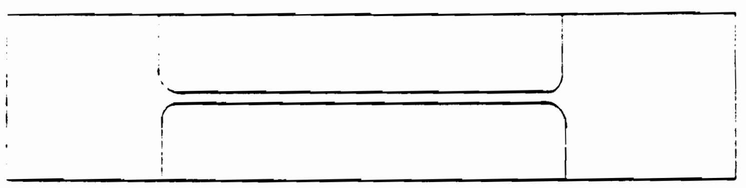

Figure 4.2 A Pattern of The Structure

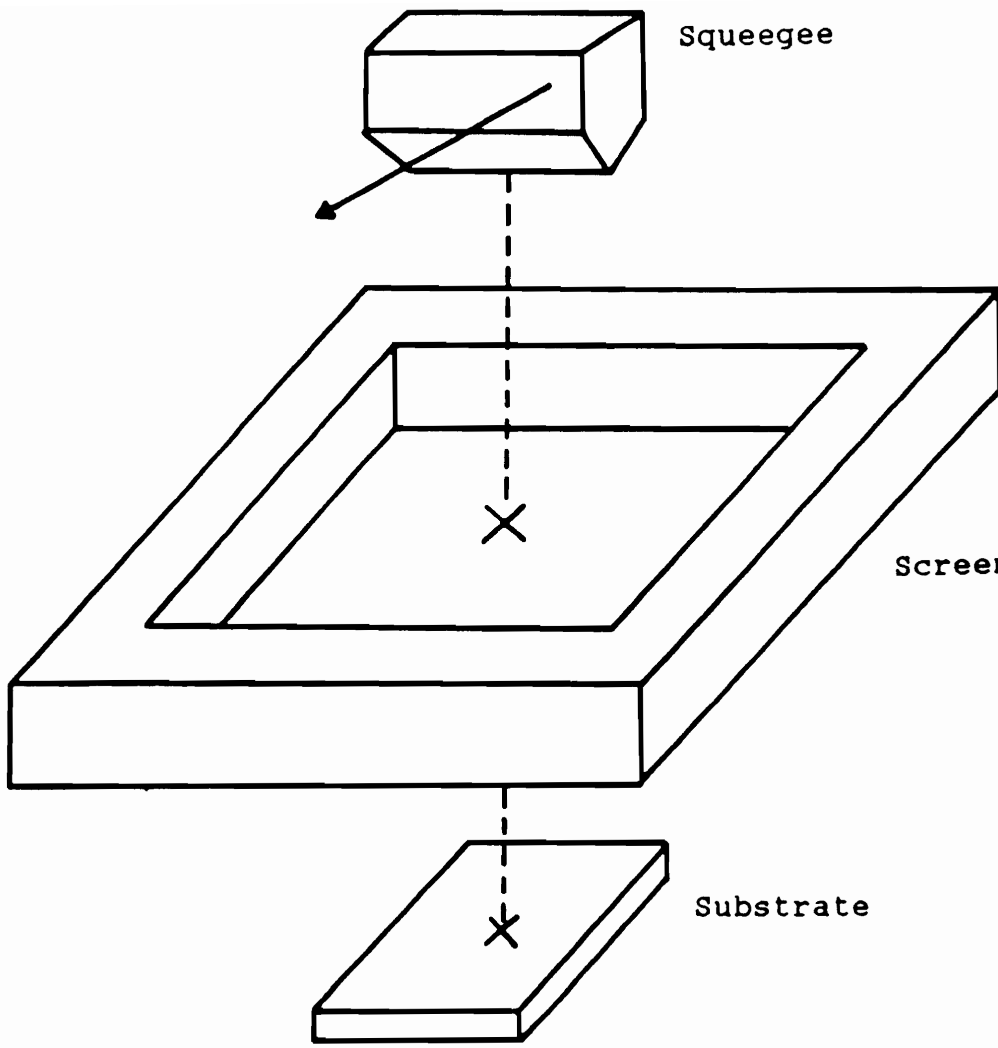

Figure 4.3 A Screen Printing Process Schematic

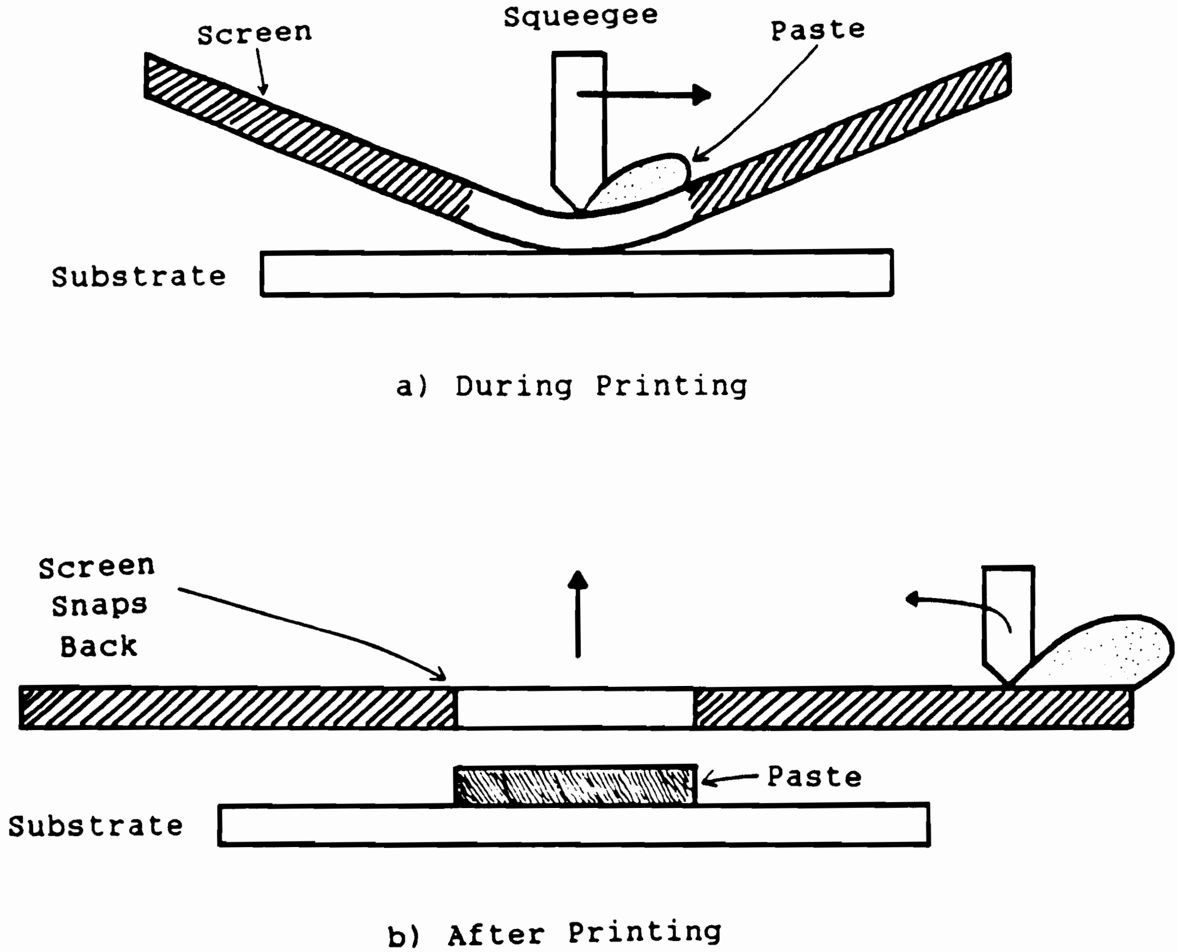

Figure 4.4 A Cross Section of The Screen,
a) During Printing and,
b) After Printing

4.3 Frequency Domain Measurement Techniques

4.3.1 Basic Concept

Since voltages and currents cannot be measured directly at microwave or radio frequencies, the representation of networks at these frequencies by impedance or admittance matrix is not a convenient procedure. The quantities, directly measurable, are transmission and reflection coefficients. These quantities form the basic concept of the scattering parameters (S parameters). The major reason the S parameters are preferred for microwave and radio circuits characterizing is the ability to measure them in a match impedance system, in contrast to the short-circuit and open-circuit types measurements required for the other network parameters. S parameters represent the relationship between the incident traveling wave coming toward the junction, and the reflected traveling wave coming outward from the junction at the n-th port, defined as follows,

$$a_n = V_n^+ \times (Z_{0n})^{-\frac{1}{2}}$$

$$b_n = V_n^- \times (Z_{0n})^{-\frac{1}{2}}$$

where V^+ and V^- represent incident and reflected waves along the line at n-th port and Z_0 is the characteristic impedance of the line. The quantities a_n and b_n are linearly related since the system is assumed to be linear throughout. The relationship between a_n and b_n can be written as,

$$[\ b\ ] = [\ S\ ]\ [\ a\ ]$$

or

$$b_1 = S11a_1 + S12a_2 + S13a_3 + \ldots\ldots\ldots\ldots\ldots + S1n\ a_1$$

$$b_2 = S22a_1 + S22a_2 + S23a_3 + \ldots\ldots\ldots\ldots\ldots + S2n\ a_2$$

....

....

$$b_n = Sn1a_1 + Sn2a_2 + Sn3a_3 + \ldots\ldots\ldots\ldots\ldots + Snn\ a_n$$

and in matrix form as

$$\begin{bmatrix} b_1 \\ b_2 \\ .. \\ .. \\ b_n \end{bmatrix} = \begin{bmatrix} S11 & S12 & S13 & .. & .. & .. & S1n \\ S22 & S22 & S23 & .. & .. & .. & S2n \\ .. & .. & .. & .. & .. & .. & .. \\ .. & .. & .. & .. & .. & .. & .. \\ Sn1 & Sn2 & Sn3 & .. & .. & .. & Snn \end{bmatrix} \begin{bmatrix} a_1 \\ a_2 \\ .. \\ .. \\ a_n \end{bmatrix}$$

The average power flowing into the port n may be evaluated by using the quantities of a_n and b_n in the form of

$$V_n = V_n^+ + V_n^- = (\ Z_{0n}\ )^{\frac{1}{2}} \times (\ a_n + b_n\ )$$

$$I_n = (\ V_n^+ + V_n^-\ )\ /\ Z_{0n}$$

$$= (\ Z_{0n}\ )^{-\frac{1}{2}} \times (\ a_n - b_n\ )$$

and the power flow at the port n can be given by,

$$P = \tfrac{1}{2}\ \mathrm{Re}\ (\ V_n\ I_n^*\ )$$

$$= \tfrac{1}{2}\ \mathrm{Re}\ [\ (\ a_n\ a_n^* - b_n\ b_n^*\ ) + (\ b_n\ a_n^* - b_n\ a_n^*\ )]$$

$$= \tfrac{1}{2}\ (\ a_n\ a_n^* - b_n\ b_n^*\ )$$

= incident power - reflected power

For a two-port network, the relationship between b_n and a_n can be expressed as,

$$b_1 = S11a_1 + S12a_2$$

$$b_2 = S21a_1 + S22a_2$$

and in matrix form as,

$$\begin{bmatrix} b_1 \\ b_2 \end{bmatrix} = \begin{bmatrix} S11 & S12 \\ S21 & S22 \end{bmatrix} \begin{bmatrix} a_1 \\ a_2 \end{bmatrix}$$

To solve for individual parameters, a_1 or a_2 must be made equal to zero. The parameters can be written as,

$$S11 = \left.\frac{b_1}{a_1}\right| a_2 = 0 \text{ (output terminated in } Z_0 \text{)}$$

$$S21 = \left.\frac{b_2}{a_1}\right| a_2 = 0 \text{ (output terminated in } Z_0 \text{)}$$

$$S12 = \left.\frac{b_1}{a_2}\right| a_1 = 0 \text{ (input terminated in } Z_0 \text{)}$$

$$S22 = \left.\frac{b_2}{a_2}\right| a_1 = 0 \text{ (input terminated in } Z_0 \text{)}$$

Figure (4.6) presents S parameters of a two-port network.

4.3.2 Experimental Techniques

The Hewlett-Packard 8510 (HP 8510) Network Analyzer is used to acquire the magnitude and phase characteristics of the quantities in frequency domain measurements. The HP 8510 Network Analyzer system, Figure (4.7), is composed of four parts: a test signal source (synthesized sweep HP 834x-series or sweep oscillator HP 835xx-series), test set (Reflection /Transmission Test Set or S Parameter Test Set HP 85xx-series), IF detector (HP 85102), and display processor (HP 85101). During a typical measurement, the test signal source generates the signal at the range of frequency between 30 MHz to 26.5 GHz to the specified port. The test set provides the input/output ports to connect the device-under-test, signal separation to sample the reference and test signals, and test signal frequency to 20 MHz conversion. In IF detector, a harmonic of voltage-tuned local oscillator (VTO) mixes with the stimulus to produce a first IF frequency close to 20 MHz. Fine tuning is achieved by comparing the IF frequency with 20 MHz crystal reference and sweeping the local oscillator to track the stimulus frequency. The frequency conversion produces an IF frequency of 100 kHz for application to the detection. With a fully calibrated system, the IF signal is maintained at optimum levels for detection over a wide range of operation.

Figure (4.8) demonstrates S-Paramter Test Set Signal Flow which shows an automatic selection of S11, S12, S21, S22. The signal is automatically switched for forward or reverse measurements. The magnitude and phase of an applied signal through the device-under-test are measured in terms of S parameters by comparing the incident signal to the transmitted signal (or to the reflected signal).

4.3.3 Test Results

The HP 8510 network analyzer is used to acquire the characteristics of crosstalk noise in frequency domain forms. The characteristics can be observed in terms of gain (dB) and phase changes (angle). The observation of phase changes is inconsiderable but the observation of gain gives some meaningful results. The crosstalk noise characteristics in terms of gain, Figures (4.9) - (4.12), depend on the spacing between the lines. As the spacing increases, the measured S21 and S31 decrease. The measured S21 and S31 of the circuit with 10 mils spacing are presented in Figure (4.9). The measured S21 and S31 match closely the simulated S21 and S31 of Figure (3.13) for a wideband of frequencies (0.045 GHz - 4.0 GHz). At 0.8 GHz operating frequency, the measured S21 and S31 provide matched results as the simulated ones and the measured S21 gives maximum crosstalk which meet the purpose of the design.

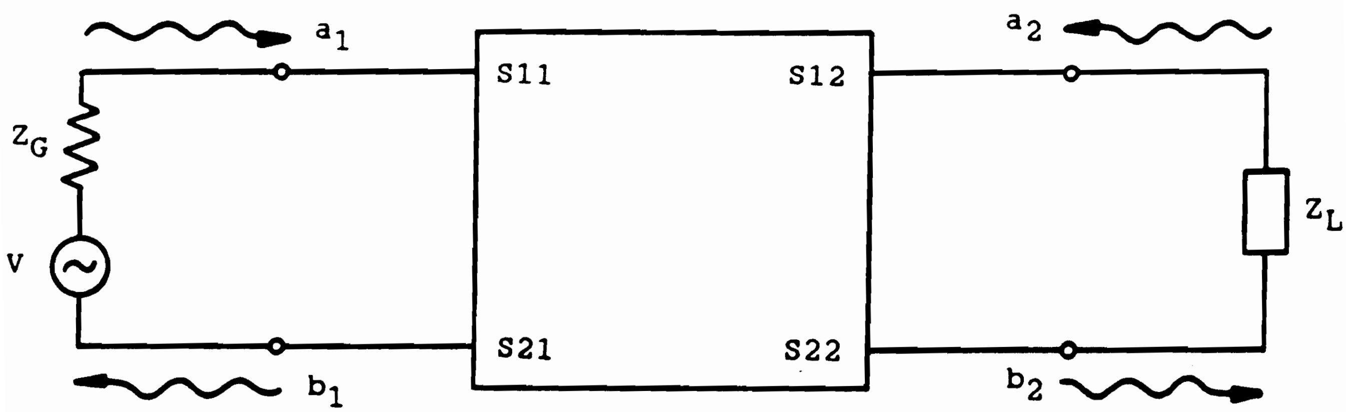

Figure 4.6 S-Parameter of A Two Port Network

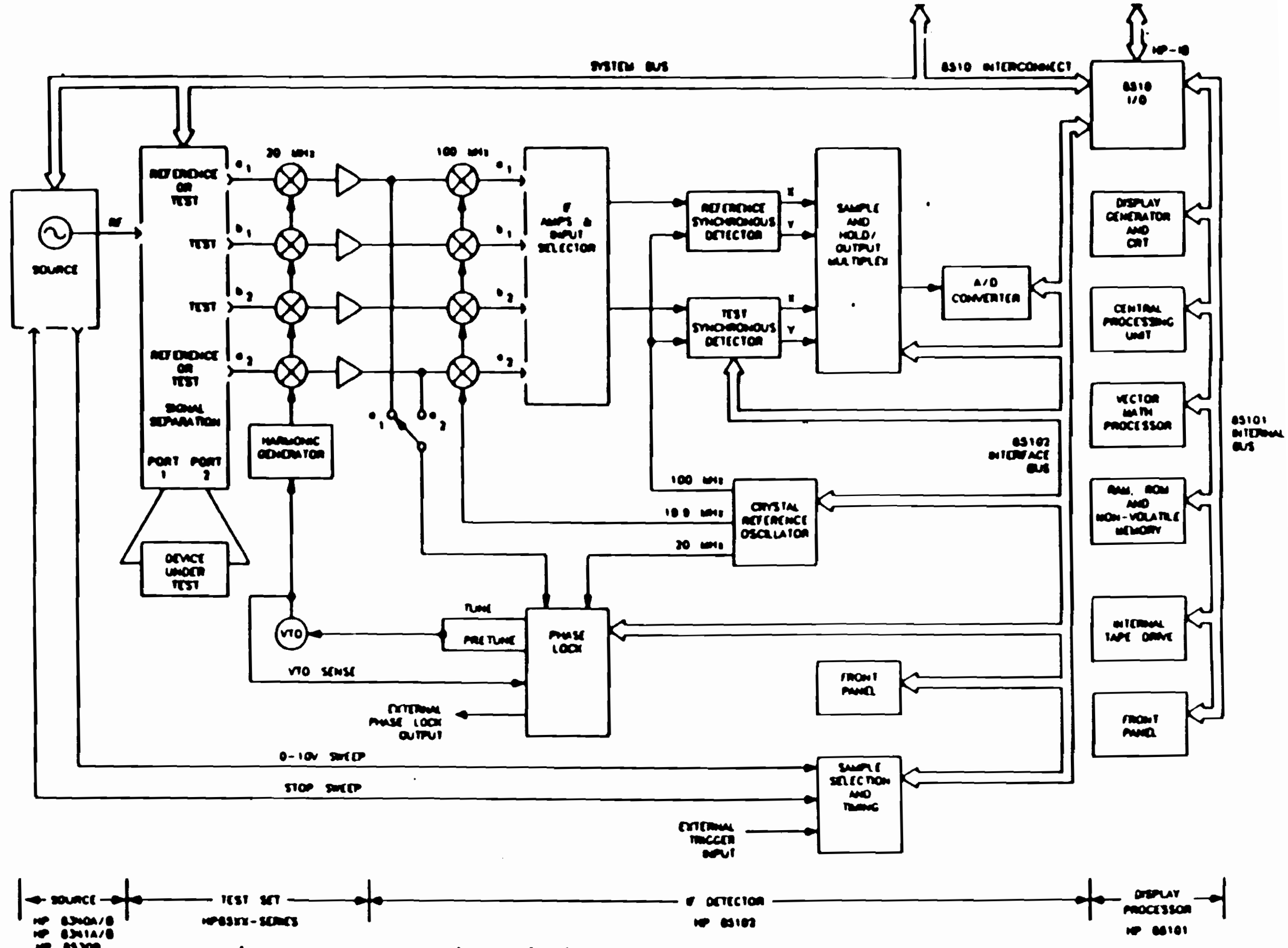

Figure 4.7 Simplified System Block Diagram

of HP 8510 Network Analyzer

(Hewlett Packard, HP 8510B Network Analyzer Manual)

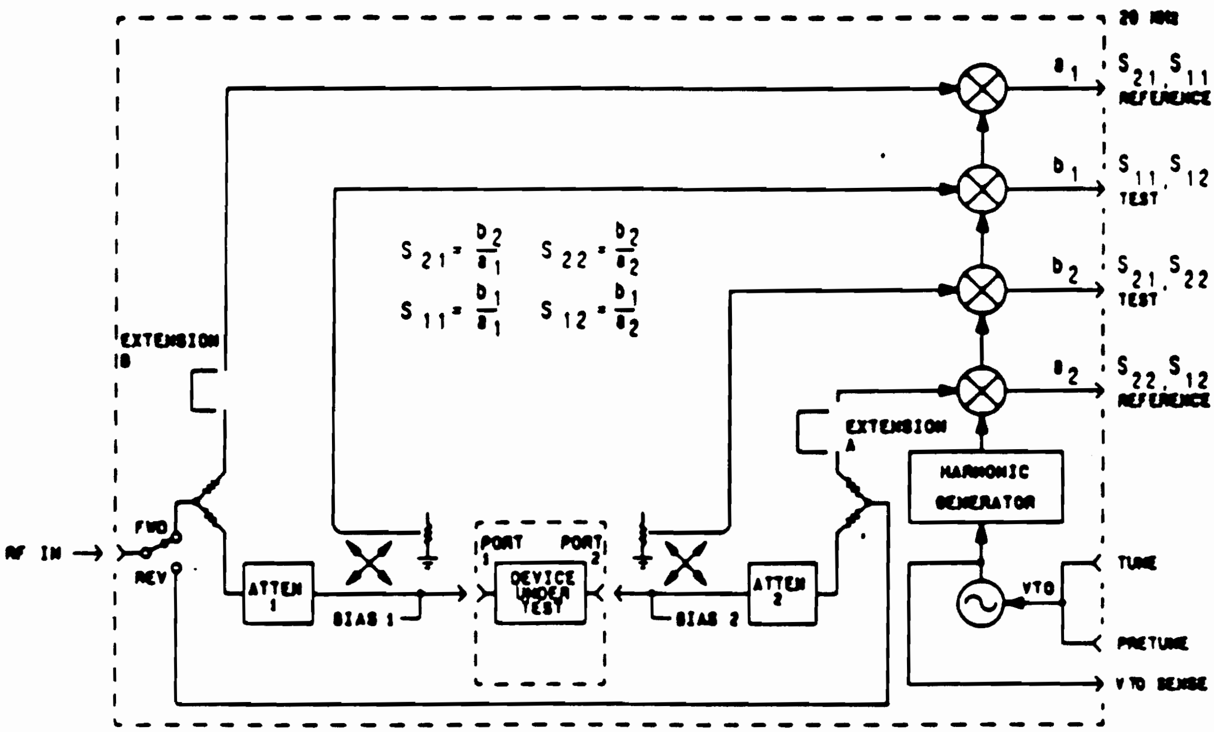

Figure 4.8 S-Parameter Test Set Signal Flow

of HP 8510 Network Analyzer

(Hewlett Packard, HP 8510B Network Analyzer Manual)

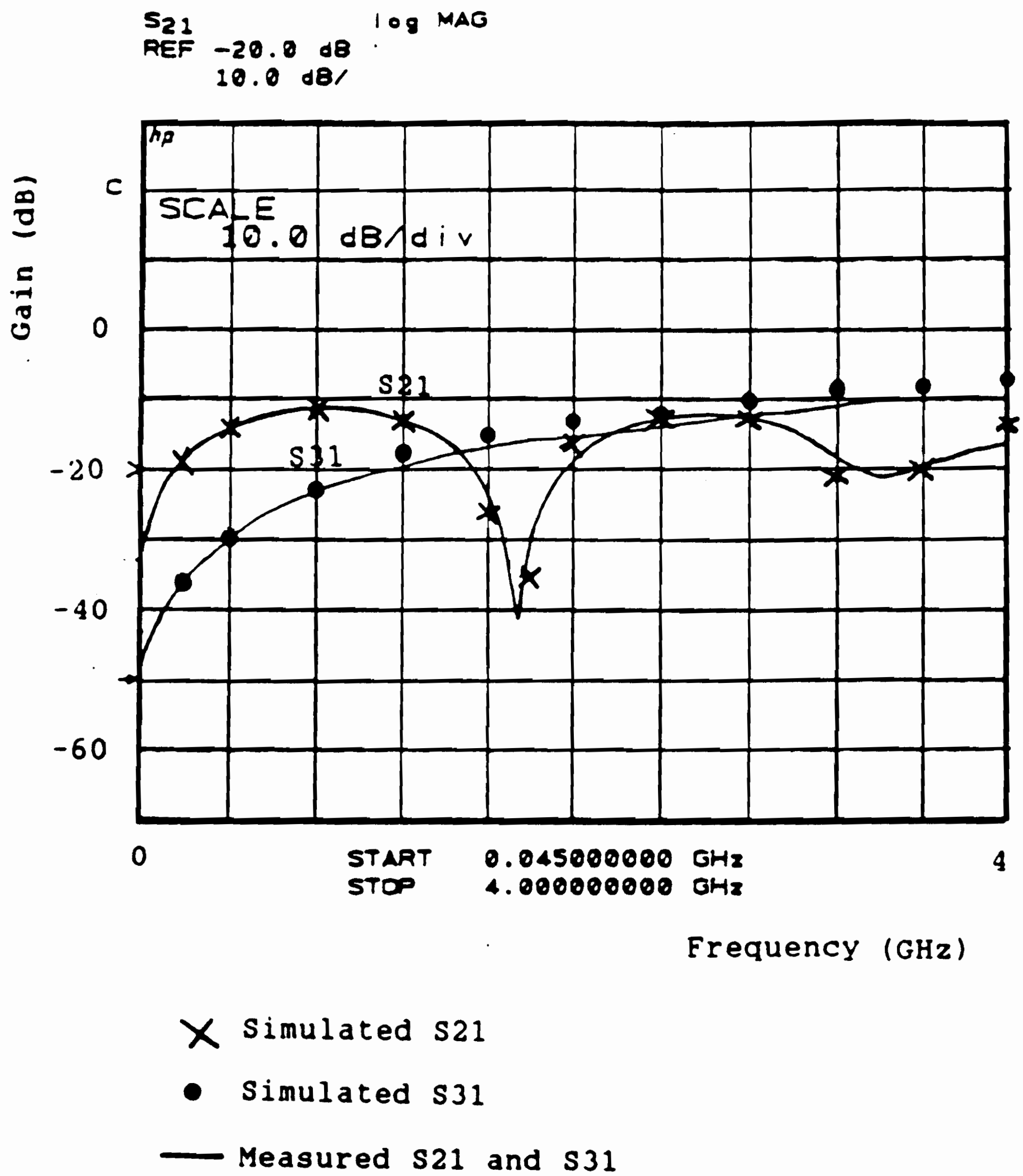

Figure 4.9 Measured S21 and S31 of The Structure, (Spacing = 10 mils)

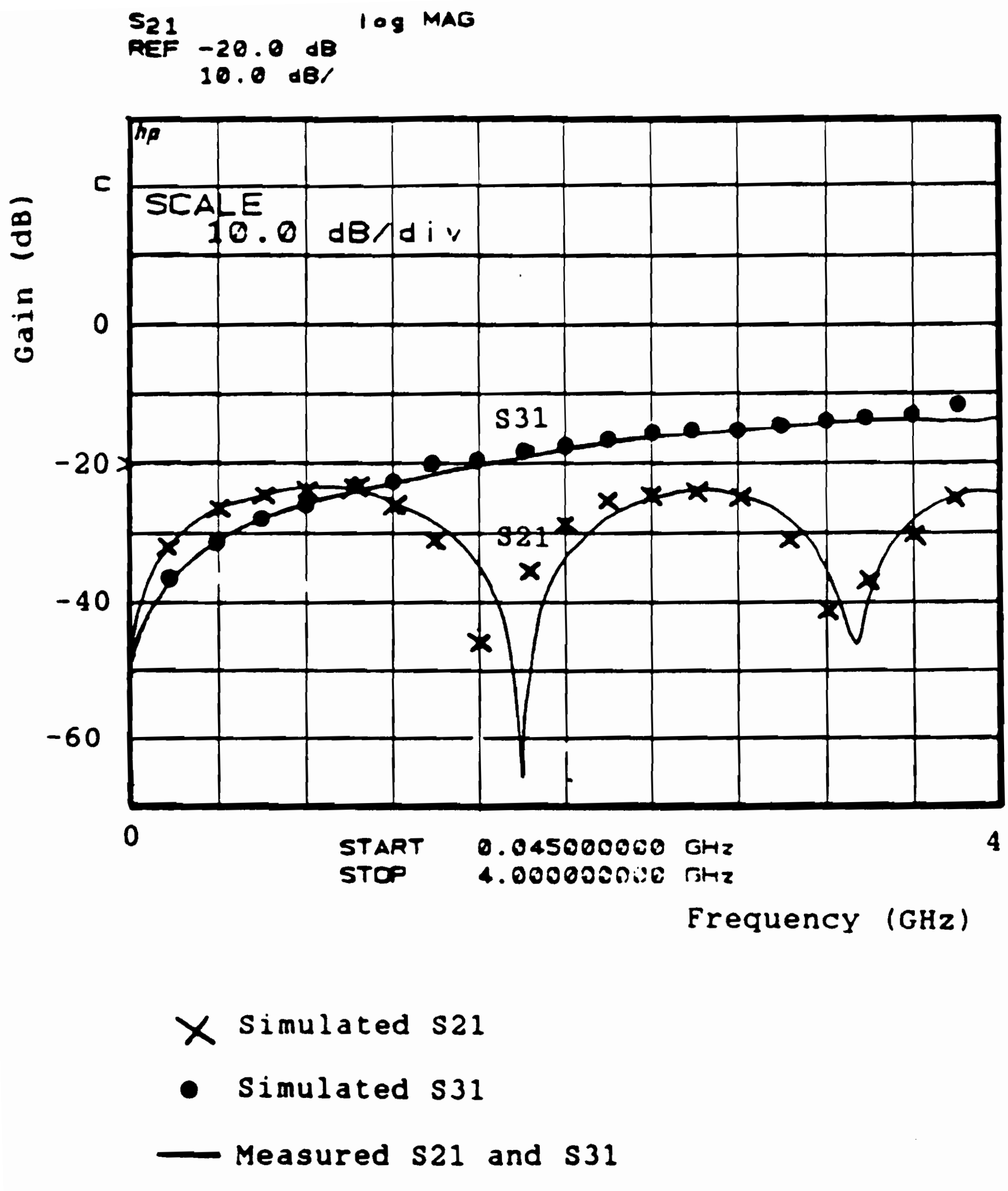

Figure 4.10 Measured S21 and S31 of The Structure, (Spacing = 50 mils)

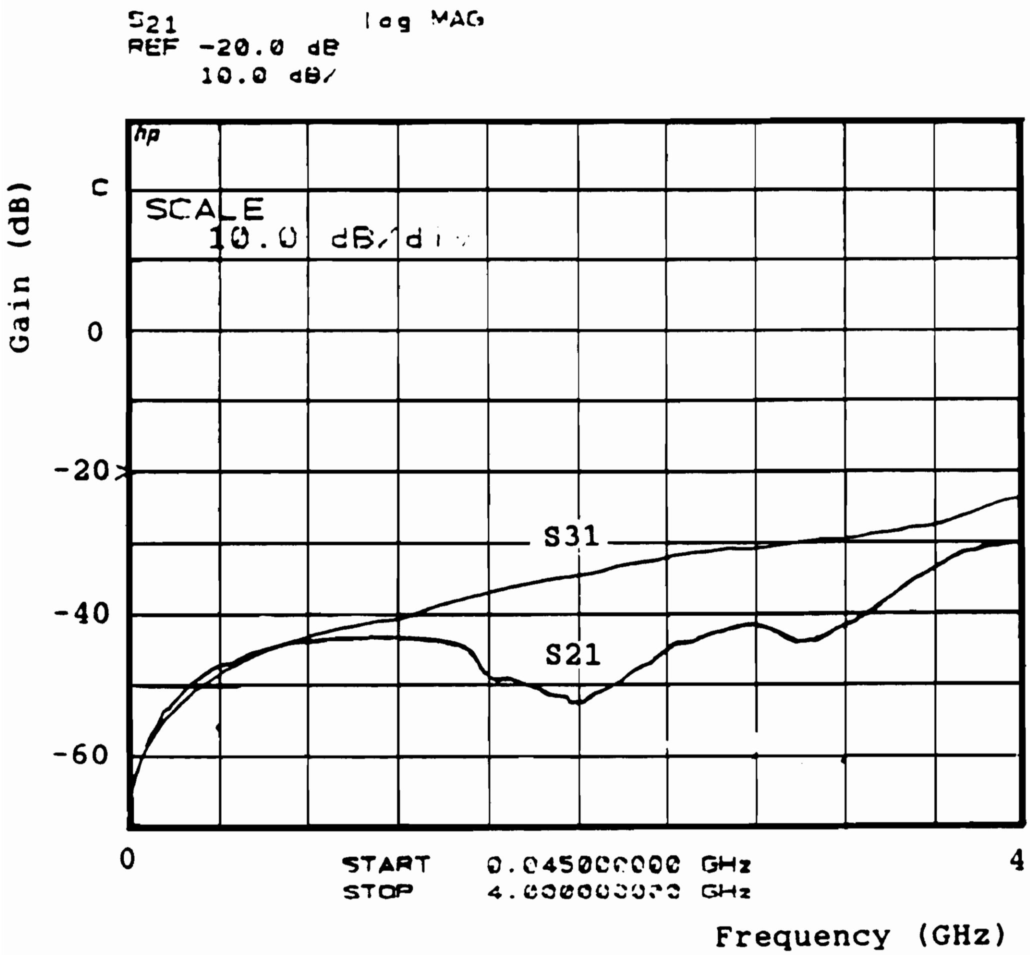

Figure 4.11 Measured S21 and S31 of The Structure, (Spacing = 200 mils)

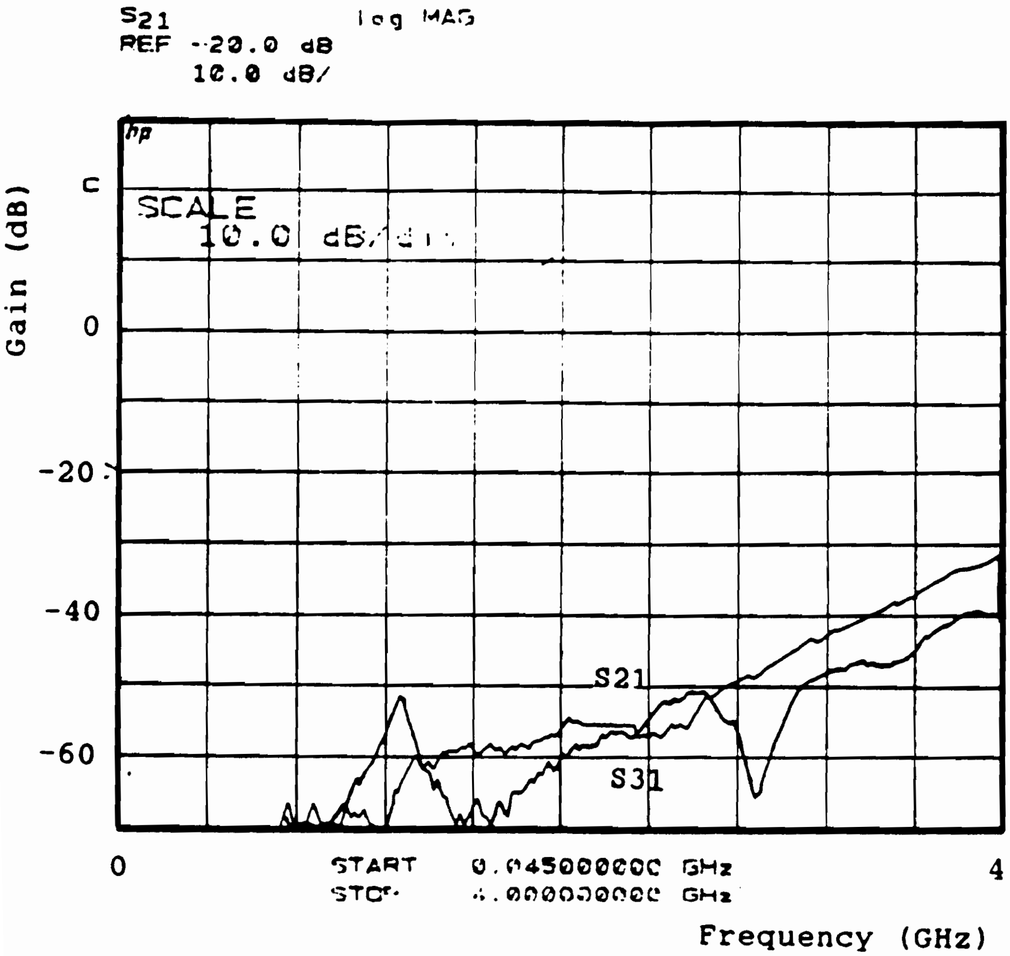

Figure 4.12 Measured S21 and S31 of The Structure, (Spacing = 1500 mils)

4.4 Time Domain Measurement Techniques

4.4.1 Basic Concept

Time domain measurement techniques can be divided into two methods, the Time Domain Reflection technique (TDR) and the Time Domain Transmission technique (TDT). The setup used for the measurements with the Time Domain Reflection technique is called the time domain reflection network analyzer (TDRNA) and that with the Time Domain Transmission technique is called the time domain transmission network analyzer (TDTNA). The concept of time domain measurement techniques is to propagate a train of generated pulses with adequately fast transition in a reference line and observe the response waveform. The TDR technique is used to observe the response or reflected waveform at the network's input port where the TDT technique is used to observe the response or transmitted waveform at the network's output port. The setup of time domain network analyzer consists of a digitizing oscilloscope interfaced to a data acquisition system and TDR or TDT unit which has a pulse generator and a feedthrough sampling head. Since distance is related to time in these techniques, the faster the pulse is, the greater the distance resolution is.

4.4.2 Experimental Techniques

The relationship between the frequency domain response and time domain response of any network or device under test (DUT) can be represented in the term of Fourier Transform. The time domain measurements of experimental circuits are used HP 5412 Digitizing Oscilloscope Mainframe. Time domain measurements in this section is used to acquire the reference and response waveforms needed to evaluate the integral part of crosstalk noise characteristics. Figure (4.13) illustrates the setup used in these measurements. This setup is composed of a digitizing oscilloscope mainframe (HP 54120 A), a four channel test set which has a pulse generator, and a feedthrough sampling head to the experimental circuits. The pulse generator has a spectral contents covering the band from DC to 18 GHz.

4.4.3 Test Results

For time domain measurements, the response of signal on the microstrip line is shown in Figure (4.14) The pulse is the same at port 1 and port 4, except for the time delay of the pulse. The crosstalk noise responses at port 2 and port 3 are shown in Figures (4.15) - (4.17) and Figures (4.18) - (4.20), respectively.

When signal is sent on the main line in the form of step function as shown in Figure (4.14), the response at the same line gives the same response but the delay time is included. This delay time can be used to calculate the line length. The crosstalk noise characteristics on the adjacent lines can be observed and the following conclusions are drawn.

At the beginning of the adjacent line,as shown in Figures (4.15) - (4.17), characteristics can be classified into three parts, a small sine wave, a big unit impulse plus a small sine wave, and a small underdamped wave before it settles. Based on the proposed theory, these crosstalk signals consist of three types of signal. The small sine wave occurs due to the resonance of inductances and capacitances in the circuit. The big unit impulse is the primary crosstalk while the underdamped portion represents the secondary crosstalk. At the end of the adjacent line, as shown in Figures (4.18) through (4.20), characteristics can be classified into two parts, a big impulse on the negative side and a small underdamped wave before it settles. These crosstalk signals are the same as those at the beginning of the line but include the loss of line. A big impulse on the negative side occurs as differential crosstalk and gives the bigger magnitude while the bandwidth is smaller.

Examining Figures (4.15)-(4.20), the measured waveforms match the simulated waveforms of Figures (3.15) - (3.17). As the spacing increases, the size of crosstalk noise waveforms decreases. Errors occurring in the fabrication process can cause some small deviations in the inductance, mutual inductance, capacitance, and mutual capacitance values of the actual circuits.

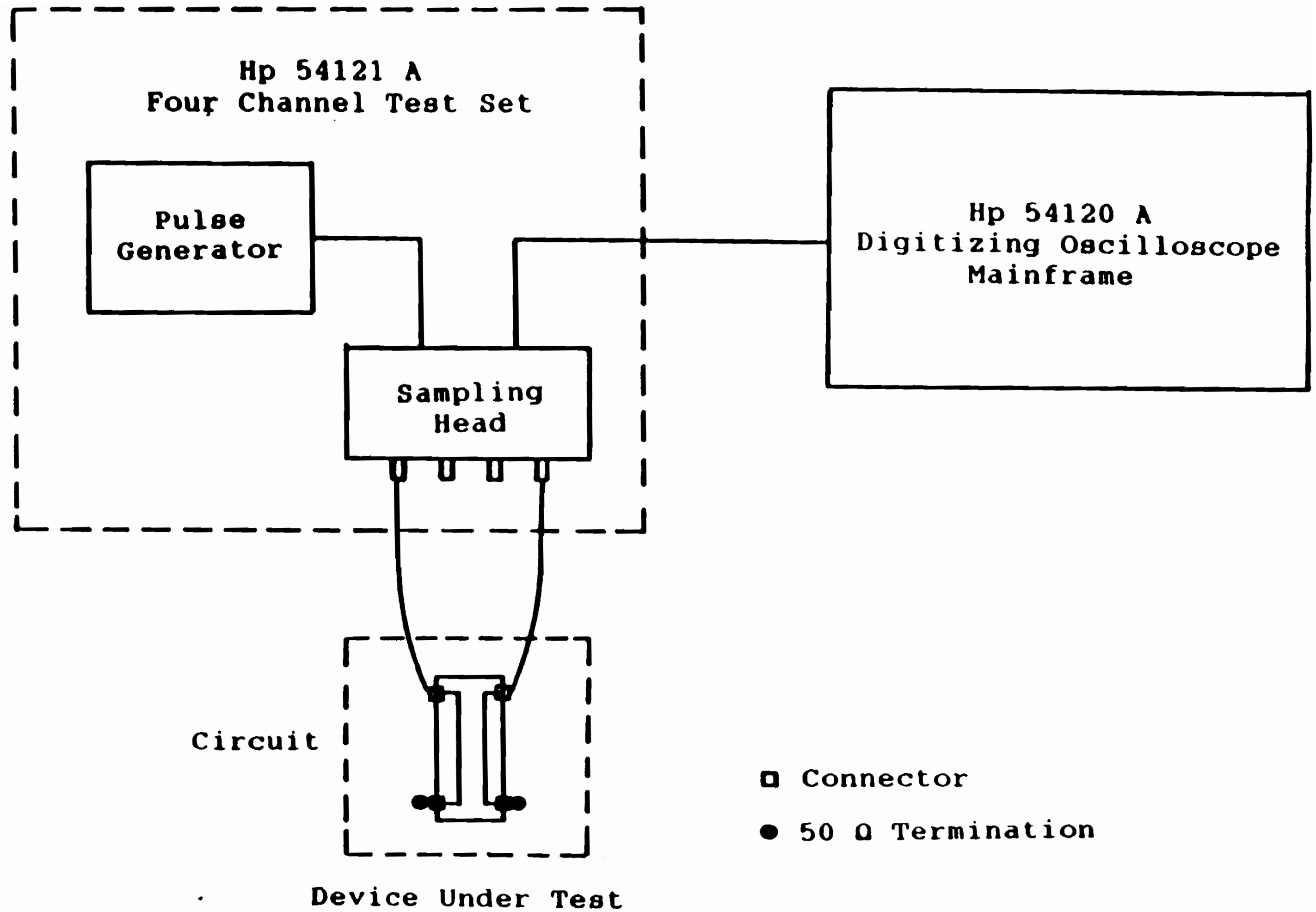

Figure 4.13 Time Domain Measurement Setup Using HP 5412 Digitizing Oscilloscope Mainframe

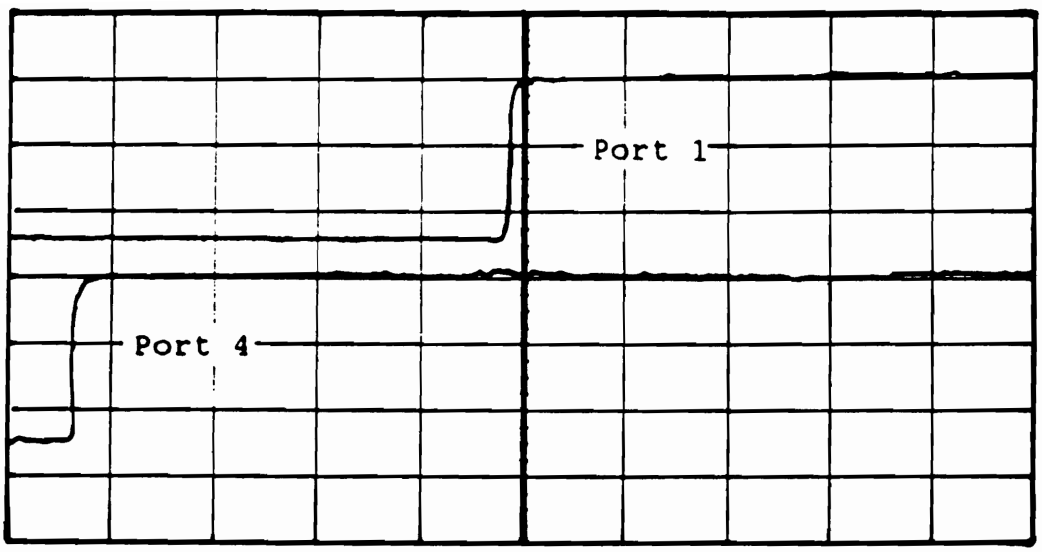

Ch.1 = 80 mVolts/div   Offset = 200 mVolts
Ch.4 = 80 mVolts/div   Offset = -40.62 mVolts
Timebase = 2.00 ns/div   Delay = 16.00 ns

Figure 4.14 Measured Responses at Port 1 and Port 4

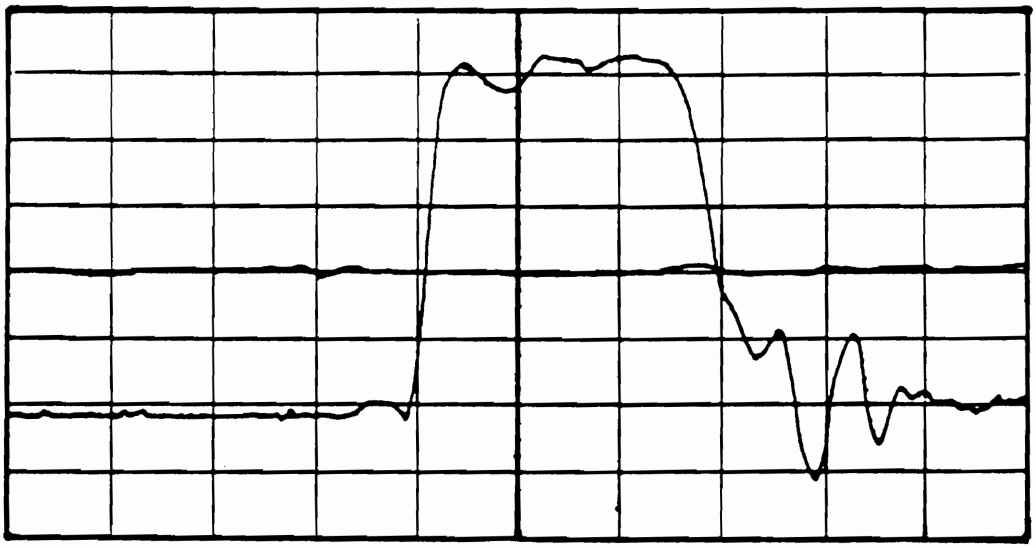

Ch.1 = 80 mVolts/div Offset = 200.0 mVolts
Ch.4 = 5 mVolts/div Offset = 16.50 mVolts
Timebase = 200 ps/div Delay = 24.57 ns

Figure 4.15 Measured Crosstalk Signal at Port 2,

(Spacing = 10 mils)

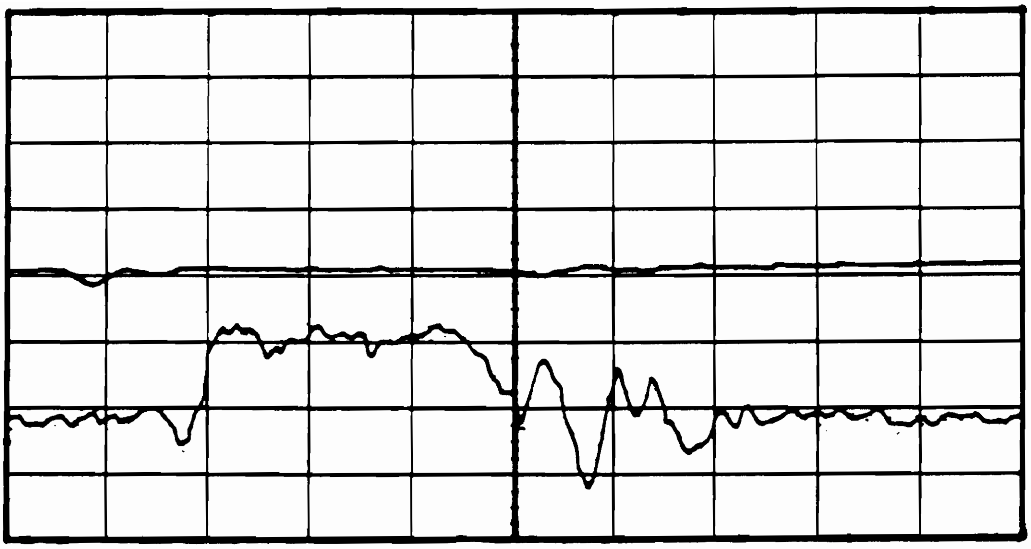

Ch.1 = 80 mVolts/div
Ch.4 = 5 mVolts/div
Timebase = 200 ps/div

Offset = 200.0 mVolts
Offset = 16.50 mVolts
Delay = 25.00 ns

Figure 4.16 Measured Crosstalk Signal at Port 2,

(Spacing = 50 mils)

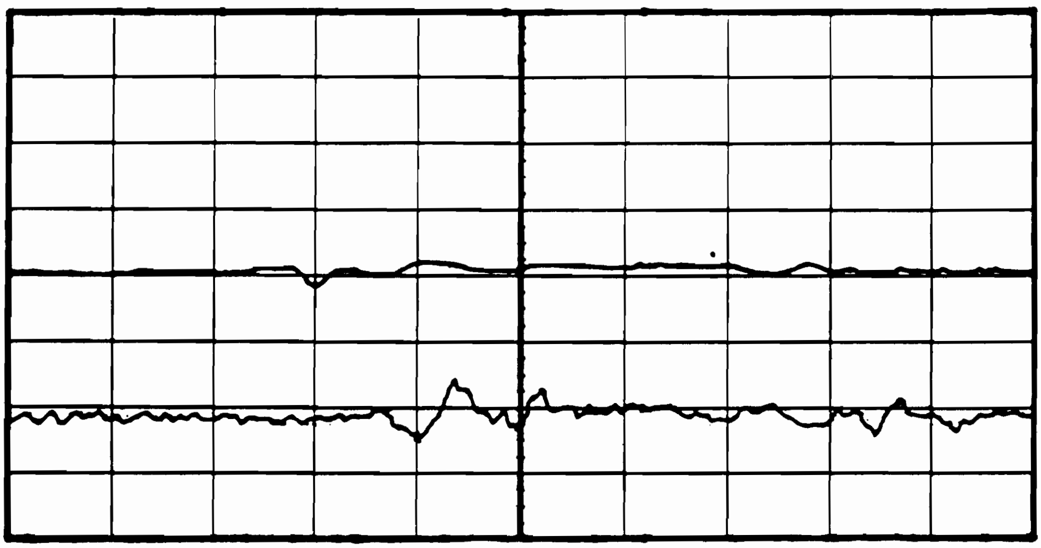

Ch.1 = 80 mVolts/div Offset = 200.0 mVolts
Ch.4 = 5 mVolts/div Offset = 16.50 mVolts
Timebase = 200 ps/div Delay = 25.00 ns

Figure 4.17 Measured Crosstalk Signal at Port 2,

(Spacing = 200 mils)

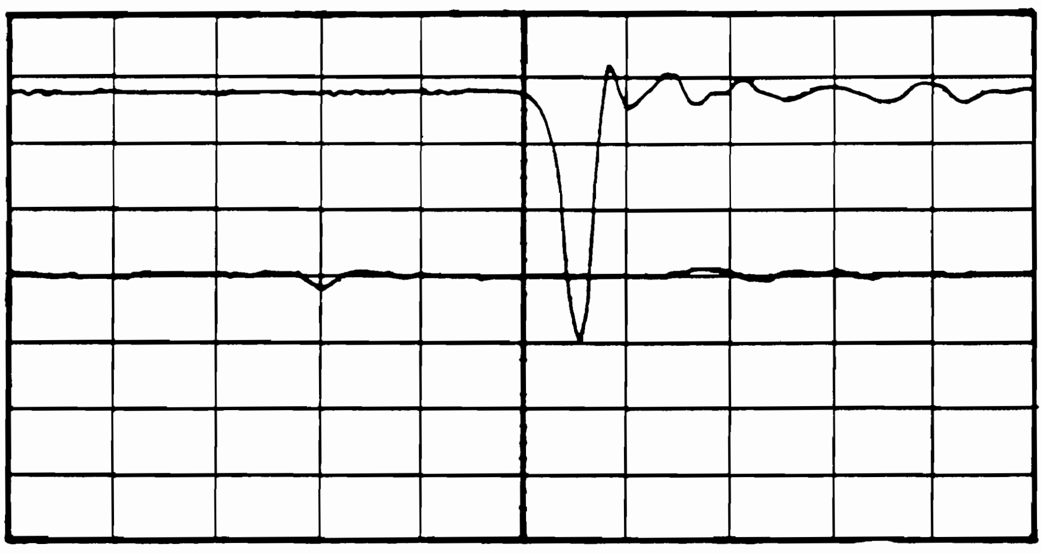

Ch.1 = 80 mVolts/div Offset = 200.0 mVolts
Ch.4 = 5 mVolts/div Offset = 16.50 mVolts
Timebase = 200 ps/div Delay = 25.00 ns

Figure 4.18 Measured Crosstalk Signal at Port 3,
(Spacing = 10 mils)

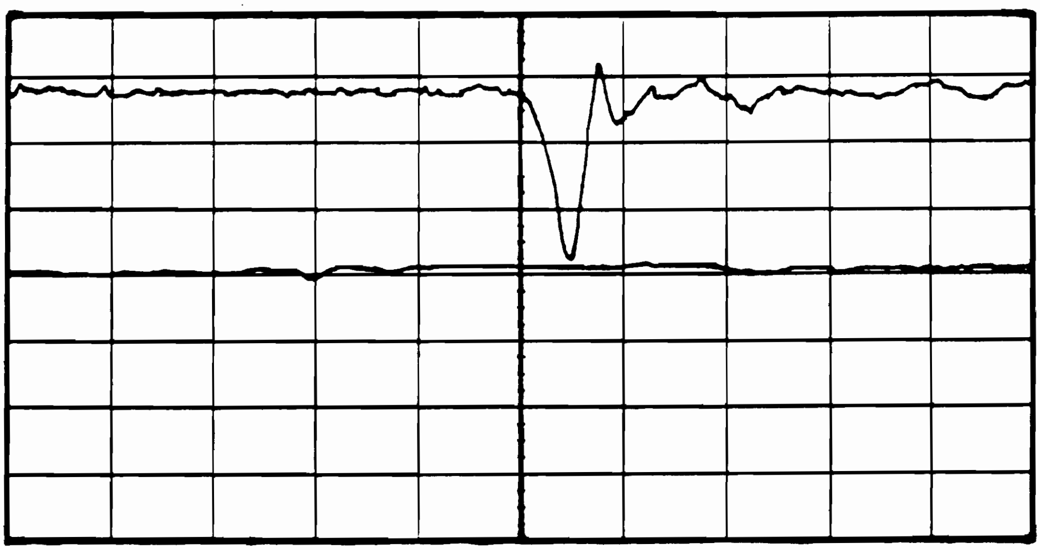

Ch.1 = 80 mVolts/div　　Offset = 200.0 mVolts
Ch.4 = 5 mVolts/div　　Offset = 16.50 mVolts
Timebase = 200 ps/div　　Delay = 25.00 ns

Figure 4.19　Measured Crosstalk Signal at Port 3,
(Spacing = 50 mils)

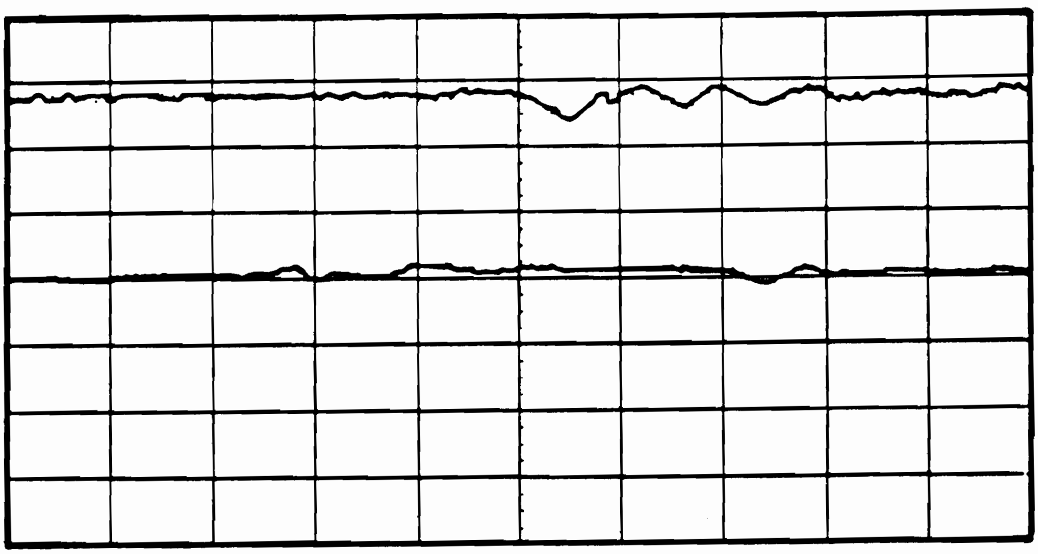

Ch.1 = 80 mVolts/div   Offset = 200.0 mVolts
Ch.4 = 5 mVolts/div   Offset = 16.50 mVolts
Timebase = 200 ps/div   Delay = 25.00 ns

Figure 4.20 Measured Crosstalk Signal at Port 3,

(Spacing = 200 mils)

4.5 Summary

The actual realization of the structures is performed using conventional thick film printing technique on alumina substrates. The fabrication process is discussed in this chapter. Measurements are conducted using frequency domain techniques, and time domain techniques. The HP 8510 network analyzer is used to acquire the characteristics of crosstalk noise in frequency domain forms. The measured S21 and S31 match closely the simulated S21 and S31 for a wideband of frequencies (0.045 GHz - 4.0 GHz). At 0.8 GHz operating frequency, the measured S21 and S31 are the same as the simulated ones and the measured S21 gives maximum crosstalk which meets the purpose of the design. As the spacing increases, the measured S21 and S31 decrease. The HP 5412 digitizing oscilloscope mainframe is used to acquire the characteristics of crosstalk noise in time domain forms. The measured waveforms match the simulated waveforms. As the spacing increases, the size of crosstalk noise waveforms decreases. Errors occurring in the fabrication process can cause some small deviations in inductance, mutual inductance, capacitance, and mutual capacitance values of the actual circuits.

The conclusion is that the model matches closely the experimental data and can give an understanding of crosstalk noise between adjacent lines in both frequency domain and time domain. In the next chapter, the crosstalk noise considerations to verify the model, such as different line lengths, different loss lines, and efficiency test on striplines are discussed.

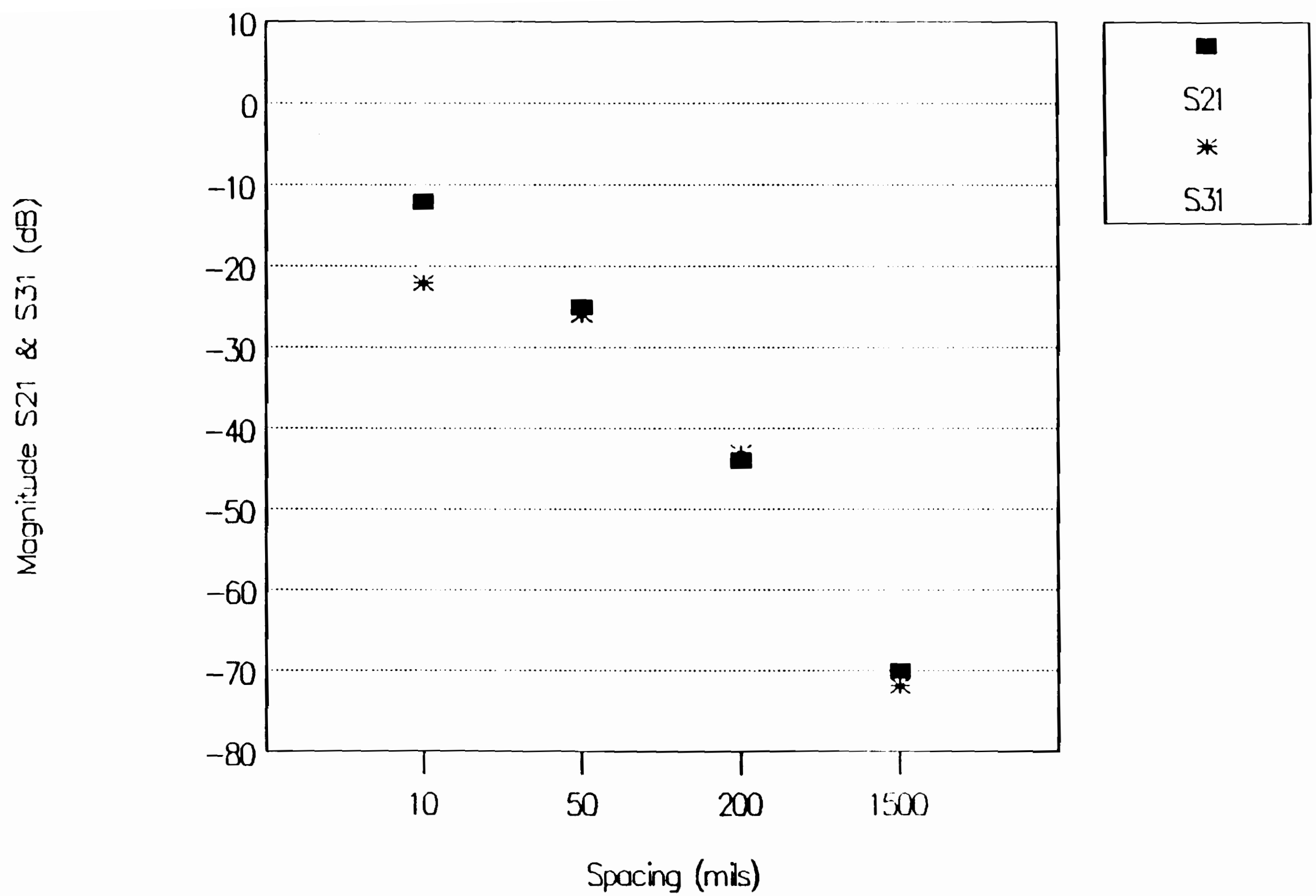

Figure 4.21 Summary of Measured S21 and S31 at .8 GHz

CHAPTER 5

VERIFICATION OF CROSSTALK NOISE MODEL IN SOME ASPECTS

5.1 Different Line Lengths

In some applications, the individual microwave component has a certain specified range of frequencies over which it is designed to operate. It does not work properly beyond this bandwidth. For instance, directional coupler is used to monitor an output power which is coupled from the forward power. The directional coupler only works as designed when power is applied to the proper port. Since the higher frequency means shorter wavelength, the line length is a factor to determine the operating frequency. With the same physical model of crosstalk noise, as shown in Figures (3.4) - (3.5), the line length can be used to predict the shape of crosstalk waveform. The bandwidth of crosstalk waveform depends on the line length. The longer the line is, the larger the bandwidth is.

Verification

The effect of line length is investigated in order to verify the crosstalk noise model in this section. The structures have the line length about a quarter wavelength at the operating frequency. In this work, a set of different line lengths having the same line width are fabricated and tested.. The operating frequencies are chosen to be 4 GHz, .8 GHz and .5 GHz, and the line lengths are taken equal to 228 mils, 1400 mils, and 2000 mils, respectively.

The actual realization of the structures is performed using selective etching of copper cladded teflon-ceramic duriod composite substrates from Rogers Corporation. The fabrication process includes artwork and layout, photoresist, etching. The artwork and layout procedure is similar to that in previous chapter. In photoresist process, the substrate needs to be cleaned and the photoresist is applied by spinning few drops in order to evenly spread the photoresist layer. After spinning, the substrate is placed in an oven for drying. Then, the pattern is exposed on the photoresist side of substrate and the substrate is developed. The substrate is etched in an etchant solution. After the etching is completed, the photoresist can be washed-off using acetone. The substrate is now completed and ready for use.

Measurements are conducted using the same procedure as shown in Chapter 4. The experimental results are shown in Figures (5.1) - (5.15). Since the maximum crosstalk noise, maximum magnitudes of S21, can be used to determine the operating frequency, Figures (5.1) - (5.3) demonstrate that the experimental circuits are to be operated at .5 GHz, .8

GHz, and 4 GHz for the line length of 2000 mils, 1400 mils, and 228 mils, respectively. This criteria meets the purpose of the design. Figures (5.4)-(5.5), Figures (5.6)-(5.7), and Figures (5.8)-(5.9) present the near-end crosstalk noise at port 2 of the circuits with line lengths of 2000 mils, 1400 mils, and 228 mils, respectively. Figures (5.10)-(5.11), Figures (5.12)-(5.13), and Figures (5.14)-(5.15) present the far-end crosstalk noise at port 3 of the circuits with line lengths of 2000 mils, 1400 mils, and 228 mils, respectively. The crosstalk waveforms of the proposed model can be applied to different line lengths. The circuits with the line length of 2000 mils give significant primary crosstalk as compared to secondary crosstalk. The bandwidths are found to be large. The circuits with the line length of 228 mils give a narrow bandwidth due to short line length. The shape of waveforms is compressed. These waveforms are similar to those in Chapter 4. As the line length increases, the crosstalk noise increases.

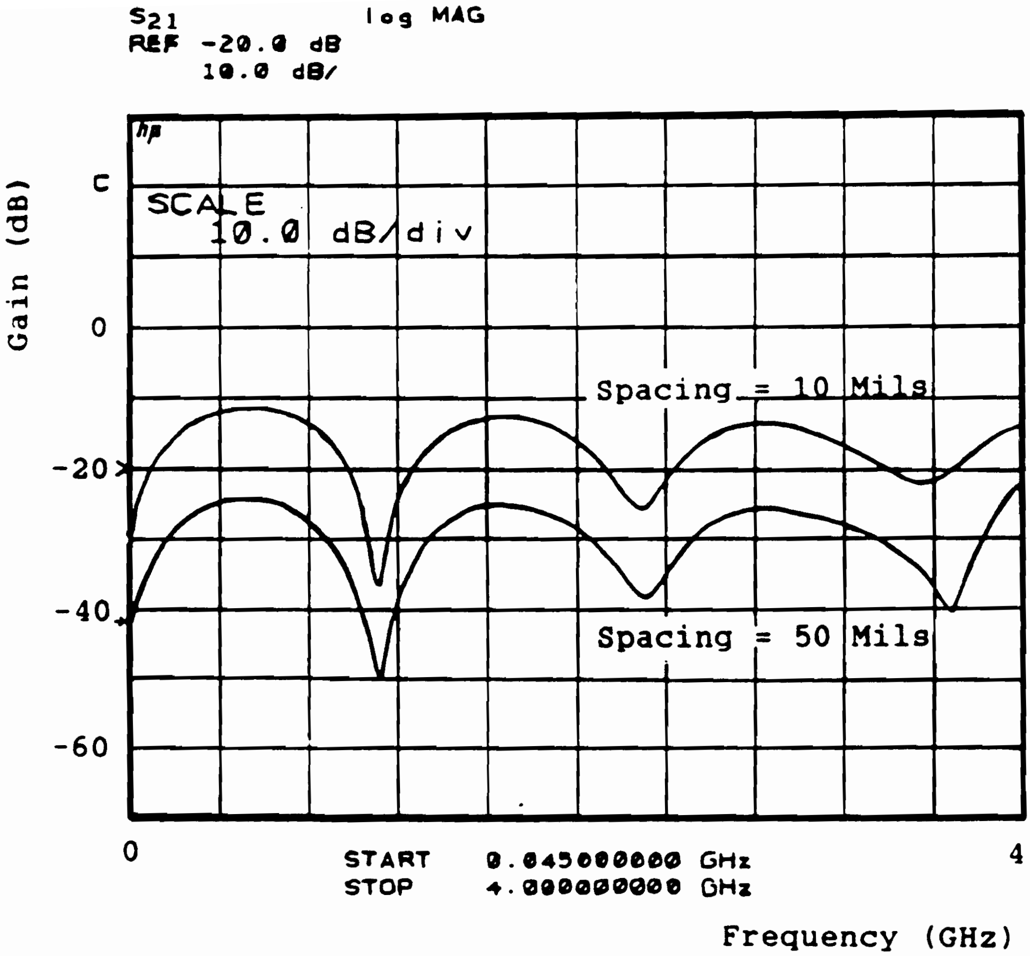

Figure 5.1 Measured S21 of The Structures, (Length = 2000 mils)

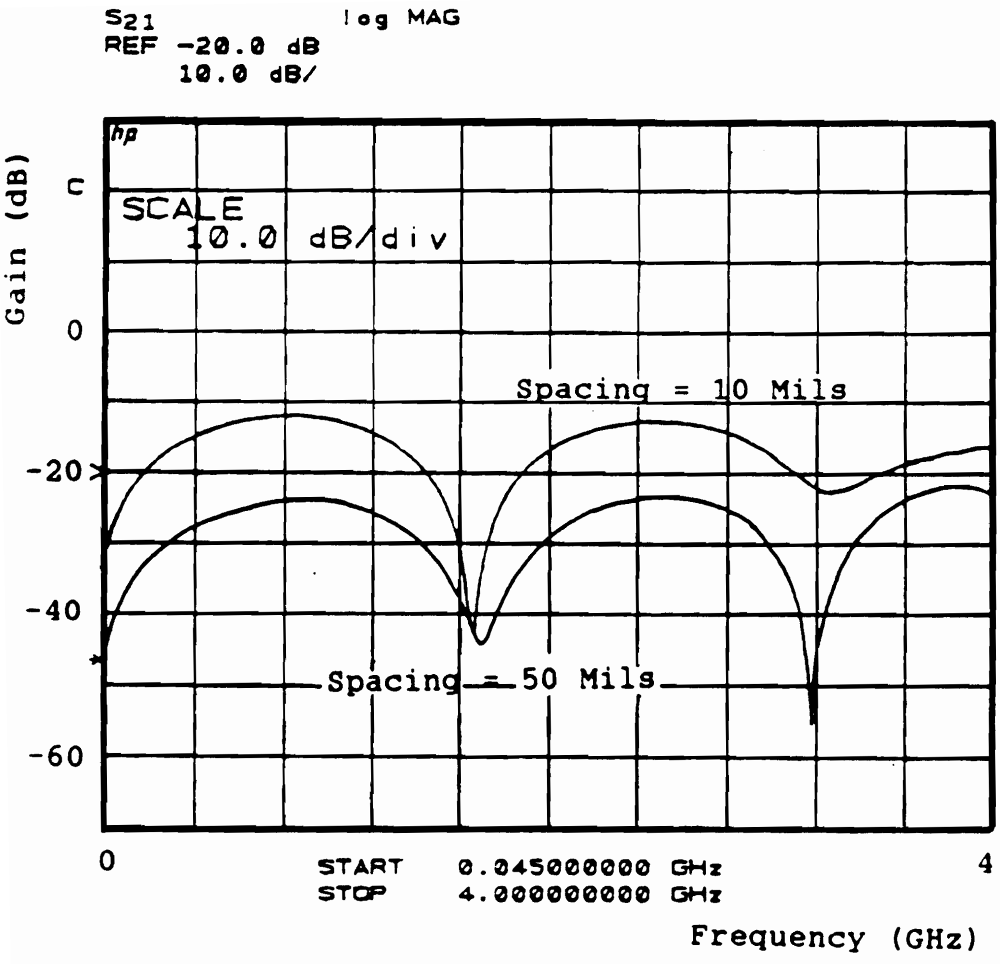

Figure 5.2 Measured S21 of The Structures,

(Length = 1400 mils)

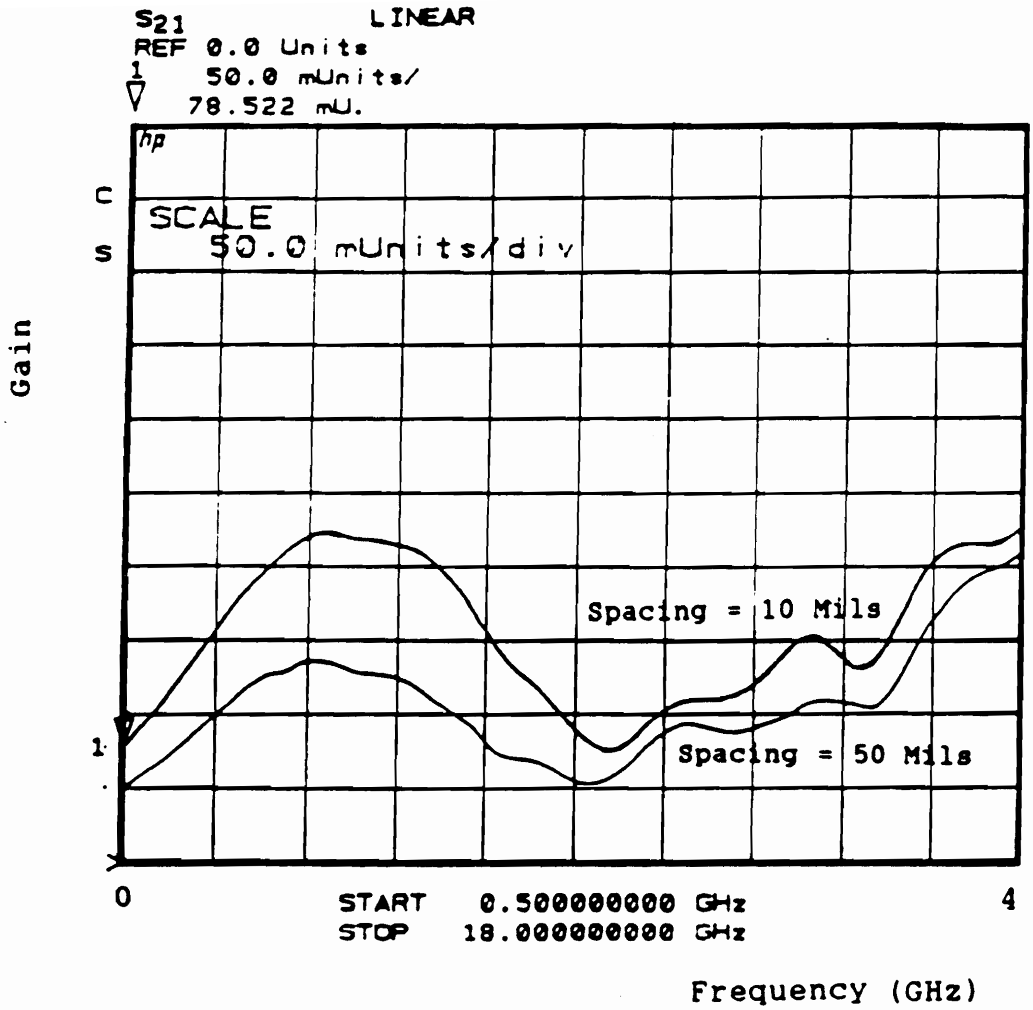

Figure 5.3 Measured S21 of The Structures,

(Length = 228 mils)

Ch.1 = 80 mVolts/div Offset = 200.0 mVolts
Ch.4 = 5 mVolts/div Offset = 16.50 mVolts
Timebase = 200 ps/div Delay = 25.00 ns

Figure 5.4 Measured Crosstalk Signal at Port 2,

(Length = 2000 mils, Spacing = 10 mils)

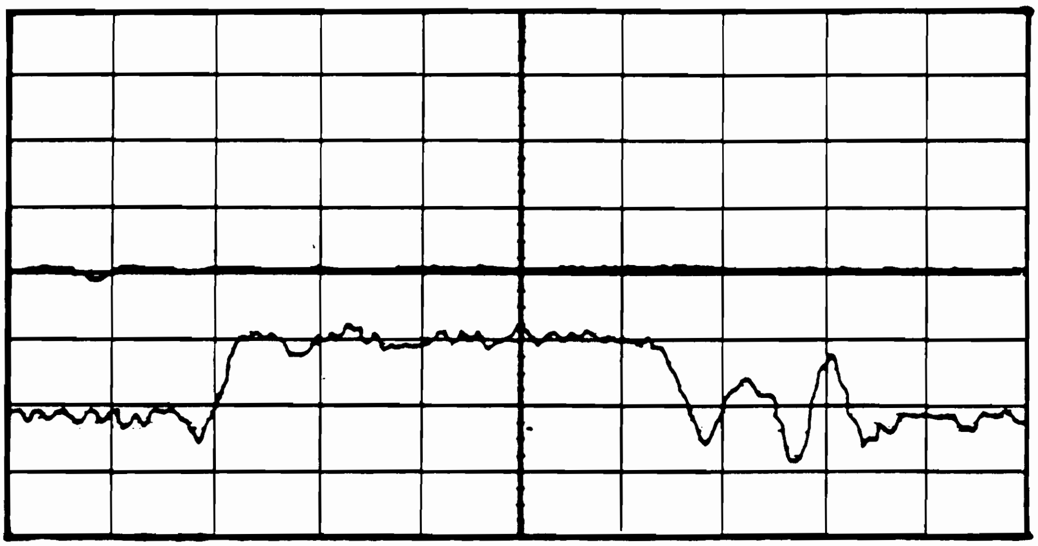

Ch.1 = 80 mVolts/div Offset = 200.0 mVolts
Ch.4 = 5 mVolts/div Offset = 16.50 mVolts
Timebase = 200 ps/div Delay = 25.00 ns

Figure 5.5 Measured Crosstalk Signal at Port 2,

(Length = 2000 mils, Spacing = 50 mils)

Ch.1 = 80 mVolts/div Offset = 200.0 mVolts
Ch.4 = 5 mVolts/div Offset = 16.50 mVolts
Timebase = 200 ps/div Delay = 24.57 ns

Figure 5.6 Measured Crosstalk Signal at Port 2,

(Length = 1400 mils, Spacing = 10 mils)

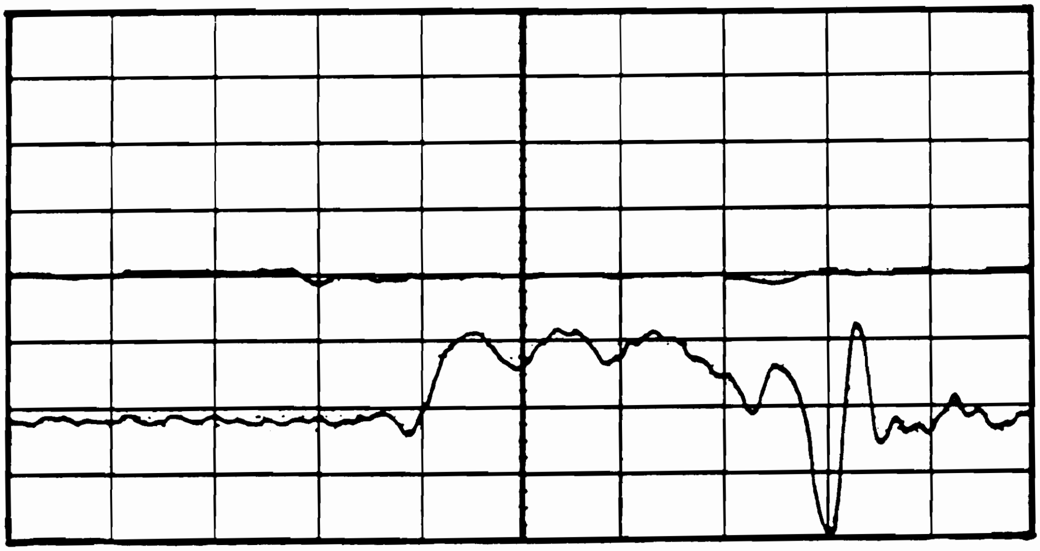

Ch.1 = 80 mVolts/div Offset = 200.0 mVolts
Ch.4 = 5 mVolts/div Offset = 16.50 mVolts
Timebase = 200 ps/div Delay = 24.57 ns

Figure 5.7 Measured Crosstalk Signal at Port 2,
(Length = 1400 mils, Spacing = 50 mils)

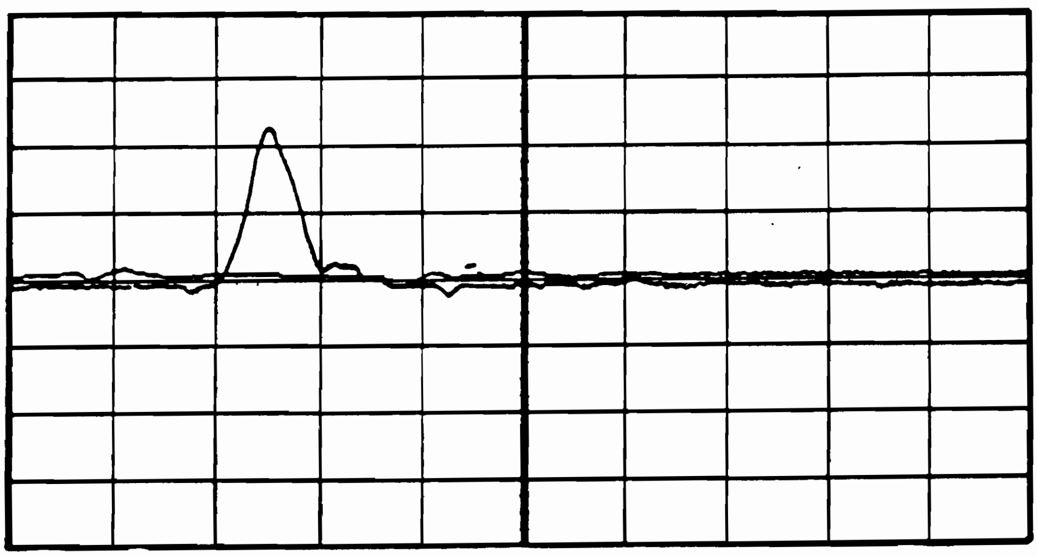

Ch.1 = 80 mVolts/div Offset = 200.0 mVolts
Ch.4 = 10 mVolts/div Offset = 3.0 mVolts
Timebase = 200 ps/div Delay = 25.00 ns

Figure 5.8 Measured Crosstalk Signal at Port 2,

(Length = 228 mils, Spacing = 10 mils)

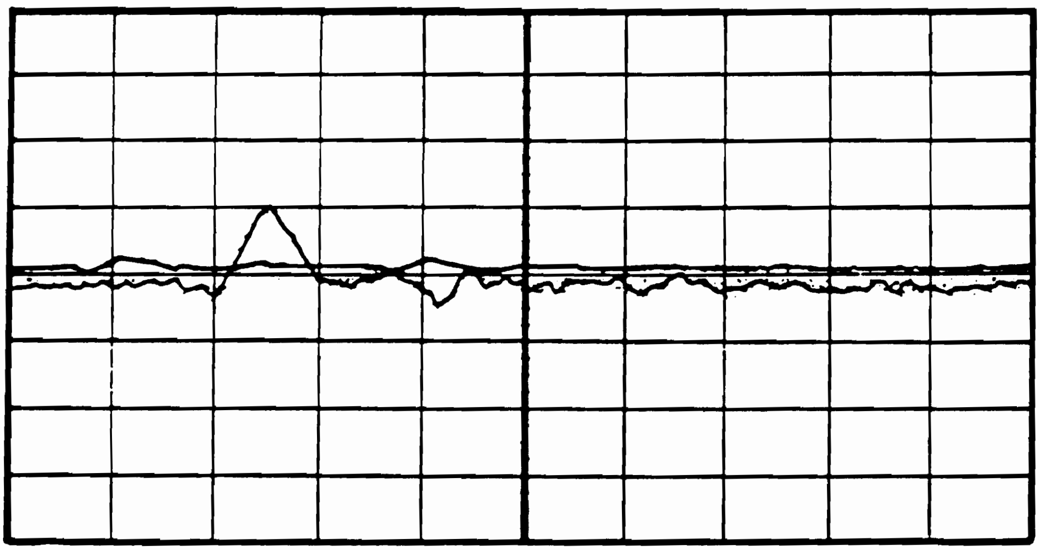

Ch.1 = 80 mVolts/div Offset = 200.0 mVolts
Ch.4 = 5 mVolts/div Offset = 3.0 mVolts
Timebase = 200 ps/div Delay = 25.00 ns

Figure 5.9 Measured Crosstalk Signal at Port 2,

(Length = 228 mils, Spacing = 50 mils)

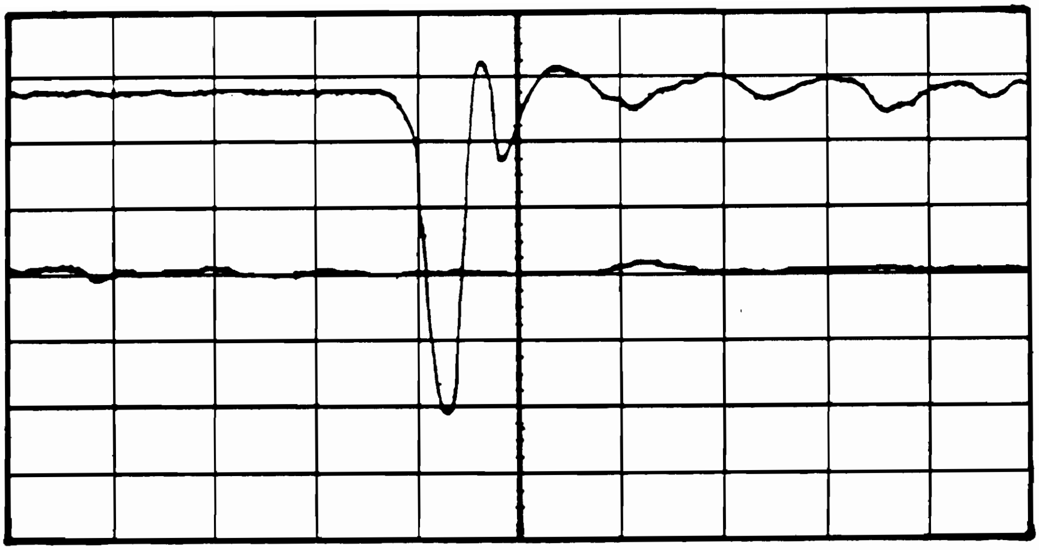

Ch.1 = 80 mVolts/div   Offset = 200.0 mVolts
Ch.4 = 10 mVolts/div   Offset = -22.0 mVolts
Timebase = 200 ps/div   Delay = 25.00 ns

Figure 5.10 Measured Crosstalk Signal at Port 3,

(Length = 2000 mils, Spacing = 10 mils)

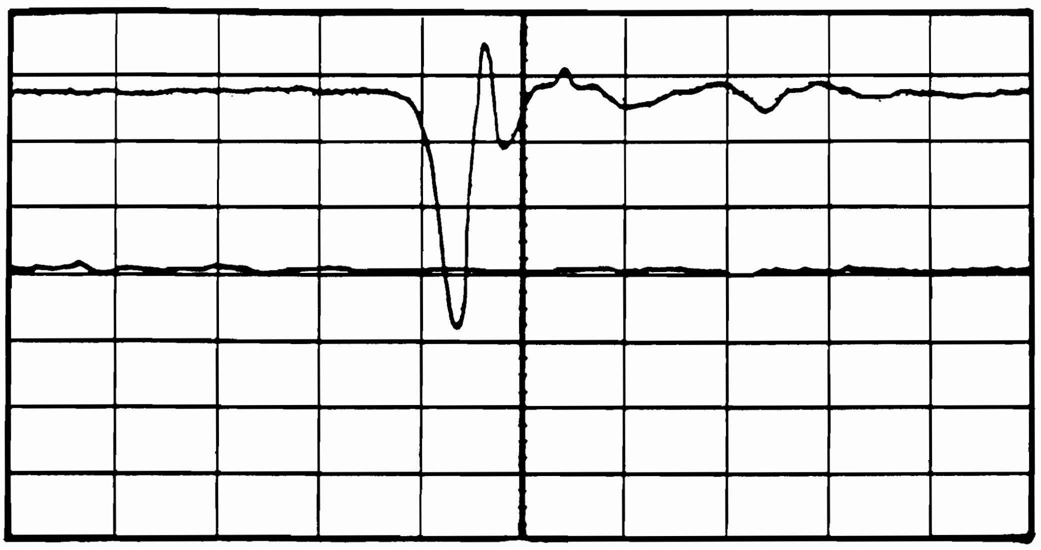

Ch.1 = 80 mVolts/div   Offset = 200.0 mVolts
Ch.4 = 10 mVolts/div   Offset = -22.0 mVolts
Timebase = 200 ps/div   Delay = 25.00 ns

Figure 5.11 Measured Crosstalk Signal at Port 3,

(Length = 2000 mils, Spacing = 50 mils)

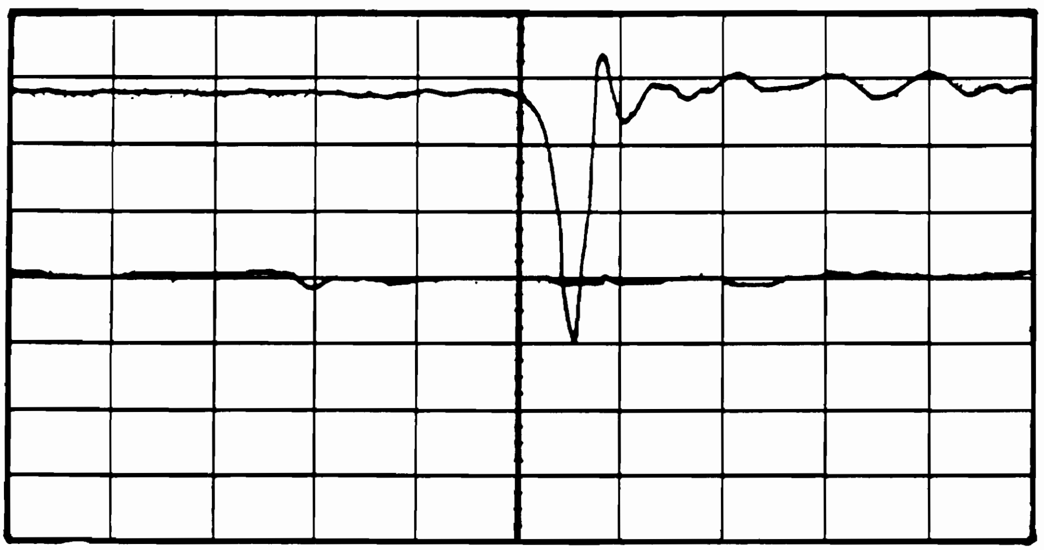

Ch.1 = 80 mVolts/div Offset = 200.0 mVolts
Ch.4 = 10 mVolts/div Offset = -22.0 mVolts
Timebase = 200 ps/div Delay = 24.57 ns

Figure 5.12 Measured Crosstalk Signal at Port 3,
(Length = 1400 mils, Spacing = 10 mils)

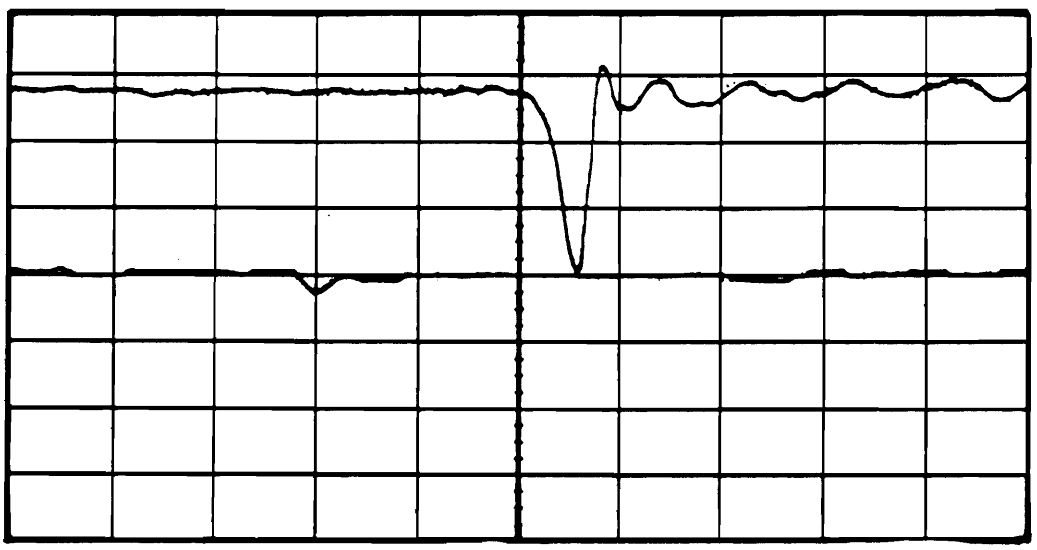

Ch.1 = 80 mVolts/div   Offset = 200.0 mVolts
Ch.4 = 10 mVolts/div   Offset = -22.0 mVolts
Timebase = 200 ps/div   Delay = 24.57 ns

Figure 5.13 Measured Crosstalk Signal at Port 3,
(Length = 1400 mils, Spacing = 50 mils)

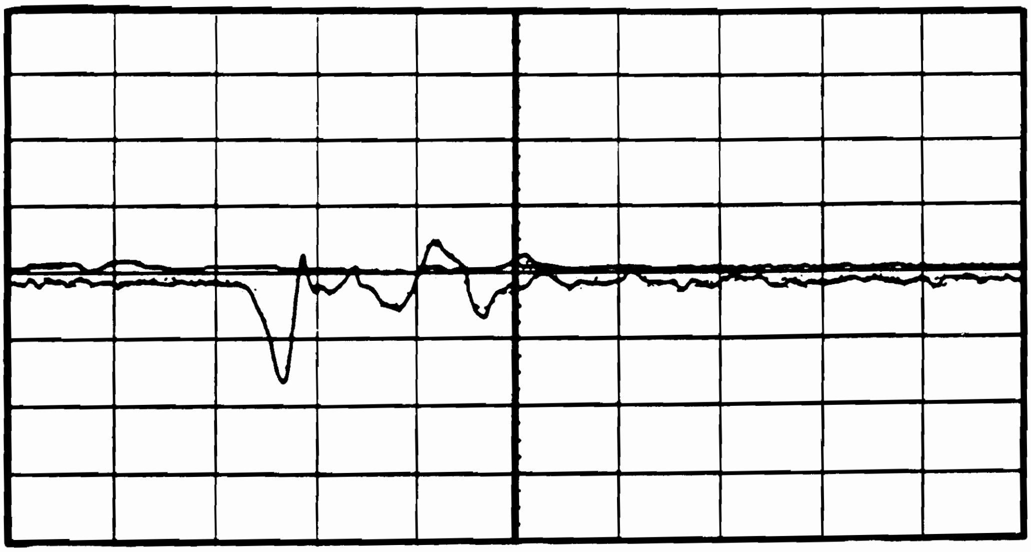

Ch.1 = 80 mVolts/div	Offset = 200.0 mVolts
Ch.4 = 5 mVolts/div	Offset = 3.0 mVolts
Timebase = 200 ps/div	Delay = 25.00 ns

Figure 5.14 Measured Crosstalk Signal at Port 3,
(Length = 228 mils, Spacing = 10 mils)

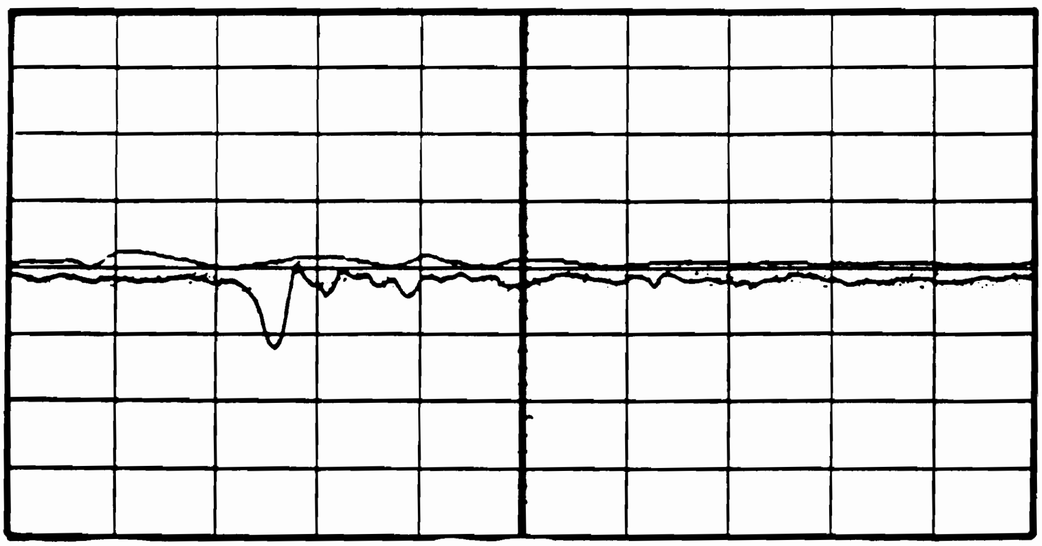

```
Ch.1 = 80 mVolts/div        Offset = 200.0 mVolts
Ch.4 =  5 mVolts/div        Offset =   3.0 mVolts
Timebase = 200 ps/div       Delay  = 25.00 ns
```

Figure 5.15 Measured Crosstalk Signal at Port 3,

(Length = 228 mils, Spacing = 50 mils)

5.2 Different Loss lines

Metal used in microwave applications must carry high frequency signal with minimum materials losses as possible. This metal may be used as a conductor for a circuit. The value of conductivity is used to indicate how well the circuit can carry signal or current. For example, the conductivities of silver, copper, gold, aluminum, and indium are of the order 6.30×10^7 mho/meter, 5.85×10^7 mho/meter, 4.25×10^7 mho/meter, 3.50×10^7 mho/meter, 1.11×10^7 mho/meter, respectively. Silver is the best conductor and indium is the worst selection of these metallizations. These bulk values are expected to vary in film form.

Verification

The effect of loss lines is investigated in order to verify the crosstalk noise model in this section. In this work, a set of experimental circuits having the same geometry is investigated. The line length is taken equal to 1400 mils. The actual realization of the structure is performed using conventional thick film printing technique on alumina substrates, as well as selective copper cladded teflon-ceramic duriod composite substrates. The conductors for the thick film process are chosen to be DuPont Ag 6160 and DuPont Ag-Pd 6134. The fabrication procedures using DuPont Ag 6160 and DuPont Ag-Pd 6134 conductors in thick film process is shown in Chapter 4, while that using selective etching of copper cladded teflon-ceramic duriod composite substrates is the same procedure as shown in Section 5.1. Measurements are conducted using frequency domain techniques and time domain techniques. The experimental results are shown in Figures (5.16) - (5.27). Figures (5.16) - (5.18) are shown the measured S21 of the circuits using Dupont Ag 6160 conductor, Dupont Ag-Pd 6134 conductor, copper cladded teflon-ceramic duriod composite substrates, respectively. Figures (5.19) - (5.21) show the measured S31 of those cases. Results show that the lines with different conductivity do not affect the crosstalk noise in the range of operation. In time domain measurements, the crosstalk noise waveforms are the same for all experimental circuits in this section. Figures (5.22) - (5.27) show the results of the crosstalk noise waveforms from the circuits made of Dupont Ag-Pd 6134 conductor where those from the circuits made of Dupont Ag 6160 are presented in Chapter 4 and those from the circuits made of copper cladded teflon-ceramic are presented in Section 5.1. Figure (5.28) Summarizes the measured S21 and S31 of the lines with different loss at operating frequency .8 GHz.

The conclusion is that the lines with different loss do not affect the crosstalk noise in the range of operation.

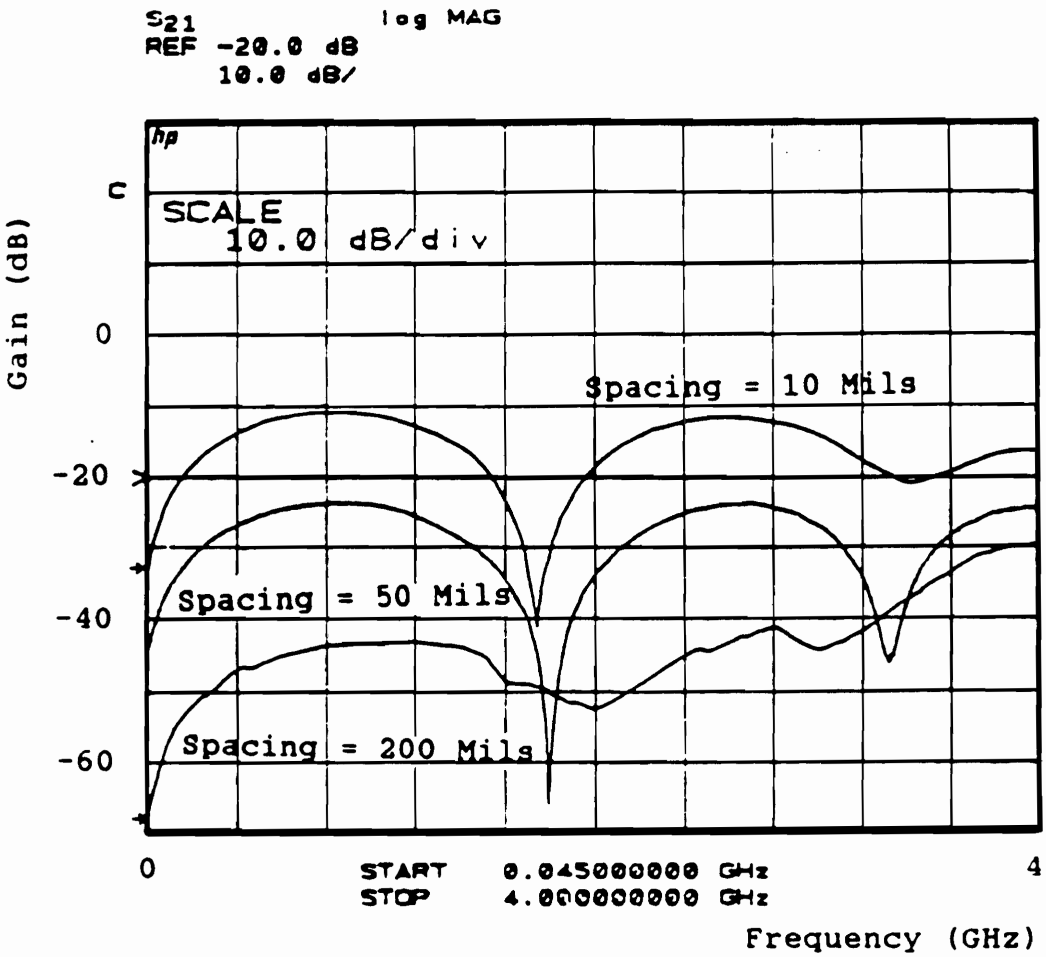

Figure 5.16 Measured S21 of The Structures,

(Made of Dupont Ag 6160 Conductor)

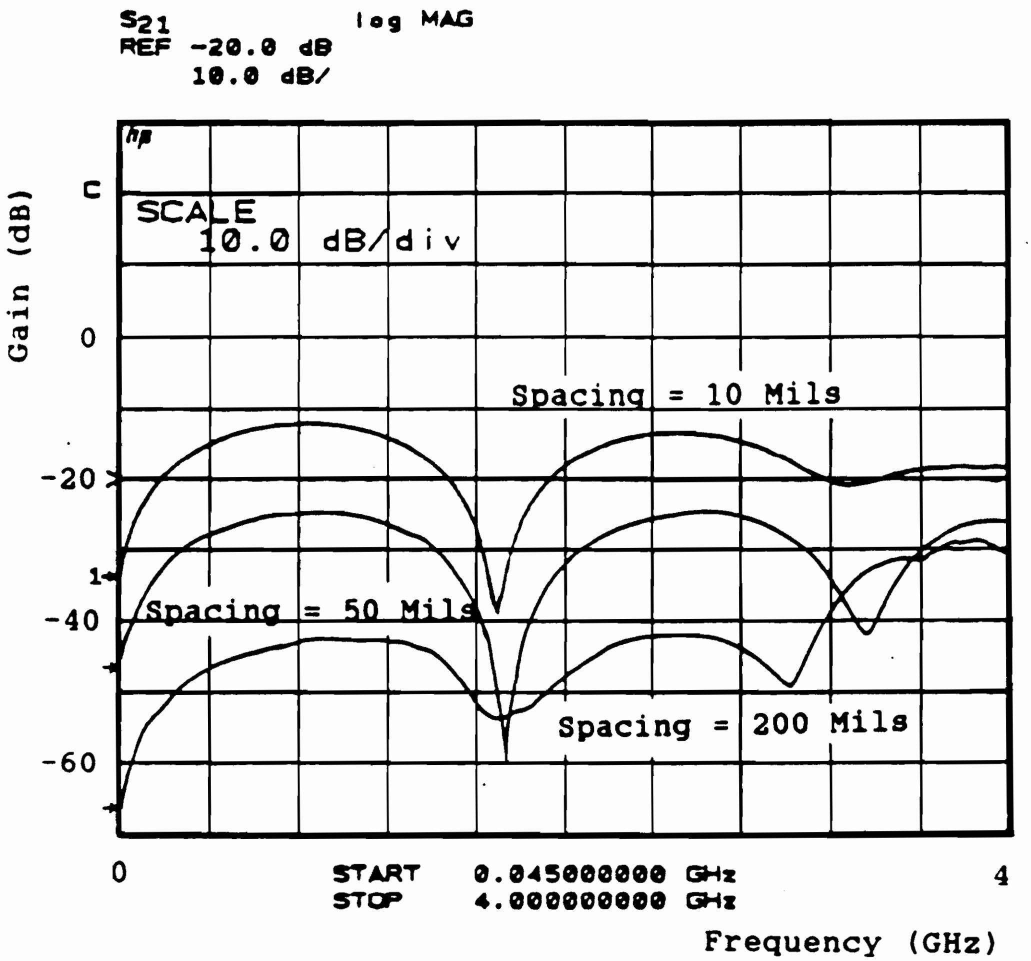

Figure 5.17 Measured S21 of The Structures, (Made of Dupont Ag-Pd 6134 Conductor)

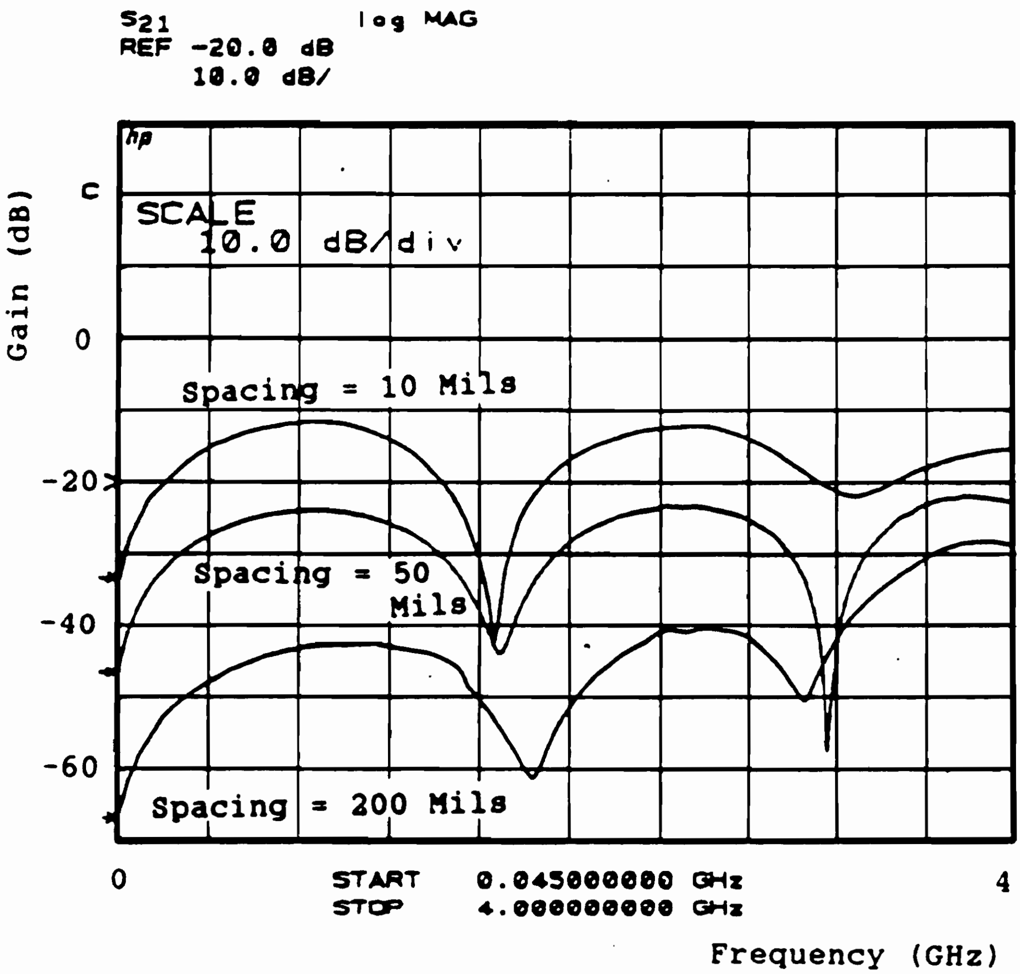

Figure 5.18 Measured S21 of The Structures, (Made of Copper Cladded Teflon-Ceramic Composites Duriod 6010)

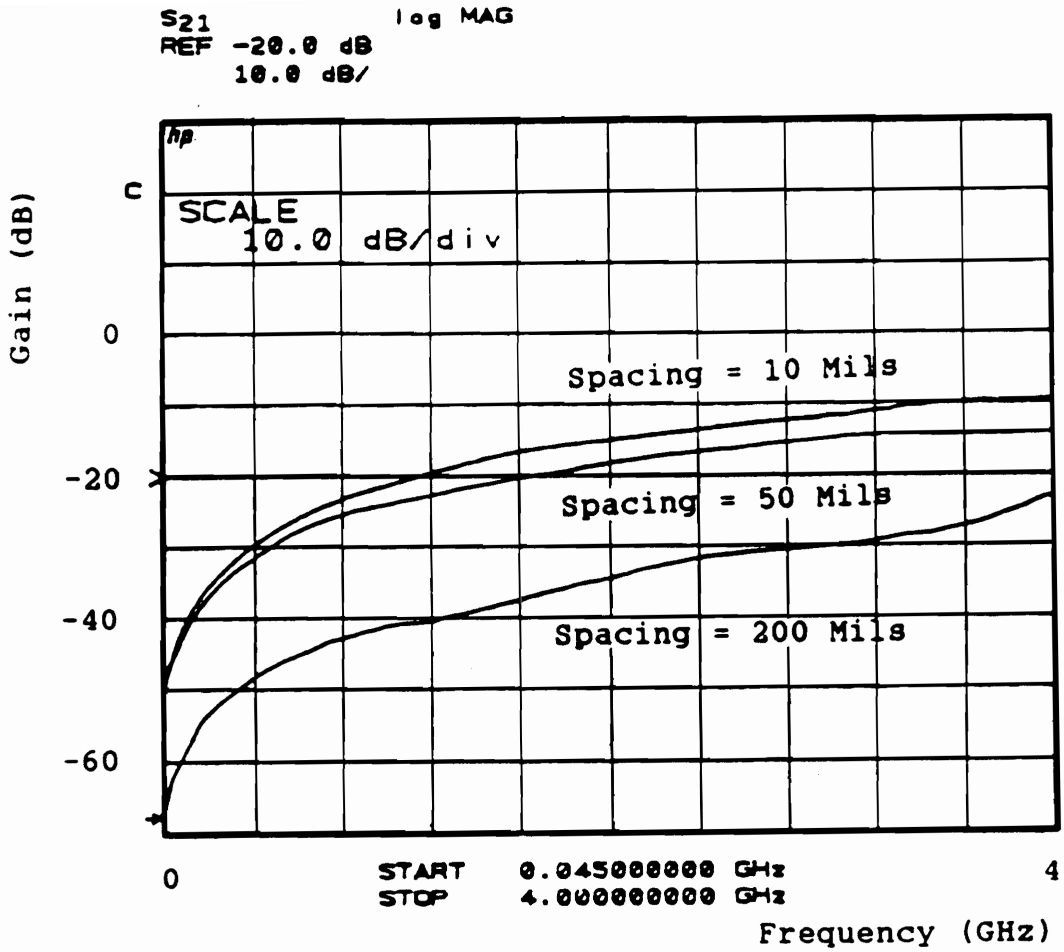

Figure 5.19 Measured S31 of The Structures, (Made of Dupont Ag 6160 Conductor)

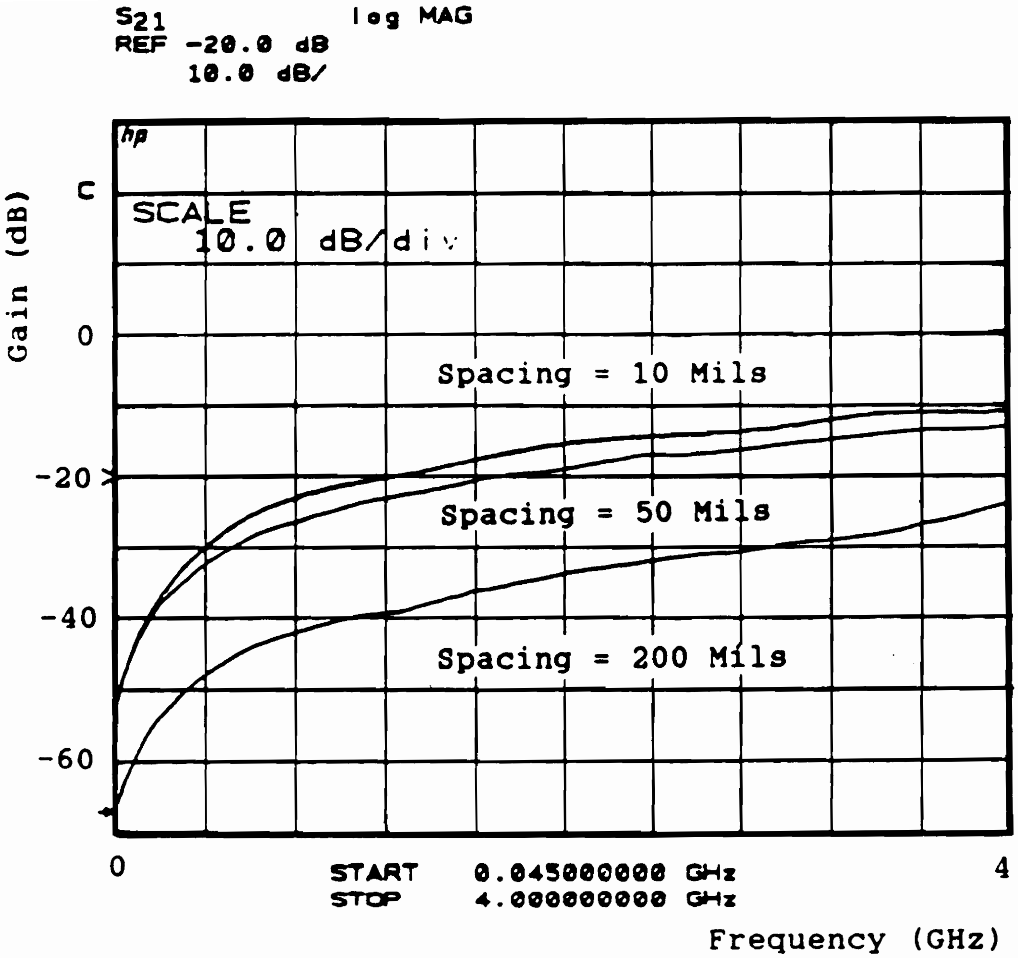

Figure 5.20 Measured S31 of The Structures,

(Made of Dupont Ag-Pd 6134 Conductor)

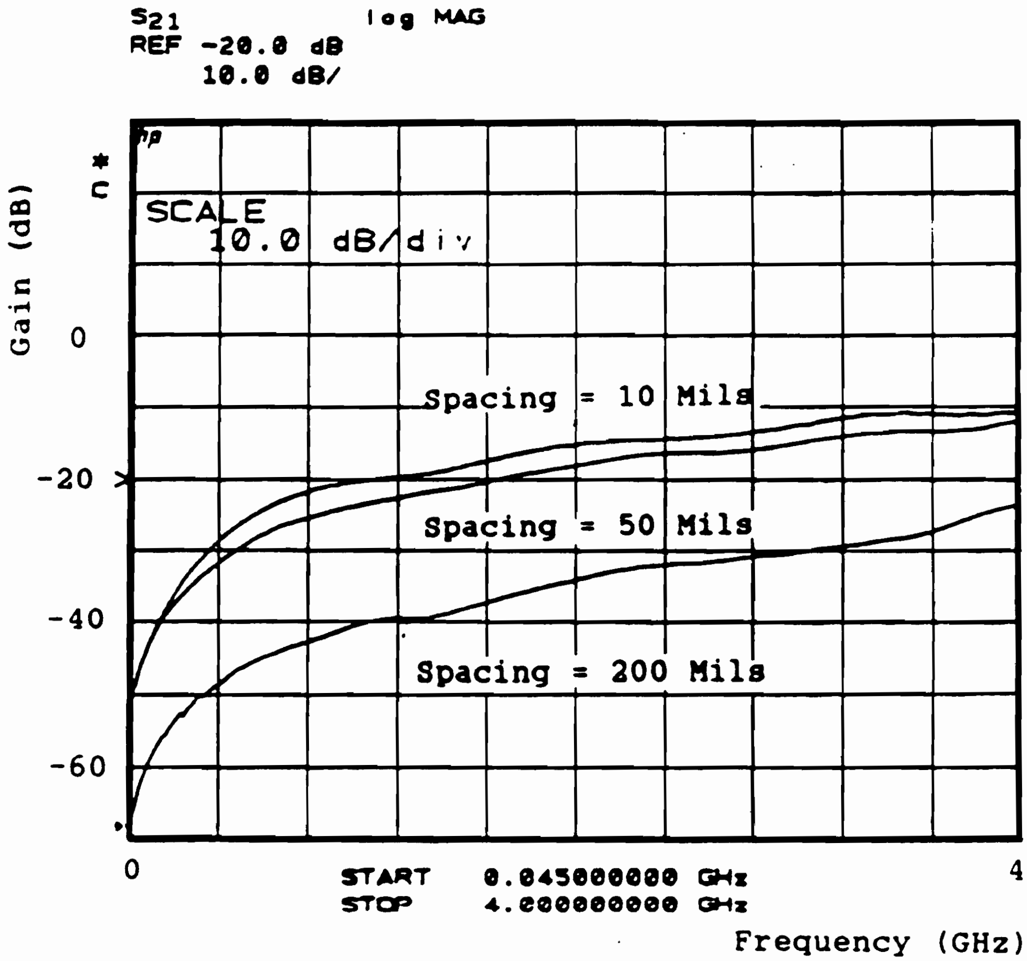

Figure 5.21 Measured S31 of The Structures, (Made of Copper Cladded Teflon-Ceramic Composites Duriod 6010)

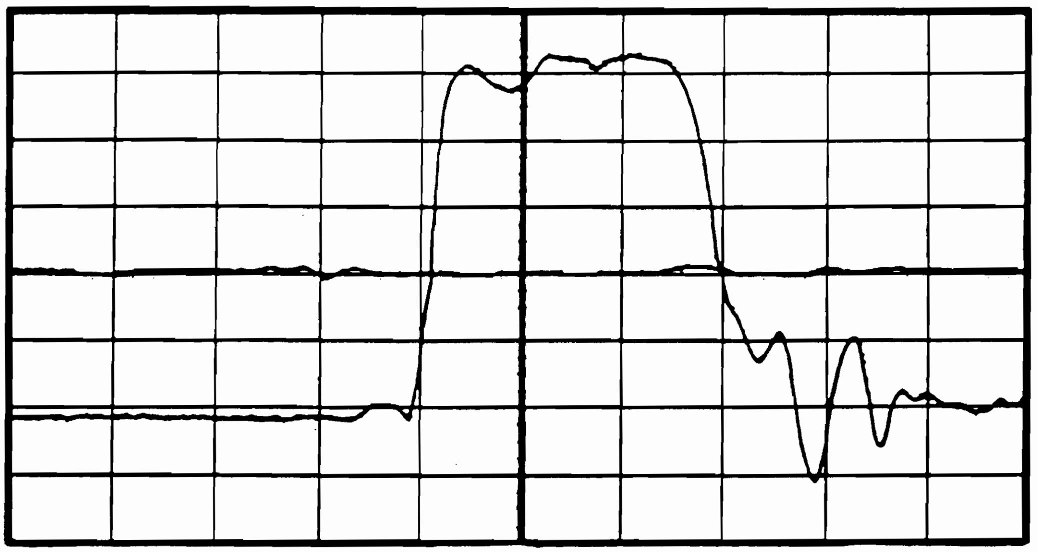

Ch.1 = 80 mVolts/div   Offset = 200.0 mVolts
Ch.4 = 5 mVolts/div   Offset = 16.50 mVolts
Timebase = 200 ps/div   Delay = 24.57 ns

Figure 5.22 Measured Crosstalk Signal at Port 2 of The Structure, (Made of Dupont Ag-Pd 6134 Conductor, Spacing = 10 mils)

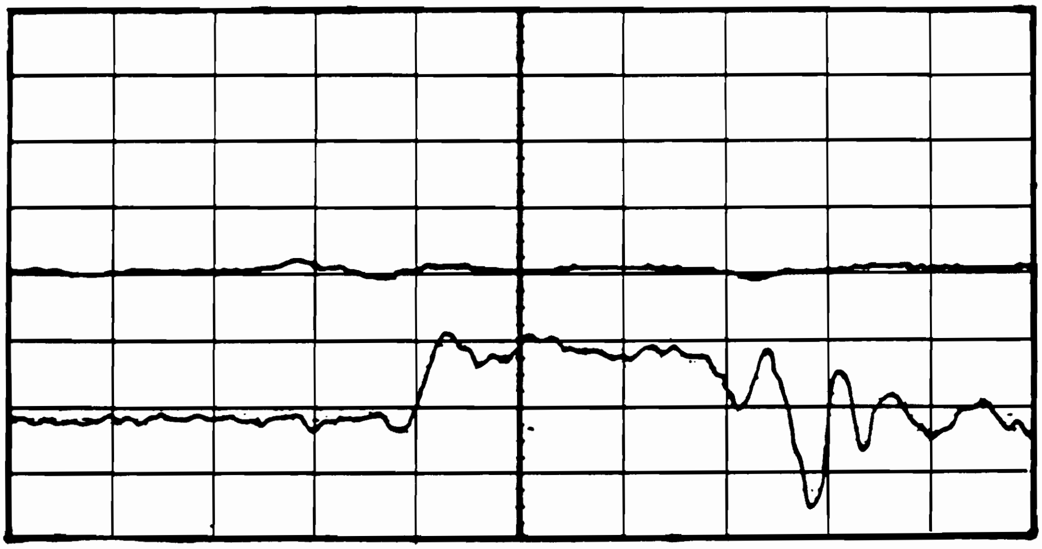

Ch.1 = 80 mVolts/div   Offset = 200.0 mVolts
Ch.4 = 5 mVolts/div   Offset = 16.50 mVolts
Timebase = 200 ps/div   Delay = 24.57 ns

Figure 5.23 Measured Crosstalk Signal at Port 2 of The Structure, (Made of Dupont Ag-Pd 6134 Conductor, Spacing = 50 mils)

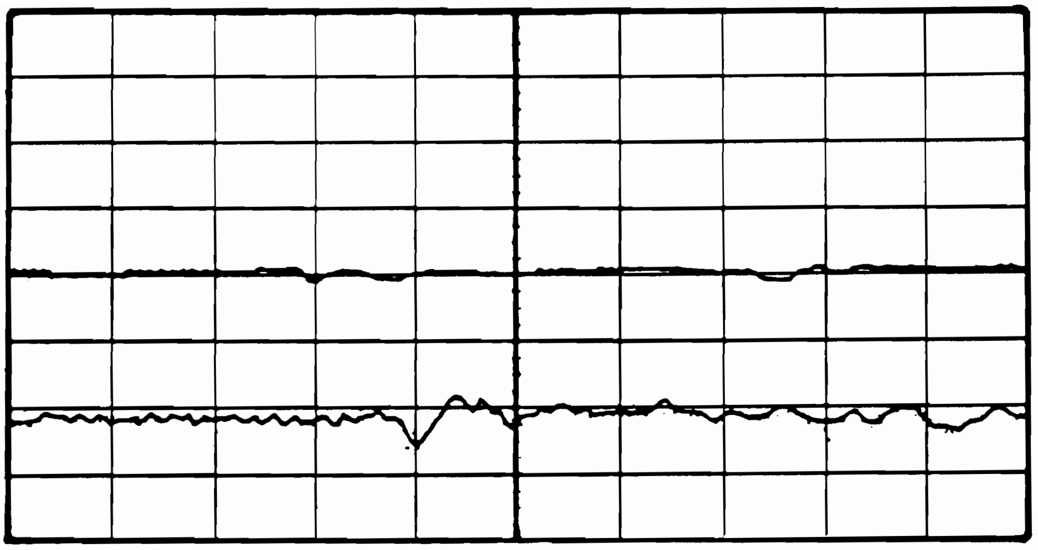

Ch.1 = 80 mVolts/div Offset = 200.0 mVolts
Ch.4 = 5 mVolts/div Offset = 16.50 mVolts
Timebase = 200 ps/div Delay = 24.57 ns

Figure 5.24 Measured Crosstalk Signal at Port 2 of The Structure, (Made of Dupont Ag-Pd 6134 Conductor, Spacing = 200 mils)

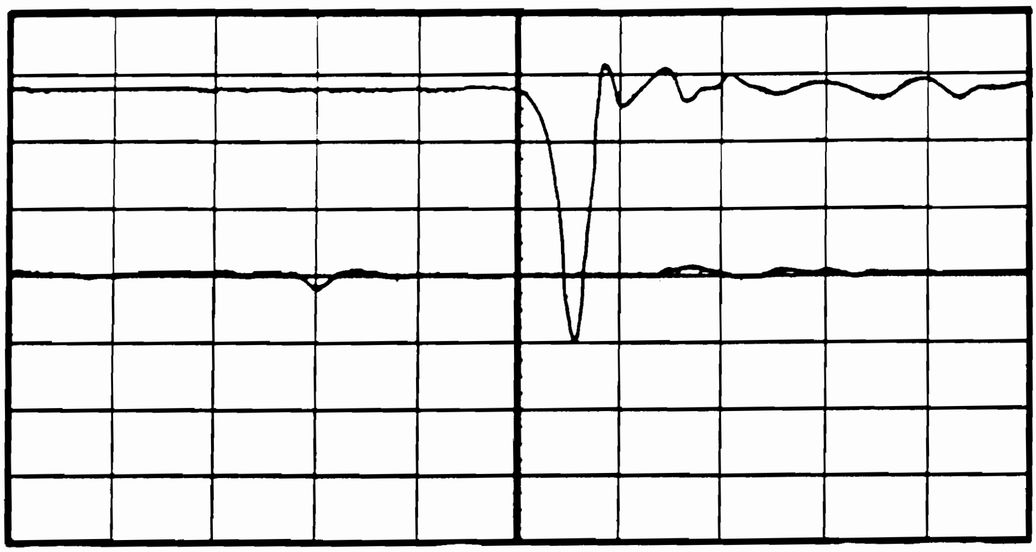

Ch.1 = 80 mVolts/div   Offset = 200.0 mVolts
Ch.4 = 10 mVolts/div   Offset = -22.0 mVolts
Timebase = 200 ps/div   Delay = 24.57 ns

Figure 5.25 Measured Crosstalk Signal at Port 3 of The Structure, (Made of Dupont Ag-Pd 6134 Conductor, Spacing = 10 mils)

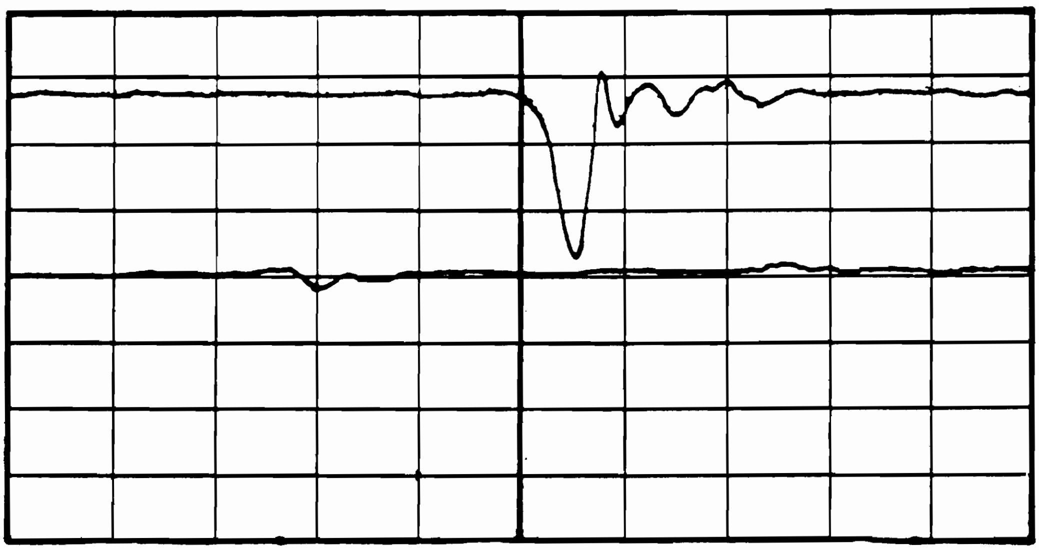

Ch.1 = 80 mVolts/div   Offset = 200.0 mVolts
Ch.4 = 10 mVolts/div   Offset = -22.0 mVolts
Timebase = 200 ps/div   Delay = 24.57 ns

Figure 5.26 Measured Crosstalk Signal at Port 3 of The Structure, (Made of Dupont Ag-Pd 6134 Conductor, Spacing = 50 mils)

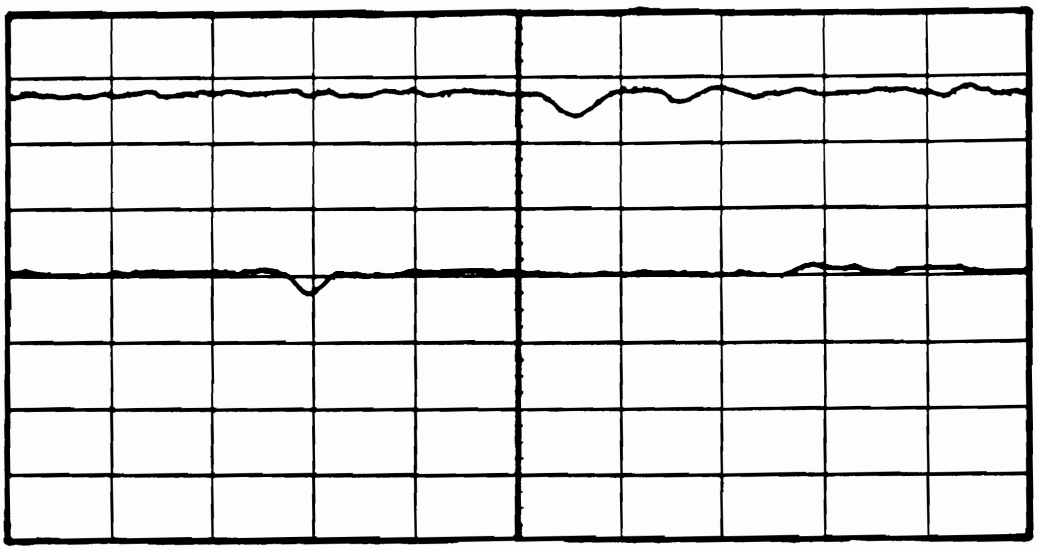

Ch.1 = 80 mVolts/div　　Offset = 200.0 mVolts
Ch.4 = 10 mVolts/div　　Offset = -22.0 mVolts
Timebase = 200 ps/div　　Delay = 24.57 ns

Figure 5.27 Measured Crosstalk Signal at Port 3 of The Structure, (Made of Dupont Ag-Pd 6134 Conductor, Spacing = 200 mils)

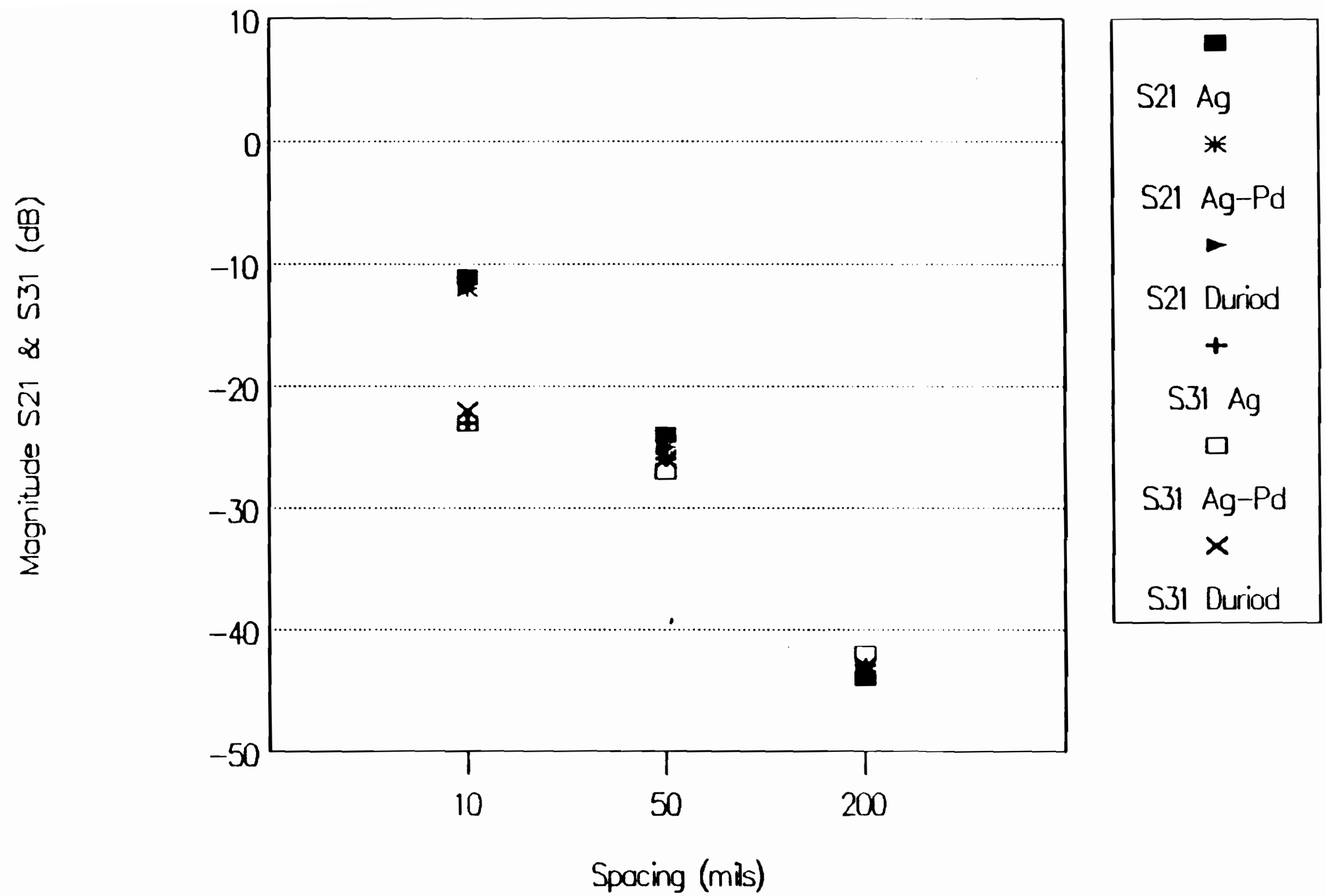

Figure 5.28 Summary of Measured S21 and S31 of Different Loss Lines at .8 GHz

5.3 Efficiency Test on Striplines

The mode of propagation along a stripline is transverse electromagnetic (TEM), where a pure TEM mode cannot propagate in a microstrip line as shown in Chapter 2. Since one of the most useful and widely applied stripline structure is the quarter-wave parallel coupled line, the purpose of this section is to test efficiency of this crosstalk noise model on stripline structures.

Verification

The line length is chosen to be 1400 mils. The materials used in this section is copper cladded teflon-ceramic duriod composite substrates. The fabrications of microstrip line circuits are made in Section 5.1. The results of measurements are shown in Section 5.1. In order to test efficiency of the model on stripline structures, the stripline circuits need to be fabricated. To obtain the stripline geometry, two laminates are used. The laminate A is the microstrip line circuit, used in Section 5.1, which is completely metallized on the bottom side and has two microstrip lines on the other side. The laminate B is metallized on the top and is clear of any metal on the bottom side. Both laminates are clamped together tightly for the stripline configuration.

To confirm the measurements results, Touchtone Software is used to simulate data related to frequency domain responses as shown in Figures (5.29)-(5.30). Because the mode of propagation along a stripline is transverse electromagnetic (TEM), the simulated frequency response at port 2, S21, has the same shape as those of port 3, S31. The magnitudes of S31 is less than those of S21 due to the loss. Figures (5.31) and (5.32) present the results of measured S21 and S31 of stripline circuits. The measurement results are close to the simulated ones of Figure (5.29) and (5.30). Comparing to the measurement results of microstrip line circuits in Figure (5.18)-(5.19), the frequency response of crosstalk noise in stripline structure is much less than in microstrip structure. At the operating frequency of .8 GHz, microstrip line circuits with spacing 10 mils and 50 mils give crosstalk noise, S21, more than those of stripline circuits 6 db and 12 dB, respectively. S31 cannot be compared with each other, due to the different mode of propagation. Since the mode of propagation along a stripline is TEM, the measured S21 and S31 have the same shape of response. Figures (5.33) - (5.36) present the crosstalk noise waveforms of stripline circuits in time domain measurements. Compared to those of microstrip line in Figures (5.5)-(5.6) and Figures (5.12)-(5.13), the crosstalk noise waveforms of stripline circuits are much smaller than those of microstip circuits and cannot be observed in the circuits with 50 mils spacing. The time domain waveforms at port 2 and port 3 have the same shape. This supports the results in frequency domain measurements that the mode of propagation in stripline structure is TEM. Since our crosstalk noise model is assumed the mode of propagation to be TEM mode in microstip line structure, the model gives a good agreement in stripline structure. One point to observe in Figures (5.33) - (5.36), the response in channel 1 is less than normal. It is due to the characteristic impedance of stripline circuit is less than that of microstrip circuit which is designed to be approximately 50 ohms. Figure (5.37) summarizes the simulated and measured S21 and S31 at operating frequency, .8 GHz.

Based on the simulation and measurements results, we can conclude that the model gives a good agreement for stripline structures.

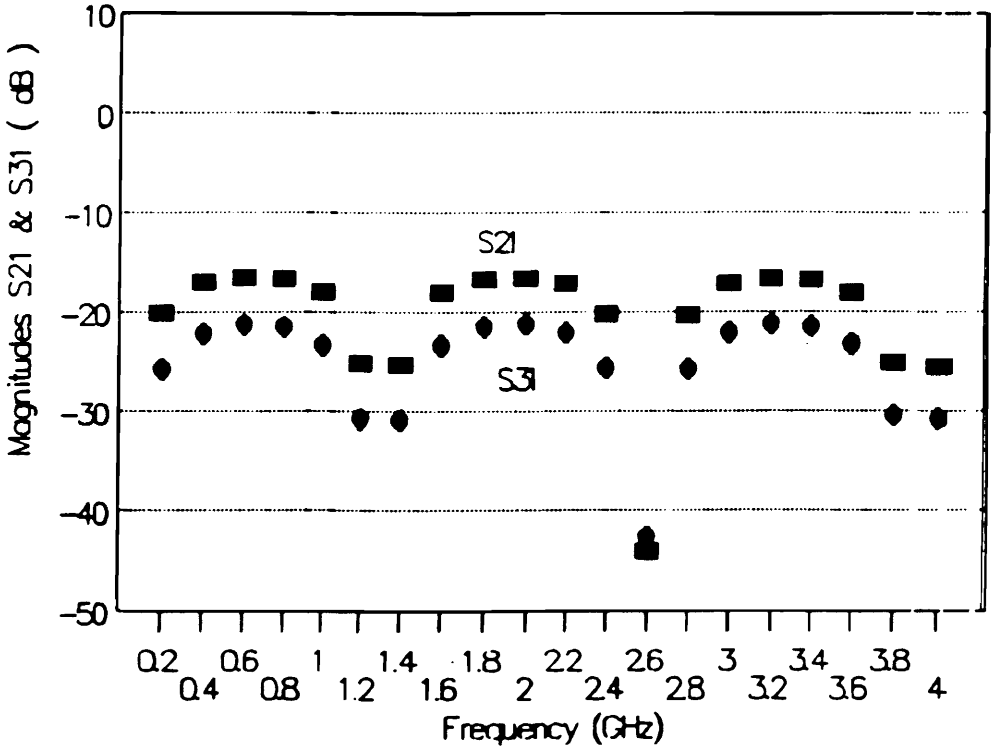

Figure 5.29 Simulated S21 and S31 of The Stripline Structure, (Spacing = 10 mils)

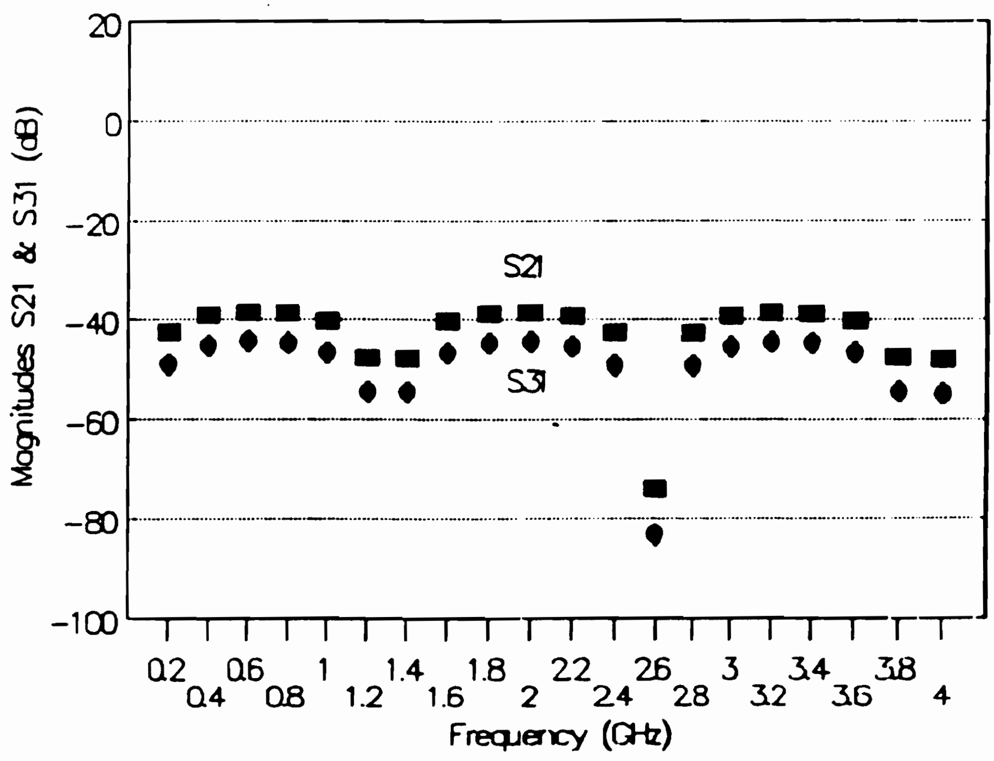

Figure 5.30 Simulated S21 and S31 of The Stripline Structure, (Spacing = 50 mils)

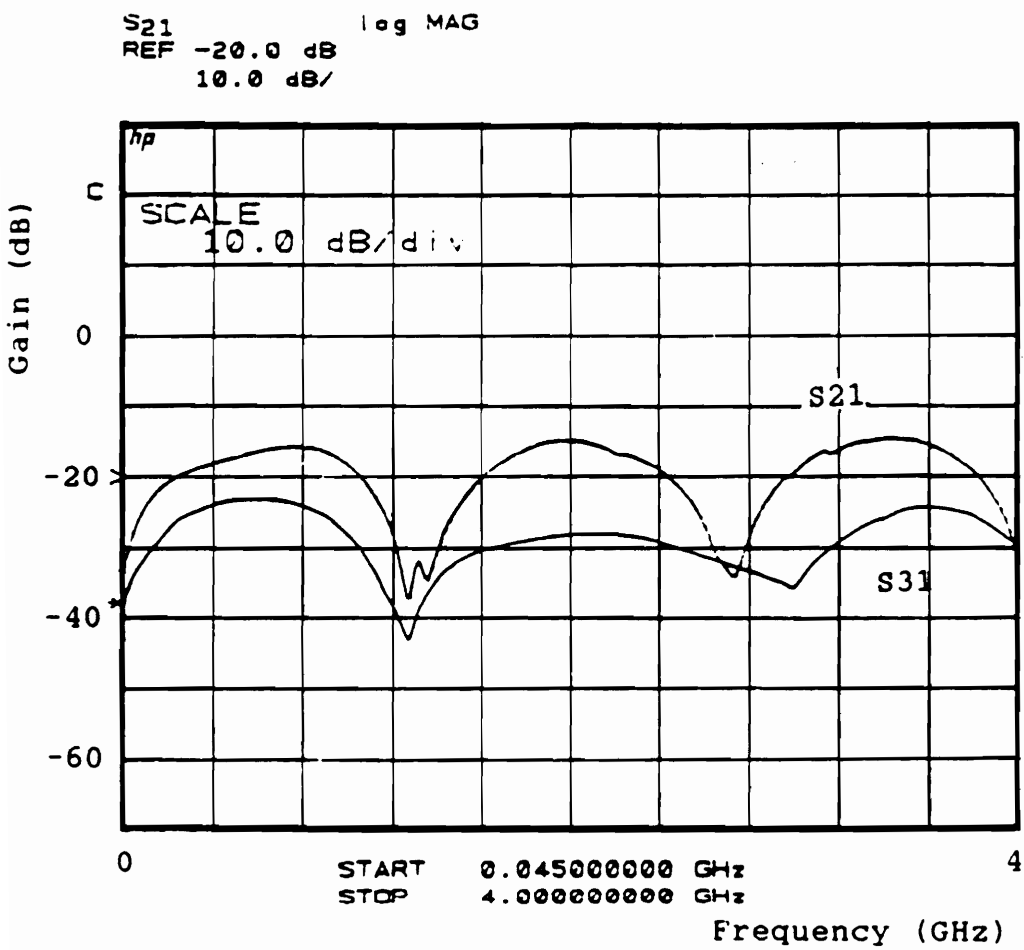

Figure 5.31 Measured S21 and S31 of The Stripline Structure, (Spacing = 10 mils)

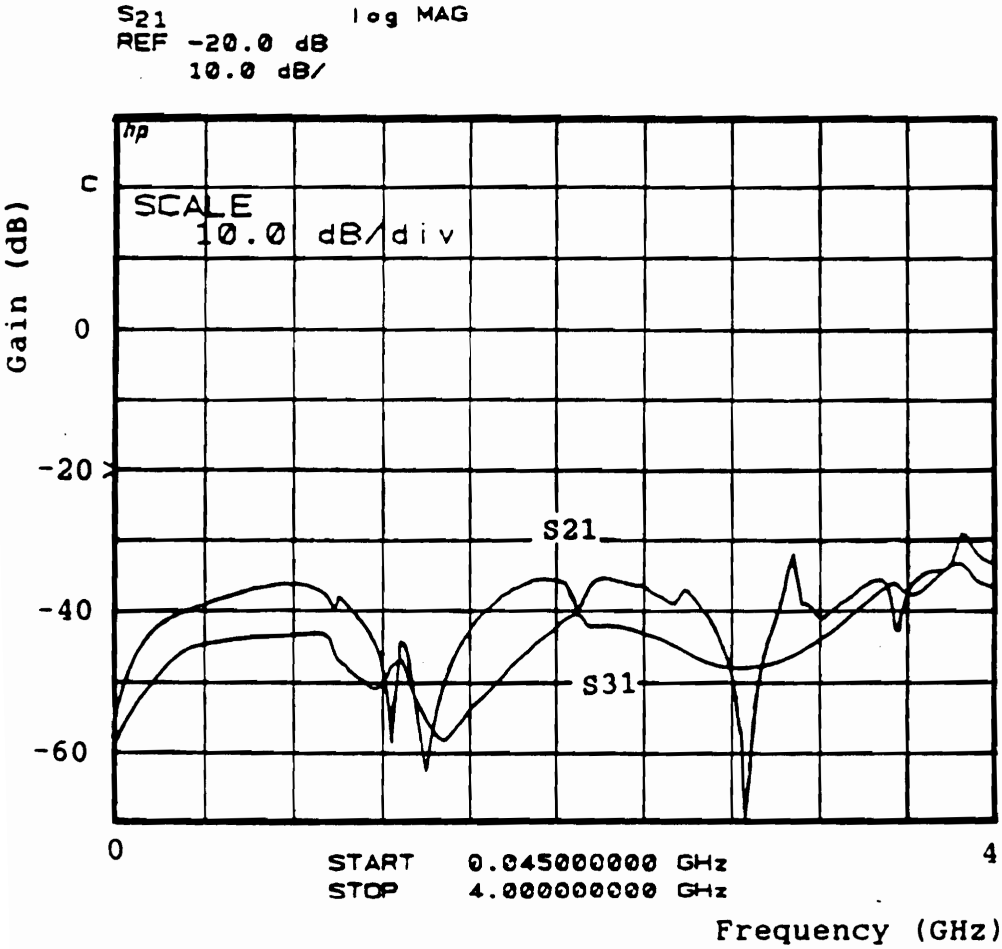

Figure 5.32 Measured S21 and S31 of The Stripline Structure, (Spacing = 50 mils)

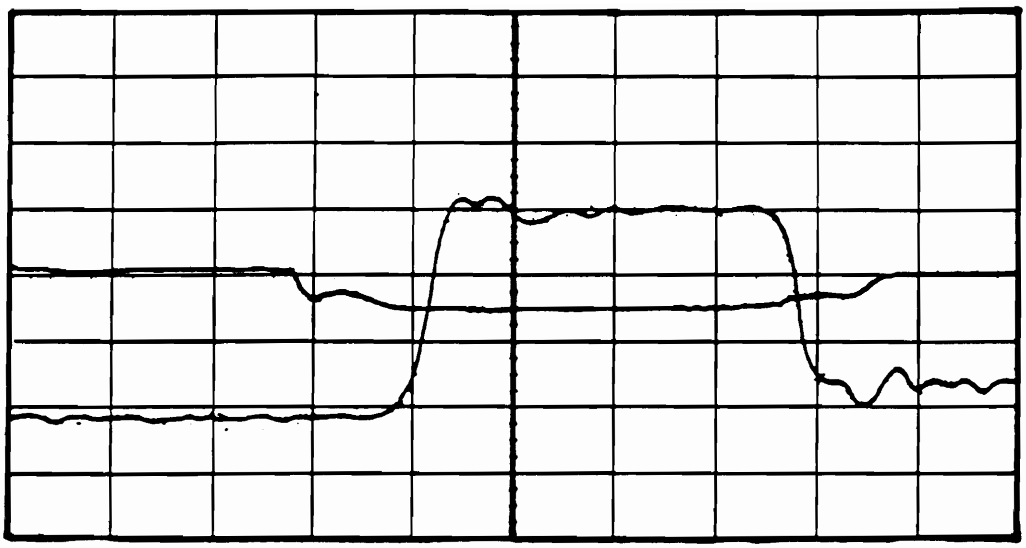

Ch.1 = 80 mVolts/div   Offset = 200.0 mVolts
Ch.4 = 5 mVolts/div   Offset = 16.50 mVolts
Timebase = 200 ps/div   Delay = 24.57 ns

Figure 5.33 Measured Crosstalk Signal at Port 2 of The Stripline Structure, (Spacing = 10 mils)

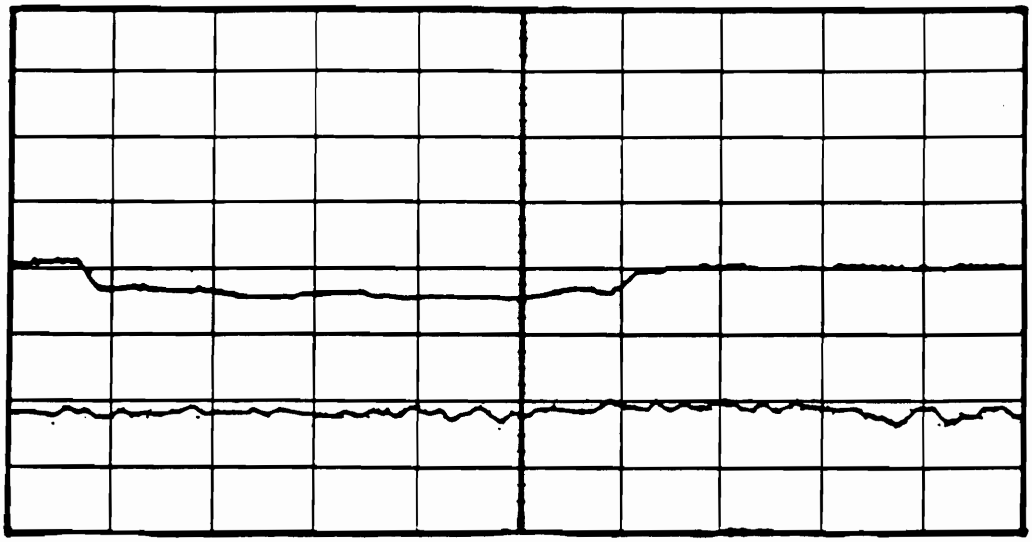

Ch.1 = 80 mVolts/div Offset = 200.0 mVolts
Ch.4 = 5 mVolts/div Offset = 16.50 mVolts
Timebase = 200 ps/div Delay = 25.00 ns

Figure 5.34 Measured Crosstalk Signal at Port 2 of The Stripline Structure, (Spacing = 50 mils)

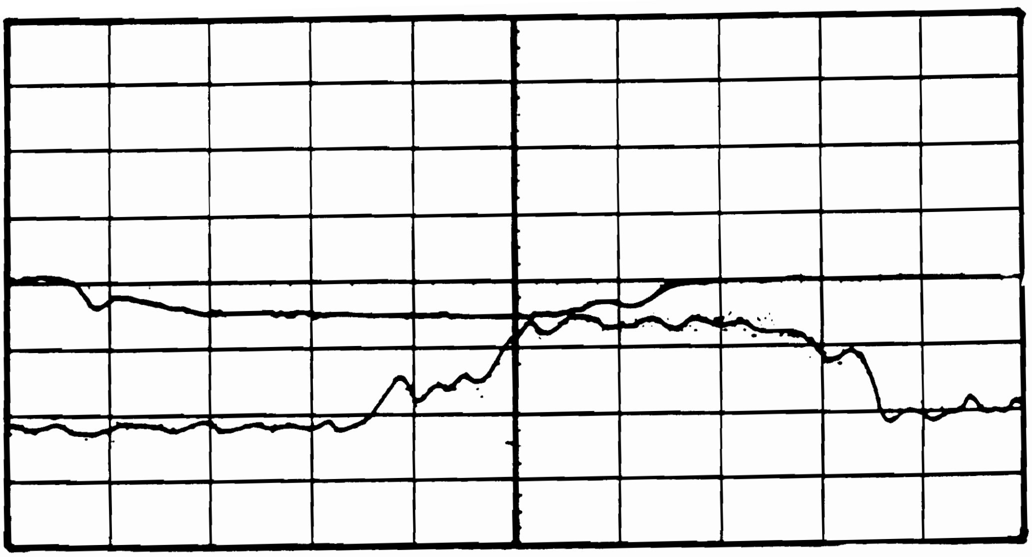

Ch.1 = 80 mVolts/div
Ch.4 = 5 mVolts/div
Timebase = 200 ps/div

Offset = 200.0 mVolts
Offset = 16.50 mVolts
Delay = 25.00 ns

Figure 5.35 Measured Crosstalk Signal at Port 3 of The Stripline Structure, (Spacing = 10 mils)

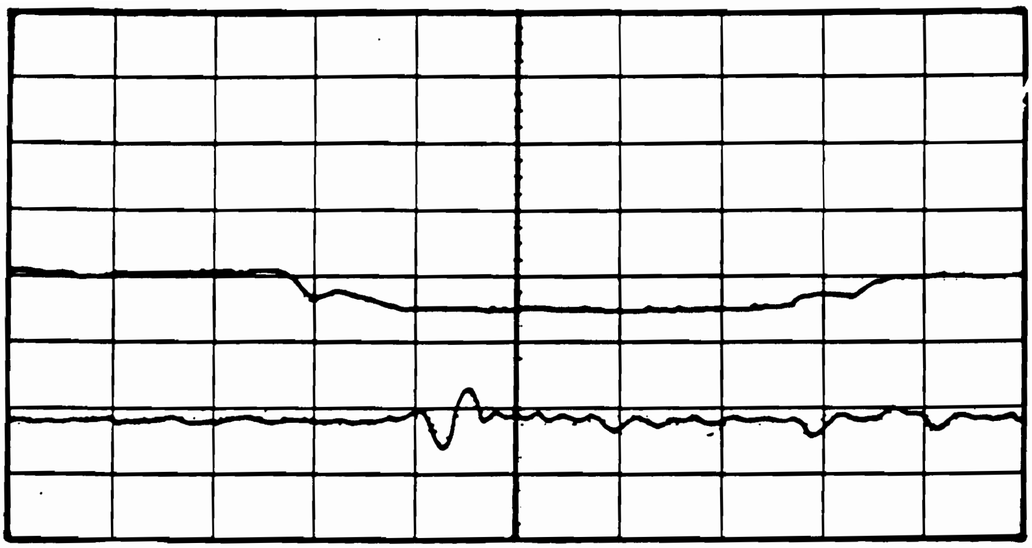

Ch.1 = 80 mVolts/div   Offset = 200.0 mVolts
Ch.4 = 5 mVolts/div   Offset = 16.50 mVolts
Timebase = 200 ps/div   Delay = 24.57 ns

Figure 5.36 Measured Crosstalk Signal at Port 3 of The Stripline Structure, (Spacing = 50 mils)

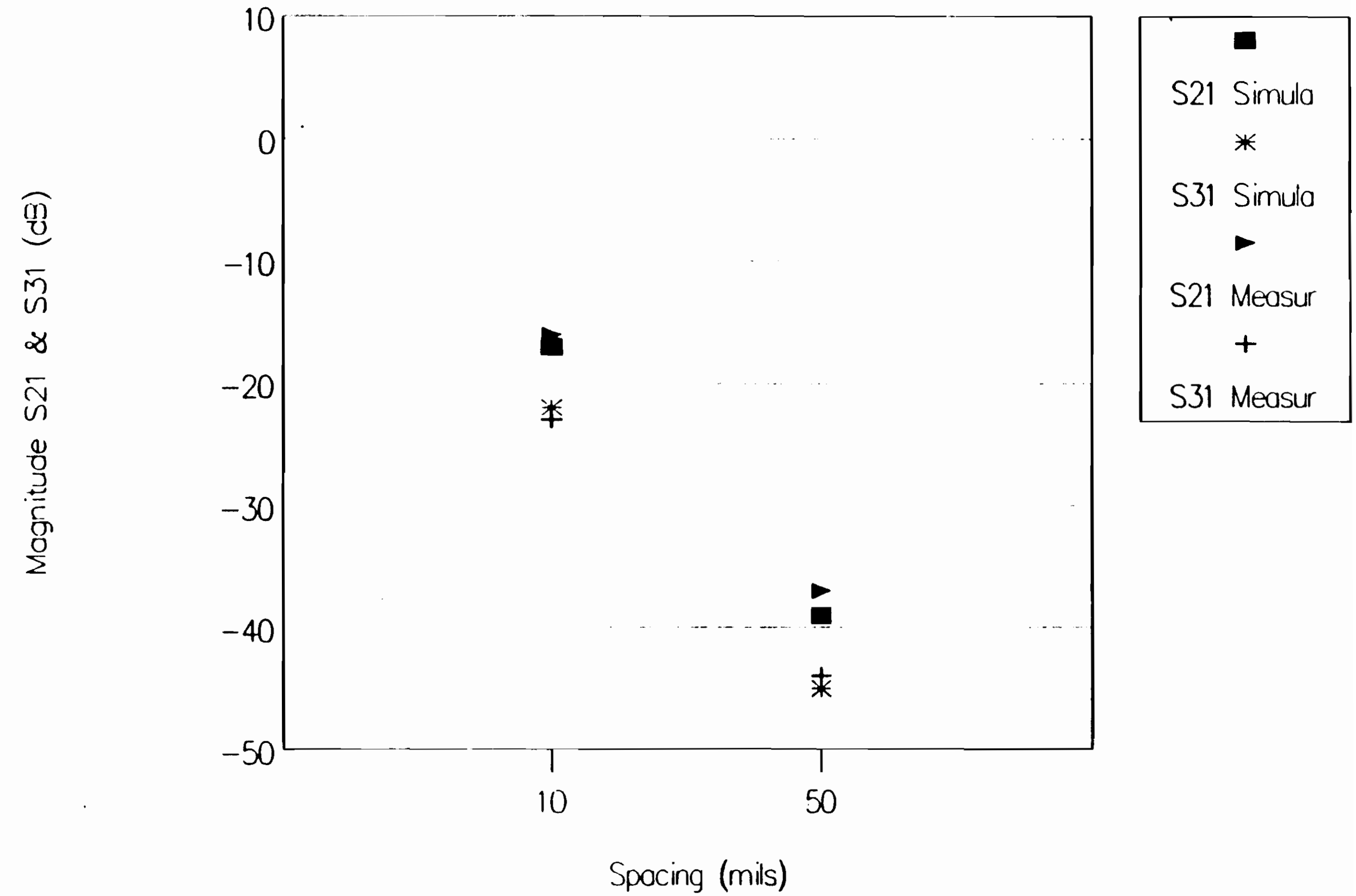

Figure 5.37 Summary of Simulated and Measured S21 and S31 of The Stripline Structures at .8 GHz

5.4 Summary

To confirm the model, the verifications model of crosstalk noise in some aspects such as, different line length, various metallization types, and efficiency test on striplines are presented. The results show that the model is suitable to these criterions. The model matches closely the experimental data in both the time domain and the frequency domain using time domain and frequency domain measurement techniques, respectively.

CHAPTER 6

CONCLUSION

The objective of this dissertation was to characterize the crosstalk noise based on the theory of coupled microstrip lines. A review covering the development of the techniques used to characterize and model crosstalk noise was discussed in Chapter 2. The theoretical background needed to develop crosstalk noise equivalent circuit model was included. An equivalent circuit model used in this work comprised of the addition of inductances and capacitances to the fundamental transmission line model. The analysis of the lines characteristics was carried out, assuming the propagation mode to be TEM mode. Characterization of crosstalk noise along adjacent lines, current-voltage characteristics, characteristic impedance, effective dielectric impedance, and maximum crosstalk was performed analytically. Computer simulation and computations of these parameters were also performed. MAXWELL Software was used to simulate data of physically based equivalent circuit model. The data was used to determine the characterization of crosstalk noise. TOUCHSTONE Software was used to simulate the data on crosstalk noise on adjacent lines in frequency domain, where SPICE Software was used to simulate the data in time domain. The circuits were also realized experimentally using both conventional thick film printing technique on alumina substrates, as well as selective etching of copper-cladded teflon-ceramic duriod composite substrates. An investigation of the crosstalk noise in both the frequency domain and the time domain using various measurement techniques was performed. The results illustrated that the computation matches closely the experimental data.

The HP 8510 network analyzer was used to acquire the characteristics of crosstalk noise in frequency domain forms. The measured S21 and S31 match closely the simulated S21 and S31. At the operating frequency, the measured S21 and S31 were the same as the simulated ones and the measured S21 gave maximum crosstalk which met the purpose of the design. As spacing increased, the measured S21 and S31 decreased.

The HP 5412 digitizing oscilloscope mainframe was used to acquire the characteristics of crosstalk noise in time domain forms. The measured waveforms of near-end and far-end crosstalk noise matched the simulated waveforms. As the spacing increased, the size of crosstalk noise waveforms decreased. Variability encountered in the fabrication process can cause some small deviations in the inductance, mutual inductance, capacitance, and mutual capacitance values of the actual circuits.

Verifications model of crosstalk noise in some aspects, such as, different line length, various metallizations, and efficiency test on striplines were also presented. The results showed that the model was suitable to meet the specified criteria. The model closely matched the experimental data in both time domain and frequency domain. The line length was used to determine the operating frequency. As the line length increased, the bandwidth of crosstalk noise waveforms increased. The various metallizations gave no difference at this operating frequency of 0.8 GHz. The model can also be applied to the stripline structure since the propagation mode on stripline structure was TEM.

It is concluded that the computation of the equivalent circuit model used in this work can successfully represent crosstalk noise on adjacent lines and explains the physical phenomena better.

BIBLIOGRAPHY

1. Ahmad, M., Characterization and Modeling of Thick Film Components for Hybrid Microwave Integrate Circuits, Ph.D. Dissertation, Virginia Polytechnic Institute and State University, Blacksburg, Virginia, Aug. 1984.
2. Alexopoulos, N.G., Integrated - Circuit Structure on Anisotropic Substrates, IEEE Trans. Microwave Theory and Techniques, Vol. MTT-33, No. 10, pp. 847-881, Oct. 1985.
3. Al-Mazroo, A.Y., Characterization and Modeling of Magnetic Materials and Structures, Ph.D. Dissertation, Virginia Polytechnic Institute and State University, Blacksburg, Virginia, Dec. 1988.
4. Atwater, H.A., Tests of Microstrip Dispersion For mulas, IEEE Trans. Microwave Theory and Techniques, Vol. 36, No. 3, pp. 619-621, Mar. 1988.
5. Babu, G.R. and Banmali, Measurement of Coupled Microstrip Line Parameters, International Journal of Electronics, Vol. 45, No. 5, pp. 551-560, 1978.
6. Bahl, I.J. and P. Bhartia, Microwave Solid State Circuit Design, John Wiley & Sons, New York, 1988.
7. Bahl, I.J. and R. Garg, Simple and Accurate Formulas For Microstrip with Finite Strip Thickness, Proc. IEEE, Vol. 65, pp. 1611-1612, Nov. 1977.

8. Bailey, A.E., Microwave Measurement, Peter Peregrinus Ltd., London, England, 1985.

9. Bakoglu, H.B. and J.D. Meindl, Optimal Interconnection Circuits for VLSI, IEEE Trans. Electron Devices, Vol. ED-32, pp. 903-909, May 1985.

10. Brews, J.R., Characteristic Impedance of Microstrip Lines, IEEE Trans. Microwave Theory and Techniques, Vol. MTT-35, No. 1, pp. 30-34, Jan. 1987.

11. Bryant, T.G., and J.A. Weiss, Parameters of Microstrip Transmission Lines of Coupled Pairs of Microstrip Lines, IEEE Trans. Microwave Theory and Techniques, Vol. MTT-16, No. 12, pp. 1021-1027, Dec. 1968.

12. Buris, N.E. and D.D. Stancil, Magnetostatic Surface Wave Propagation in Ferrite Thin Films with Arbitrary Variations of the Magnetization Through the Film Thickness, IEEE Trans. Microwave Theory and Techniques, Vol. MTT-33, No. 6, pp. 484-491, June 1985.

13. Catt, I., Crosstalk (Noise) in Digital Systems, IEEE Trans Electronic Computers, Vol. EC-16, No. 6, pp. 743-763, Dec. 1967.

14. Caulton, M., J.J. Hughes, and H. Sobol, Measurements on the Properties of Microstrip Transmission Lines for Microwave Integrated Circuits, RCA Review, Vol. 27, pp. 377-391, 1966.

15. Chang, F.Y., Transient Analysis of Lossless Coupled Transmission Lines in a Nonhomogeneous Dielectric Medium, IEEE Trans Microwave Theory and Techniques, Vol. MTT-18, No. 9, pp. 616-626, Sept. 1970.

16. Chatterjee, R., Elements of Microwave Engineering, John Wiley & Sons, New York, 1986.

17. Cohn, S.B., Problems in Strip Transmission Line, IRE Trans. Microwave Theory and Techniques, Vol. MTT-3, pp. 119-126, Mar. 1955.

18. Cohn, S.B., Shielded Coupled Strip Transmission Line, IRE Trans. Microwave Theory and Techniques, Vol. MTT-3, pp. 29-38, Oct 1955.

19. Connolly, J.B., Cross Coupling in High Speed Digital Systems, IEEE Trans. Electronic Computers, Vol. EC-15, No. 3, pp. 323-327, June 1966.

20. Deibele, S. and J.B. Beyer, Measurements of Microstrip Effective Relative Permittivities, IEEE Trans. Microwave Theory and Techniques, Vol. MTT-35, No. 5, pp. 535-538, May 1987.

21. Edwards, T.C., Foundations for Microstrip Circuit Design, John Wiley & Sons, Chichester and New York, 1981.

22. Edwards, T.C. and R.P. Owens, 2 - 18 Ghz Dispersion Measurements on 10 - 100 Ohm Microstrip Line on

Sapphire, IEEE Trans. Microwave Theory and Techniques, Vol. MTT - 24, pp. 506-513, Aug. 1976.

23. Getsinger, W.J., Microstrip Dispersion Model, IEEE Trans. Microwave Theory and Techniques, Vol. MTT-21, pp. 34-39, 1973.

24. Getsinger, W.J., Measurement and Modeling of the Apparent Characteristic Impedance of Microstrip, IEEE Trans. Microwave Theory and Techniques, Vol. MTT-31, pp. 624-632, 1983.

25. Greg, R. and I.J. Bahl, Characteristics of Coupled Microstriplines, IEEE Trans. Microwave Theory and Techniques, Vol. MTT-27, No. 7, pp. 700-705, July 1979.

26. Gupta, K.C., R. Garg, and I.J. Bahl, Microstrip Lines and Slotlines, Artech House Inc., Dedham, Massachusetts, 1979.

27. Gupta, K.C., R. Garg, and R. Chadha, Computer-Aided Design of Microwave Circuits, Artech House Inc., Dedham, Mass-achusetts, 1981.

28. Gupta, K.C. and A. Singh, Microwave Integrated Circuits, John Wiley & Sons, Inc., New York, 1974.

29. Hamilton, C.A., High Speed, Low Crosstalk Chip Holder for Josephson Integrated Circuits, IEEE Trans. Instrumentation and Measurement, Vol. IM-31, No. 2, pp. 129-131, June 1982.

30. Hammestrand, E.O., Equations for Microstrip Circuit Design, Proc. European Microwave Conf., pp. 268-272, 1975.

31. Hashimoto, M., A Rigorous Solution for Dispersive Microstrip, IEEE Trans. Microwave Theory and Techniques, Vol. MTT-33, No. 11, pp. 1131-1137, Nov. 1985.

32. Hassan,E.F., Field Solution, Polarization, and Eigen modes of Shield Microstrip Transmission Line, IEEE Trans. Microwave Theory and Techniques, Vol. MTT-34, No. 8, pp. 845-852, Aug. 1986.

33. Hatta, T., T. Kusakabe, and T. Asai, Influence of Crosstalk in Transmission Line on Accuracy in Inductive Radio System for Detecting the Position of Linear Motro Vehicles, Electronics and Communications in Japan, Part 2, Vol. 71, No. 3, pp. 46-57, 1988.

34. Hewlett Packard, HP 8510B Network Analyzer Manual

35. Holloway, A.L., Generalized Microstrip on A Dielectric Sheet, IEEE Trans. Microwave Theory and Techniques, Vol. 36, No. 6, pp. 939-951, June 1988.

36. Howe, H.,Jr., Stripline Circuit Design, Artech House, Dedham, Massachusetts, 1974.

37. Huang, W. and T. Itoh, Complex Modes in Lossless Shielded Microstrip Lines, IEEE Trans. Microwave Theory and Techniques, Vol. 36, No. 1, pp. 163-165, Jan. 1988.

38. James,J.R. and A.Henderson, High Frequency Beh- avior of Microstrip, IEE Journal on Microwaves, Optics and Acoustics, Vol. 3, No. 5, pp. 205-218, Sept. 1979.

39. Jansen, R.H., High-Speed Computation of Single and Coupled Microstrip Parameters Including Dispersion, High-Order Modes, Loss and Finite Strip Thickness, IEEE Trans. Microwave Theory and Techniques, Vol. MTT-26, No. 2, pp. 75-82, Feb. 1978.

40. Jarvis, D.B., The Effect of Interconnections on High Speed Logic Circuits, IEEE Trans on Electronic Computer, Vol. EC-12, pp. 476-487, Oct. 1963.

41. Kami, Y. and R. Sato, Coupling of Electromagnetic Waves to Transmission Lines, Electronics and Communications in Japan, Vol. 67-B, No. 4, pp. 76-84, 1984.

42. Kirschning, M. and R.H. Jansen, Accurate Model for Effective Dielectric Constant of Microstrip with Validity up to Millimeter-Wave Frequencies, Electronics Letters, Vol. 18, pp. 272-273, 1982.

43. Kirschning,M. and R.H.Jansen, Accurate Wide Range Design Equations for the Frequency-Dependent Characteristic of Parallel Coupled Microstrip Lines, IEEE Trans. Microwave Theory and Techniques, Vol. MTT-32, No. 1, pp. 83-90, Jan. 1984.

44. Kobayashi, M. and F. Ando, Dispersion Characteristics of Open Microstrip Lines, IEEE Trans. Microwave Theory and Techniques, Vol. MTT-35, No. 2, pp. 101-105, Feb. 1987.

45. Kobayashi, M., Longitudinal and Transverse Current Distributions on Microstrip Lines and Their Closed Form Expression, IEEE Trans. Microwave Theory and Techniques, Vol. MTT-33, No. 9, pp. 784-788, Sept. 1985.

46. Koike, S., N. Yoshida, and I. Fukai, Transient Analysis of Microstrip Line on Anisotropic Substrate in Three - Dimensional Space, IEEE Trans. Microwave Theory and Techniques, Vol. 36, No. 1, pp. 34-42, Jan. 1988.

47. Kretch, B.E. and R.E. Collin, Microstrip Dispersion Including Anisotropic Substrates, IEEE Trans. Microwave Theory and Techniques, Vol. MTT-35, No. 8, pp. 710-718, Aug. 1987.

48. Kwon, O., R. Fabian, and W. Pease, Closely Packed Microstrip Lines as Very High-Speed Chip-to-Chip Interconnects, IEEE Trans. Components, Hybrids, and Manufaturing Technology, Vol. CHMT-10, No. 3, pp. 314-320, Sept. 1987.

49. Lane, T.A., F.J. Belcourt, and R.J. Jensen, Electrical Characteristics of Copper/Polyimide Thin - Film Multilayer Interconnects, IEEE Trans. Components, Hybrids, and Manufaturing Technology, Vol. CHMT-12, No. 4, pp. 577-585, Dec. 1987.

50. Laverghetta, T.S., Microwave Materials and Fabrication Techniques, Artech House, Dedham, Massachusetts, 1984.

51. Laverghetta, T.S., Practical Microwaves, Howard W.- Sams & Co, Inc., Indianapolis, Indiana, 1984.

52. Leung, T. and C.A. Balanis, Attenuation Distribution of Transient Signals in Microstrip, IEEE Trans. Microwave Theory and Techniques, Vol. 36, No. 4, pp. 765-769, April 1988.

53. Maia, M.R., A.G. Assuncao, and A.J. Giarola, Dynamic Analysis of Microstrip Lines and Finlines on Uniaxial Anisotropic Substrates, IEEE Trans. Microwave Theory and Techniques, Vol. MTT-35, No. 10, pp. 881-886, Oct. 1987.

54. Mariki, G.E. and C. Yeh, Dynamic Three Dimensional TLM Analysis of Microstriplines on Anisotropic Substrate, IEEE Trans. Microwave Theory and Techniques, Vol. MTT-33, No. 9, pp. 789-799, Sept. 1985.

55. Matthaei, G.L., D.C. Park, Y.M. Kim, and D.L. Johnson, A Study of The Filter Properties of Single and Parallel-Coupled Dielectric-Waveguide Grating, IEEE Trans. Microwave Theory and Techniques, Vol. MTT-31, No. 10, pp. 825-835, Oct. 1983.

56. Naiheng, Y. and R.F. Harrington, Characteristic Impedance of Transmission Lines with Arbitrary Dielectrics under the TEM Approximation, IEEE Trans.

Microwave Theory and Techniques, Vol. MTT-34, No. 4, pp. 472-475, April 1986.

57. Napoli, L.S. and J.J. Hughes, Characteristics of Coupled Microstrip Lines, RCA Review, pp. 479-498, Sept. 1970.

58. Okugawa, S. and H. Hagawara, Analysis and Computation of Crosstalk Noise between Microstrip Transmission Lines, Electronics and Communications in Japan, Vol. 53-C, No. 7, pp. 128-135, 1970.

59. Oliver, B.M., Directional Electromagnetic Couplers, Proc. IRE, Vol. 42, No. 11, pp. 1686-1692, Nov. 1954.

60. Owens, R.P., Accurate Analytical Determination of Quasi-Static Microstrip Line Parameters, Radio and Electronic Engineer, Vol. 46, No. 7, pp. 360-364, July 1976.

61. Pauw, L.J., The Radiation of Electromagnetic Power by Microstrip Configurations, IEEE Trans. Microwave Theory and Techniques, Vol. MTT-25, No. 9, pp. 719-725, Sept. 1977.

62. Podell, A., A High Directivity Microstrip Coupler Technique, G-MTT 1970 Internatinal Microwave Symposium Digest, pp. 33-36, May 1970.

63. Pramanick, P. and P. Bhartia, An Accurate Description of Dispersion in Microstrip, Microwave Journal, No. 26, pp. 89-93, Dec. 1983.

64. Pramanick, P. and P. Bhartia, Computer - Aided Design Models for Millimeter - Wave Finlines and Suspended

Substrate Microstrip Lines, IEEE Trans. Microwave Theory and Techniques, Vol. MTT-33, No. 12, pp. 1429-1434, Dec. 1985.

65. Pucel, R.A., et al, Losses in Microstrip, IEEE Trans. Microwave Theory and Techniques, Vol. MTT-16, pp. 342-350, 1968.

66. Saad, T.S., R.C. Hansen, and G.J. Wheeler, Microwave Engineers' Handbook Volume 1 & 2, Artech House, Dedham, Massachusetts, 1971.

67. Schneider, M.V., Microstrip Lines for Microwave Integrated Circuits, Bell System Tech. Journal, Vol. 48, pp. 1421-1444, 1969.

68. Schutt-Aine, J.E. and R. Mittra, Analysis of Pulse Propagation in Coupled Transmission Lines, IEEE Trans Circuits and Systems, Vol. CAS-32, No. 12, pp. 1214-1219, Dec. 1985.

69. Seckelmann, R., On Measurements of Microstrip Properties, Microwave Journal, Vol. 11, pp. 61-64, 1968.

70. Seki, S. and H. Hasegawa, Analysis of Crosstalk in Very High-Speed LSI/VLSI's Using a Coupled Multiconductor MIS Microstrip Line Model, IEEE Trans. Microwave Theory and Techniques, Vol. MTT-32, No. 12, pp. 1715-1720, Dec. 1984.

71. Senthinathan, R., J.L. Prince, and M.R. Scheinfein, Characteristics of Coupled Buried Microstrip Lines by

Modeling and Simulation, IEEE Trans. Components, Hybrids, and Manufacturing Technology, Vol. CHMT-12, No. 4, pp. 604-611, Dec. 1987.

72. Shepherd, P.R. and R.D. Pollard, Direct Calibration and Measurement of Microstrip Structures on Gallium Arsenide, IEEE Trans. Microwave Theory and Techniques, Vol. MTT-34, No. 12, pp. 1421-1426, Dec. 1986.

73. Sherrill, B.M. and N.G. Alexopoulos, The Method of Lines Applied to a Finline / Strip Configuration on A Anisotropic Substrate, IEEE Trans. Microwave Theory and Techniques, Vol. MTT-35, No. 6, pp. 568-574, June 1987.

74. Silvester, P., TEM Wave Properties of Microstrip Transmission Lines, Proc. Instn. Elect. Engrs., Vol. 115, No. 1, p. 43, Jan. 1968.

75. Thomas, H.E., Handbook of Microwave Technique and Equipment, Prentice - Hall, Englewood Cliffs, N.J, 1972.

76. Tripathi, V.K. and A. Hill, Equivalent Circuit Modeling of Losses and Dispersion in Single and Coupled Lines for Microwave and Millimeter-Wave Integrated Circuits, IEEE Trans. Microwave Theory and Techniques, Vol. 36, No. 2, pp. 256-262, Feb. 1988.

77. Tsalamengas, J.L., N.K. Uzunoglu, and N.G.Alexopoulos, Propagation Characteristics of A Microstrip Line Printed on A General Anisotropic Substrate,IEEE Trans. Microwave

Theory and Techniques, Vol. MTT-33, No. 10, pp. 941-945, Oct. 1985.

78. U.S. Department of Commerce / National Bureau of Standards, NBS Technical Note 672, Time Domain Automatic Network Analyzer for Measurement of RF and Microwave, Boulder, Colorado, Sept. 1975.

79. Veghte, R.L. and C.A. Balanis, Dispersion of Transient Signals in Microstrip Transmission Lines, IEEE Trans. Microwave Theory and Techniques, Vol. MTT-34, No. 12, pp. 1427- 1436, Dec. 1986.

80. Venkataraman, J., S. Rao, A.R. Djordjevic, J.K. Sarkar, and Y. Naiheng, Analysis of Arbitrarily Oriented Microstrip Transmission Lines in Arbitrarily Shaped Dielectric Media over A Finite Ground Plane,IEEE Trans. Microwave Theory and Techniques, Vol. MTT-33, No. 10, pp. 952-959, Oct. 1985.

81. Waldow, P. and I. Wolff, The Skin - Effect at High Frequencies, IEEE Trans. Microwave Theory and Techniques, Vol. MTT-33, No. 10, pp. 1076-1081, Oct. 1985.

82. Wheeler, H.A., Transmission-line Properties of A Strip on A Dielectric Sheet on A Plane, IEEE Trans. Microwave Theory and Techniques, Vol. MTT-25, No. 8, pp. 631-647, Aug. 1977.

83. Whitaker, J.F., T.B. Norris, G. Mourou, and T.Y. Hsiang, Pulse Dispersion and Shaping in Microstrip Lines, IEEE Trans. Microwave Theory and Techniques, Vol. MTT-35, No. 1, pp. 41-47, Jan. 1987.

84. Zehentner, J., Characteristic Impedance and Effective Permittivity of Modified Microstrip Line for High Power Transmission, IEEE Trans. Microwave Theory and Techniques, Vol. MTT-35, No. 7, pp. 615-620, July 1987.

85. Zhang, X., J. Fang, K.K. Mei, and Liu, Calculation of The Dispersive Characteristics of Microstrips by The Time Domain Finite Difference Method, IEEE Trans. Microwave Theory and Techniques, Vol. 36, No. 2, pp. 263-266, Feb 1988.

Appendix I

Program for Microstrip Line Computations

```
C***********************************************************
C
C
C
C
C                         MICROSTRIP
C                      CHARACTERISTICS
C
C
C
C
C*********************************************************

      REAL Z0,Er,Eeff,EeffT,EeffF,E1,ERR,ERROR,
     &     F(1000),W(1000),WH(1000),We,
     &     STARTF,STOPF,STEPF,STARTW,STOPW,STEPW,
     &     SUMF,SUMW,H,SCALE,TBAR,T1,T2,FT1,FT2,
     &     FTBAR,LENGTH,LAMDA

      INTEGER  I,J,NF,NW
      CHARACTER*80  FILEIN, FILEOUT

      PI = 3.14159265


      WRITE ( *, * ) ' PROCEDURE OF CALCULATION '
      WRITE ( *, * ) ' ENTER FILENAME FOR INPUT: '
      READ  ( *, '(A)' ) FILEIN

      OPEN  ( UNIT = 1, FILE = FILEIN )
      WRITE ( *, * ) ' ENTER FILENAME FOR OUTPUT: '
      READ  ( *, '(A)' ) FILEOUT
      OPEN  ( UNIT = 6, FILE = FILEOUT )


      WRITE ( *, * ) 'ENTER SCALE FOR ERROR CORRECTION '
      READ  ( 1, * ) SCALE

      WRITE ( *, * )'ENTER CHARACTERISTIC IMPEDANCE (Z0)'

      READ  ( 1, * )  Z0

      WRITE ( *, * ) ' ENTER RELATIVE DIELECTRIC CONSTANT
     &                 (Er) '
      READ  ( 1, * )   Er

      WRITE ( *, * ) ' ENTER FREQUENCY RANGE
     &                 IN THIS CALCULATION (<1000):'
      WRITE ( *, * ) ' START STOP STEP  FREQUENCIES
                       IN GHZ (F)'
      READ  ( 1, * ) STARTF,STOPF,STEPF
```

```
      WRITE ( *, * ) ' ENTER WIDTH OF MICROSTRIP LINE
     &                  (<1000):'
      WRITE ( *, * ) ' START STOP STEP  WIDTH IN MIL (W)'
      READ  ( 1, * ) STARTW,STOPW,STEPW

      WRITE ( *, * )' ENTER THICKNESS OF MICROSTRIP LINE'

      WRITE ( *, * ) ' ACCEPTABLE RANGE  AND % OF ERROR '
      WRITE ( *, * ) ' IN MIL (T1,T2) AND ERROR
                       ( eg. 0.0000001 )'

      READ  ( 1, * )   T1,T2,ERR


      H  = 25.
      We = 100.

      WRITE ( 6, * ) '      MICROSTRIP CHARACTERISTICS '
      WRITE ( 6, * )
      WRITE ( 6, * ) 'CHARACTERISTIC IMPEDANCE (Z0) =',Z0
      WRITE ( 6, * ) 'RELATIVE DIELECTRIC CONSTANT
     &                ( Er ) =',Er
      WRITE ( 6, * ) 'THICKNESS OF MICROSTRIP LINE
     &                ( H ) IN MIL =',H
      WRITE ( 6, * ) 'ACCEPTABLE RANGE OF METAL THICKNESS
     &                ( T ) IN MIL', ' AND  % OF ERROR'
      WRITE ( 6, * )  T1, T2, ERR
      WRITE ( 6, * )
      WRITE ( 6, * )

C.........................................MAIN PROGRAM

      NF   = ( STOPF - STARTF ) / STEPF + 1
      NW   = ( STOPW - STARTW ) / STEPW + 1


      SUMW = STARTW

      DO 10 I = 1 , NW

        WRITE ( 6, 100 )
100     FORMAT ('FREQUENCY','    W    ','       T  ',
     &          '    W/H    ', '  EeffF ',
     &          '     LAMDA   ','     LENGTH')

        WRITE ( 6, 200 )
200     FORMAT ('   GHZ    ','   MIL   ','     MIL ',
     &          '          ', '          ','      MIL   ',
     &          '         MIL')
```

```
      W ( I ) = SUMW
      WH (I) = W (I) / H

C................................BEGIN CALCULATION

C.............................FIND Eeff FROM Er AND Z0

      IF  ( W ( I ) .LT. We ) THEN

         E1 = ( Er + 1.0 ) / 2.0

         Eeff = E1 * ((1. + 29.98 / Z0 * SQRT (1 / E1 )
     &         * ( Er - 1.) / ( 2. * E1 ) * (LOG ( PI /
     &          2.) + LOG ( 4. / PI ) / Er ) ) ) ** 2

C..............................FIND EFFECTIVE WIDTH

         IF ( WH (I) .LT. 1.0 ) THEN

            C1 =  Z0 * SQRT ( Eeff ) / 60.
            B  =  4  * EXP ( C1 )
            C  =  32.
            We =  H * ( B - SQRT ( B**2 - 4*C ) ) / 2.

         ELSE

            C2 = 120. * PI / (Z0 * SQRT (Eeff ) )
            C3 = 1.393 + ( .667 * 1.444 )
            We = H * ( C2 - C3 ) / 1.667

         END IF

C..................................EFFECT OF THICKNESS

         CALL THICKNESS ( T, W(I),We,T1,T2 ,ERR, SCALE)

         Edel = ( Er-1.) * T / ( H * 4.6 * SQRT( W(I)
     &           / H ) )
         EeffT = Eeff - Edel

C        WRITE ( 6, * ) ' We    = ' ,We
C        WRITE ( 6, * ) ' Eeff  = ' ,Eeff
C        WRITE ( 6, * ) ' Edel  = ' ,Edel
C        WRITE ( 6, * ) ' EeffT = ' ,EeffT

C.........EFFECT OF DISPERSION (FREQUENCY) ON ERE AND Z0

         SUMF  = STARTF

         DO 20  J = 1,NF
```

```
               F(J)   = SUMF
               H1     = H * 2.54 / 100

               EeffF = Er - ( ( Er - EeffT ) /
     &                 ( 1.0 + ( H1 / Z0 )**1.33 * ( .43 *
     &                 F ( J )**2 - .009 * F ( J )**3 )) )

               LAMDA = 3.0E4 / ( 2.54 * F ( J )
     &                 * SQRT ( EeffF ) )

               LENGTH = LAMDA / 4.0

               WRITE  ( 6, 300 ) F(J),W(I),T,WH(I),
     &                           EeffF,LAMDA,LENGTH
300            FORMAT ( F6.2,2x,F7.3,2x,F10.9,2X,F5.3,4x,
     &                  F6.3,4X,F8.3,4X,F8.3)

               SUMF   = SUMF + STEPF
20          CONTINUE

            WRITE ( 6,*)

         ELSE

            WRITE ( 6, * )  ' NO SOLUTION DUE TO W > We '

            GO TO 999

         END IF

         SUMW = SUMW + STEPW
10    CONTINUE

      CLOSE (1)
      CLOSE (6)

999   END

C..............................THICKNESS CALCULATION

      SUBROUTINE THICKNESS (T, WSUB, We,T1,T2,ERR, SCALE)

         PI = 3.14159265

         TL = T1
         TR = T2

         ERROR = ( T2 - T1 ) * ERR

1        TBAR = ( TL + TR ) / 2.
```

```
      IF ( ( TR - TL ) .GT. ERROR ) THEN

        FTL = F ( TL, WSUB, We )
        FTBAR = F ( TBAR, WSUB, We )

        IF ( ABS ( FTBAR ) .GT. SCALE * ERROR ) THEN

           IF ( ( FTL  * FTBAR ) .GT. 0. ) THEN

              TL = TBAR

           ELSE

              TR = TBAR

           END IF
           GO TO 1

        ELSE

           T = TBAR
           GO TO 33

      . END IF

      ELSE
           WRITE ( 6, * ) 'NO SOLUTION FOUND'

33    END IF

      END

    FUNCTION F ( X, Wsub, We )

      PI = 3.14159265
      H  = 25.

      IF ( WH .LT. ( 1/ ( 2 * PI ) ) )  THEN

         F = ( We - Wsub ) * PI / ( 1.25 * X )
   &        - LOG ( 4 * PI * Wsub / X ) - 1.

      ELSE

         F = ( We - Wsub ) * PI / ( 1.25 * X )
   &        - LOG ( 2 * H / X ) - 1.

      END IF
      RETURN
      END
```

Appendix II

Program for Coupled Microstrip Lines Computations

```
C*******************************************************
C
C
C
C        Effects of Strip Thickness, Width, Frequency
C
C                      and
C
C                   Crosstalk
C
C                    Between
C
C                Microstrip Lines
C
C*******************************************************

      REAL Z0,Er,H,T,
     &     F(1000),W(1000),S(1000),WH(1000),We,
     &     STARTF,STOPF,STEPF,SUMF,
     &     STARTW,STOPW,STEPW,SUMW,
     &     STARTS,STOPS,STEPS,SUMS,
     &     E0,HALFPI,DELW,CONST1,Eeff,EeffA,WTO,WTE,
     &     Z0O,Z0E,Z0FO,Z0FE,Z0SO,Z0SE,EeffO,EeffE,
     &     EeffFO,EeffFE,GO,GE,FPO,FPE,CO,CE,COA,CEA
      INTEGER  I,J,K,NF,NW,NS
      CHARACTER*80  FILEIN, FILEOUT

      PI = 3.14159265
      E0 = ( 1 / ( 36. * PI) ) * 10E-9
      C = 3. E+08

      WRITE ( *, * ) ' ENTER INPUT FILE '
      READ  ( *, '(A)' ) FILEIN
      OPEN  ( UNIT = 1, FILE = FILEIN )
      WRITE ( *, * ) ' ENTER OUTPUT FILE '
      READ  ( *, '(A)' ) FILEOUT
      OPEN  ( UNIT = 6, FILE = FILEOUT )

      HALFPI = 1/ ( 2 * PI )
      ErA = 1.0
      EeffA = 1.0

      READ ( 1, * ) Z0
      READ ( 1, * ) Er
      READ ( 1, * ) H
      READ ( 1, * ) T
      READ  ( 1, * ) STARTW,STOPW,STEPW
      READ  ( 1, * ) STARTS,STOPS,STEPS
      READ  ( 1, * ) STARTF,STOPF,STEPF

      WRITE ( 6, * ) ' Z0 ( ohm )  =', Z0
```

```
      WRITE ( 6, * ) ' Er            = ', Er
      WRITE ( 6, * ) ' H   ( mil )   = ', H
      WRITE ( 6, * ) ' T   ( mil )   = ', T
      WRITE ( 6, * )
      WRITE ( 6, * )

C..............................Begin Calculation

      SUMW = STARTW

      NF   = ( STOPF - STARTF ) / STEPF + 1
      NW   = ( STOPW - STARTW ) / STEPW + 1
      NS   = ( STOPS - STARTS ) / STEPS + 1

      DO 10 I = 1 , NW

        W ( I ) = SUMW
        WH (I) = W (I) / H
        SUMS = STARTS

        DO 15 K = 1 , NS

          S ( K ) = SUMS
          IF ( WH (I) .LT. HALFPI ) THEN

            DELW = ( 1.25 * T/ PI )
     &             * ( 1. + LOG ( 4. * PI * W(I) / T ))

          ELSE

            DELW = ( 1.25 * T/ PI )
     &             * ( 1. + LOG ( 2. * H / T ) )

          END IF

          We = W(I) + DELW
          IF ( WH (I) .LT. 1.0 ) THEN

            CONST1 = ( 60./ Z0 ) * LOG ( (8.* H / We)
     &               + (.25 * We / H) )

          ELSE

            CONST1 = 376.7 / ( Z0 * ( ( We / H )
                     + 1.393 + ( .667
     &               * LOG ( We / H + 1.444 ) ) ) )
          END IF

          Eeff = CONST1**2

          DELT = H * T / ( Er * S(K) )
```

```
      WTE = W(I) + DELW * ( 1. - 0.5 * EXP ( -.69
   &        * DELW / DELT ) )
      WTO = WTE + DELT

      CALL CAPA ( CO, CE, Er, Eeff, W(I),S(K),H, Z0 )
      CALL CAPA ( COA, CEA, ErA, EeffA, W(I), S(K),
   &              H, Z0 )

      Z0O = 1 / ( C * SQRT ( CO * COA ) )
      Z0E = 1 / ( C * SQRT ( CE * CEA ) )

      EeffO = CO / COA
      EeffE = CE / CEA

      WRITE ( 6, * ) ' W          = ', W(I)
      WRITE ( 6, * ) ' S          = ', S(K)
      WRITE ( 6, * ) ' Effects Of Strip Thickness'
   &                 ,'and Width'
      WRITE ( 6, * ) ' ODD  Eeff = ', EeffO
      WRITE ( 6, * ) ' EVEN Eeff = ', EeffE
      WRITE ( 6, * ) ' ODD  Z0   = ', Z0O
      WRITE ( 6, * ) ' EVEN Z0   = ', Z0E
      WRITE ( 6, * )
      WRITE ( 6, * ) 'Including Effects Of Frequency'
   &                ,' and Crosstalk'
      WRITE ( 6, * )

      WRITE ( 6, 100)
100   FORMAT (' Freq','          Eeff     ',
   &          '    Z0 (Ohm)    Net Z0',
   &          '      Crosstalk ')
      WRITE  ( 6, 200)
200   FORMAT (' GHz ','      Odd      Even ',
   &          '    Odd      Even     (Ohm)',
   &              '        Unit       dB ')
      WRITE ( 6, * )

      SUMF  = STARTF

      DO 20  J = 1,NF

        F(J)   = SUMF

        GO = .6 + .018 * Z0O
        GE = .6 + .0045 * Z0E

        FPO = 31.32 * Z0O / H
        FPE = 7.83 * Z0E / H

        EeffFO = Er - ( Er - EeffO )
   &             / ( 1+ GO * (F(J)/FPO)**2 )
```

```
         EeffFE = Er - ( Er - EeffE )
     &               / ( 1+ GE * (F(J)/FPE)**2 )

         CALL CSTRIP ( Z0SO, Z0SE, W(I), S(K), H, Er )

         Z0FO = Z0SO - (Z0SO -Z0O)
     &              / ( 1 + GO * ((F(J) /FPO)**1.6 ))
         Z0FE = Z0SE - (Z0SE -Z0E)
     &              / ( 1 + GE * ((F(J) /FPE)**1.6 ))

         Z0F = SQRT ( Z0FO * Z0FE )
         CTK = ( Z0FE - Z0FO ) / ( Z0FE + Z0FO )
         CTKDB =  20. * LOG10 ( CTK )

         WRITE ( 6,300 ) F(J),EeffFO,EeffFE,Z0FO,Z0FE,
     &                             Z0F,CTK,CTKDB

300      FORMAT ( F5.2,2x,F6.3,2X,F6.3,2X,
     &                F6.3,2x,F7.3,
     &                2X,F7.3,2X,F6.3,2X,F7.3)

         SUMF   = SUMF + STEPF
20     CONTINUE

       WRITE ( 6,*)

       SUMS = SUMS + STEPS
15   CONTINUE

     SUMW = SUMW + STEPW
10   CONTINUE

     CLOSE (1)
     CLOSE (6)

999  END

C...................... Capacitance Model Calculation

     SUBROUTINE CAPA ( CO, CE, Er, Ere, W, S, H, Z0 )

       PI = 3.14159265
       E0 = ( 1 / ( 36. * PI) ) * 10E-9
       C = 3. * 10E8

       CP = E0*Er * W/H

       CF = .5 * ( SQRT ( Ere ) / ( C * Z0 ) - CP )

       CFF = ( CF* SQRT (Er/Ere) )
     &        / ( 1. + EXP ( -.1 * EXP (2.33 -2.53*W/H ))
```

```
     &         * ( H / S )* TANH ( 10.* S / H ) )

          CGD = ( E0 * Er / PI ) * LOG ( 1/ TANH ( PI* S
     &          / ( 4. * H ) )
     &        + .65 * CF * ( (.02 * SQRT (Er) / (S/H) )
     &        + 1. - 1/Er**2 ) )

          Z = S / ( S + 2. * W )
          ZZ = SQRT ( 1. - Z*Z )
          ZZZ = F (Z,ZZ )

          CGA = E0 / ZZZ

          CE = CP + CF + CFF
          CO = CP + CF + CGA + CGD

          RETURN

          END

C.............Impedance Of Coupled Striplines Calculation

         SUBROUTINE  CSTRIP ( Z0SO, Z0SE, W, S, H, Er )

           PI = 3.14159265

           YE = TANH ( PI * W / (4*H) )
     &          * TANH ( PI * ( W+S ) / (4* H ))

           YO = TANH ( PI * W / (4*H) )
     &          / TANH ( PI * ( W+S ) / (4* H ))

           YYE = SQRT ( 1. - YE**2 )
           YYO = SQRT ( 1. - YO**2 )

           YYYE = F ( YE, YYE )
           YYYO = F ( YO, YYO )

           Z0SO = 30. * PI / ( YYYO * SQRT ( Er ) )
           Z0SE = 30. * PI / ( YYYE * SQRT ( Er ) )

           RETURN
           END


        FUNCTION F ( Z, ZZ )

           PI = 3.14159265
```

```
    IF ( Z .LT. .7 ) THEN
       F = PI/ LOG ( 2.* ( 1. + SQRT (ZZ) )
&            / ( 1.- SQRT(ZZ) ))
    ELSE

       F = LOG ( 2 * ( 1. + SQRT (Z) )
&            / ( 1.- SQRT (Z) )) / PI
    END IF

    RETURN

    END
```

Appendix III

A Program for Crosstalk Noise Computations
(Microstrip circuit)

Using TOUCHSTONE Software

```
! A10.CKT
!
!                  Crosstalk Study
!                    Ideal Case
!
!                  Spacing = 10 mils
!
!                    50 ohm Lines
!              Actual Lines Length = 1400 mils
!
!              Coupled Microstrip Lines Model
!
DIM
  FREQ GHZ
  RES OH
  IND NH
  CAP PF
  LNG MIL
  TIME PS
  COND /OH
  ANG DEG

CKT
  MSUB   ER=9.8 H=25 T=.6  RHO=1  RGH=0
  MCLIN  1  2  3  4  W=24 S=10 L=1400
  DEF4P  1  2  3  4  TSMCLIN

FREQ
  SWEEP  0.2 18.0 0.2

OUT
  TSMCLIN DB[S21]  GR1
  TSMCLIN DB[S31]  GR1
  TSMCLIN MAG[S21]  GR2
  TSMCLIN ANG[S21]  GR3
  TSMCLIN MAG[S31]  GR2
  TSMCLIN ANG[S31]  GR3

GRID
  RANGE 0 10 1
  GR1  50 -100 -20
  GR2 0 1 .2
  GR3 -180 180 45
```

Appendix IV

A Program for Crosstalk Noise Computations
(Microstrip circuit)

Using SPICE Software

```
VSW 23 0 PULSE(0V .2V 0 0 0 4nS)
R1 1 23 50

.SUBCKT CRX 31 32 33 34
  LA 31 35 .00132639uH
  RA 35 34 .1778ohm
  CA 35 0 .65430pF

  LB 32 36 .00132639uH
  RB 36 33 .1778ohm
  CB 36 0 .65430pF

  CM 35 36 .0238676pF
  K  LA LB .10
.ENDS

X1 1 2 21 22 CRX
X2 22 21 5 6 CRX
X3 6 5 7 8 CRX
X4 8 7 9 10 CRX
X5 10 9 11 12 CRX
X6 12 11 13 14 CRX
X7 14 13 15 16 CRX
X8 16 15 17 18 CRX
X9 18 17 19 20 CRX
X10 20 19 3 4 CRX

R2 2 0 50
R3 3 0 50
R4 4 0 50

.TRAN 0.1nS 2nS
.PROBE V(2) V(3)

.END
```

Appendix V

A Program for Crosstalk Noise Computations
(Stripline circuit)

Using TOUCHSTONE Software

```
! C10.CKT
!
!               Teflon - Ceramic Copper Claded
!
!                    Stripline Circuit
!
!                   Crosstalk Study
!                     Ideal Case
!
!                   Spacing = 10 mils
!
!               Actual Lines Length = 1400 mils
!
!               Coupled Striplines Model
!
DIM
  FREQ GHZ
  RES OH
  IND NH
  CAP PF
  LNG MIL
  TIME PS
  COND /OH
  ANG DEG

CKT
  SSUB  ER=10.5 B=50 T=1.5 RHO=1
  SCLIN  1  2  3  4  W=24 S=10 L=1400
  DEF4P  1  2  3  4  TSSCLIN

FREQ
  SWEEP  0.2 18.0 0.2

OUT
  TSSCLIN DB[S21]  GR1
  TSSCLIN DB[S31]  GR1
  TSSCLIN MAG[S21]  GR2
  TSSCLIN ANG[S21]  GR3
  TSSCLIN MAG[S31]  GR2
  TSSCLIN ANG[S31]  GR3

GRID
  RANGE 0 10 1
  GR1  50 -100 -20
  GR2 0 1 .2
  GR3 -180 180 45
```

VITA

Mr. Prasit Teekaput was born in Bangkok, Thailand, on November 4, 1959. He received the B.Sc. degree in Electrical Engineering from Chulalongkorn University, Bangkok, Thailand, in 1982. He worked as a Research Assistant in the field of antenna design and fabrication at the department of Electrical Engineering, Chulalongkorn University during his freshman and sophomore years. He had his training in satellite communications at the Satellite Communication Earth Station of Thailand during his junior year and his training in telephone communications at the Ericsson Telephone Far East Corporation Ltd., Bangkok, during his senior year. Before he came to continue his studies in the U.S.A., he worked as an Engineer on a special research project related to circuit breakers at Thai Electric Equipments Co. Ltd. and on installation and maintenance of load cell instruments at Berli Jucker Co. Ltd., Bangkok.

He received the M.S. degree in Electrical Engineering from the University of Texas at Arlington in 1984. At the University of Texas at Arlington, he worked as a research assistant on microwave devices and semiconductors in the Center for Advanced Electron Devices and Systems. His thesis topic was on the design and fabrication of C band active phase shifters. He worked on his Ph.D. Program at The University of Texas at Arlington until 1986 and then transferred to Virginia Polytechnic Institute and State University.

At Virginia Polytechnic Institute and State University, he worked as a teaching assistant in partial of his Ph.D. Program and as a technician at the Universal Control Engineering Co. Ltd. His areas of interest include crosstalk noise characteristics, microwave measurements of material properties, and hybrid microelectronics.